

**POLAR CODE DESIGN AND DECODING
FOR MAGNETIC RECORDING**

A Thesis
Presented to
The Academic Faculty

by

Ubaid U. Fayyaz

In Partial Fulfillment
of the Requirements for the Degree
Doctor of Philosophy in the
School of Electrical and Computer Engineering

Georgia Institute of Technology
December 2014

Copyright © 2014 by Ubaid U. Fayyaz

**POLAR CODE DESIGN AND DECODING
FOR MAGNETIC RECORDING**

Approved by:

Dr. John R. Barry, Advisor
School of Electrical and Computer
Engineering
Georgia Institute of Technology

Dr. Faramarz Fekri
School of Electrical and Computer
Engineering
Georgia Institute of Technology

Dr. Steven W. McLaughlin
School of Electrical and Computer
Engineering
Georgia Institute of Technology

Dr. Matthieu Bloch
School of Electrical and Computer
Engineering
Georgia Institute of Technology

Dr. David Goldsman
School of Industrial and Systems
Engineering
Georgia Institute of Technology

Date Approved: August 4th, 2014

To my parents,

Bano & Abdullah.

ACKNOWLEDGEMENTS

First of all, I would like to express my deepest gratitude to my PhD advisor Dr. John Barry. This thesis would not have been in current shape without his patient mentoring despite my frequent mistakes and constructive criticism. His eagerness to present difficult concepts in a simple and elegant way has inspired me to take academia as a career. He has set standards of being a good teacher for me, and I will consider myself successful if I achieve a small fraction of those standards some day.

I would like to thank Dr. Steven W. McLaughlin and Dr. Faramarz Fekri for taking out time from their busy schedules and being a part of my reading committee. I would also like to thank Dr. Goldsman and Dr. Bloch for serving on my dissertation defense committee.

I would like to thank all my lab mates in Communication and Information Theory Lab. Sarwat and Elnaz helped me in the hours of distress and made my journey through PhD a lot easier. Talking to them was always refreshing, and their continuous encouragement kept me focused on my goals.

I would like to express my heartfelt thanks to my friends Wasif, Muqarrab, Shoaib, Hassan, Sajid, Bashir, Usman, Saad, Faisal and Waseem who made my life at Tech enjoyable and delightful.

My words cannot express my gratitude toward my parents who, despite all hardships, provided me with everything I ever needed. At times, the prayers of my parents were the only thing to give me the confidence to overcome my problems. Being away from my parents was the biggest sacrifice I made for graduate studies. In addition to my parents, my sisters Saima, Sadia and Nadia supported me throughout my life, and without them, I would not have achieved anything in my life. Thank you, my family.

TABLE OF CONTENTS

DEDICATION	iii
ACKNOWLEDGEMENTS	iv
LIST OF TABLES	viii
LIST OF FIGURES	ix
LIST OF SYMBOLS OR ABBREVIATIONS	xiii
SUMMARY	xiv
I INTRODUCTION	1
1.1 Magnetic Recording Channel as a Communication Channel	2
1.2 History of Error-Correcting Codes in Magnetic Recording	3
1.3 Polar Codes in Magnetic Recording	4
1.4 Thesis Goal: A Tale of Four Metrics	6
1.4.1 Requirements from a Decoder	6
1.4.2 Requirements from a Code/Encoder	7
1.4.3 Summary	9
II BACKGROUND	12
2.1 An Introduction to Block Codes	12
2.1.1 Single Parity-Check Codes	12
2.1.2 Repetition Codes	17
2.2 An Introduction to Polar Codes	19
2.2.1 Generator Matrix and Encoding	19
2.2.2 The Factor Graph Representation of Polar Codes	22
2.2.3 Hard-Output Successive Cancellation Decoder	24
2.3 The Construction of Polar Codes	26
2.3.1 Construction for the BEC	28
2.3.2 Construction for the AWGN Channel	28
2.4 System Model	29
2.5 Advanced Decoders for Polar Codes	30
2.5.1 Hard-Output Successive Cancellation List Decoder	30

2.5.2	Hard-Output Simplified Successive Cancellation Decoder	32
2.5.3	Soft-Output Belief Propagation Decoder	33
III	IMPROVED BELIEF-PROPAGATION SCHEDULE FOR POLAR CODES	37
3.1	The Soft-Cancellation (SCAN) Schedule and Decoder	38
3.2	Reducing the Memory of the SCAN Decoder	41
3.3	A Comparison with the Flooding Schedule	48
3.4	Performance Results	51
3.4.1	The AWGN Channel	51
3.4.2	Partial Response Channels	52
3.5	Complexity Analysis	54
3.6	Summary	56
IV	AN ENHANCED SCAN DECODER WITH HIGH THROUGHPUT AND LOW COMPLEXITY	58
4.1	The Properties of Polar Codes	59
4.2	Discussion on the Properties of Polar Codes	70
4.3	A High-Throughput, Low-Complexity Soft-Output Decoder for Polar Codes	72
4.4	Latency and Complexity Analysis	78
4.5	Summary	81
V	OPTIMIZED POLAR CODE DESIGN FOR INTERSYMBOL INTERFERENCE CHANNELS	82
5.1	Polar Codes as Generalized Concatenated Codes	83
5.2	An Introduction to EXIT Charts	84
5.3	EXIT Chart Analysis of Polar Codes with Multistage Decoding	87
5.3.1	Multistage Decoding with Two Stages	87
5.3.2	Multistage Decoding with Four Stages	90
5.4	EXIT Chart Based Design of Polar Codes	93
5.4.1	For Decoding with Two Stages	94
5.4.2	For Decoding with Four Stages	95
5.4.3	Computation of Design SNR	96
5.5	Simulation Results	99

5.5.1	Accuracy of EXIT Curve Approximation	100
5.5.2	Code Performance	100
5.6	Summary	102
VI	CONTRIBUTIONS AND FUTURE RESEARCH	103
6.1	Contributions	103
6.2	Future Directions	104
6.2.1	Error Floor Analysis of Polar Codes with the SCAN Decoder	104
6.2.2	Analysis of the SCAN Decoder	105
6.2.3	Performance of the SCAN Decoder in Turbo Decoding	106
APPENDIX A	— PROOF OF THE PROPERTIES OF THE SCAN	
	DECODER	108
REFERENCES	110
VITA	113

LIST OF TABLES

1	Complexity Comparison of Different Decoders	56
2	Protograph Input/Output Set Relationship	62
3	Design Parameters	100

LIST OF FIGURES

1.1	A magnetic recording device consists of a magnetic recording medium and a read/write head. The write head writes data bits on the magnetic recording medium in concentric rings called tracks.	2
1.2	The write head writes data bits on a track by changing the polarity of small magnetized regions.	2
1.3	Hard-disk write/read process is similar to transmitting on a traditional communication channel except that instead of transmitting from one physical location to the other, hard-disk drives transmit data from one time instant (when the user writes the data) to the other (when the user reads the data). An example of mapping between message and coded bits is also shown below the encoder. In this example, the transmitter sends the message bit twice and for this repetition, the code is called the <i>repetition code</i>	3
1.4	In turbo equalization, the receiver iteratively exchanges the soft information between the soft-output detector and the decoder for error-correcting code.	5
1.5	The majority of the area in the die micrograph of this LDPC decoder chip is occupied by computational and memory units shown as SISO engine and Γ -, π -SRAM, respectively. Most of the rest of the area is occupied by the wiring network connecting different parts of the chip shown as Ω -NETWORK. The image is taken from Mansour, M.M.; Shanbhag, N.R., "A 640-Mb/s 2048-bit programmable LDPC decoder chip," <i>Solid-State Circuits, IEEE Journal of</i> , vol.41, no.3, pp.684,698, March 2006 ©2006 IEEE.	8
1.6	A good decoder lies in the region close to the origin in three dimensional space of power, area and latency. This region directly corresponds to a region close to the origin in three dimensional space of computational complexity, memory requirement and latency.	8
1.7	An ideal system consisting of polar codes and their soft-output decoder should lie in the highlighted region of the four-dimensional space.	10
2.1	In a block code, the message is divided into blocks of K bits. Each block is then independently encoded to a block of N coded bits using an encoder.	13
2.2	The parity-check node takes all the input <i>messages</i> in the form of intrinsic LLRs and produces the outbound <i>message</i> $L_{N-1}^{(e)}$	18
2.3	A $(N, 1, 1/N)$ repetition code repeats the message bit N times giving rise to $N - 1$ trivial parity-check nodes with two edges as shown on the left. The right-hand side image is the rearranged version of the left-hand side image with the equality-check node corresponding to c_0 summing all incoming LLRs to produce an outgoing extrinsic LLR for c_0	19
2.4	The encoder represents the relationship between encoded and uncoded bits of a rate one-half polar code with $\mathcal{S} = \{3, 5, 6, 7\}$. The rectangles with '+' sign represents binary XOR operation.	22

2.5	The basic structure in the encoder of polar code represents polar codes of length two. This basic encoder correspond to a parity-check and an equality-check constraint.	23
2.6	The factor graph represents the relationship between encoded and uncoded bits of a rate one-half polar code with $\mathcal{S} = \{3, 5, 6, 7\}$	24
2.7	The trio (λ, ϕ, ω) can index all the nodes in the factor graph of polar codes.	25
2.8	The difference between the SC and the SCL decoder lies in the number of paths they keep while detecting any message bit.	31
2.9	The BP decoder updates LLRs on a protograph-by-protograph basis. In a single protograph, it updates four LLRs with two LLRs in both L and B	34
2.10	The polar code with BP decoding performs worse than the LDPC code with BP decoding on both the fronts: it requires a larger number of computations while requiring a larger E_b/N_0 to achieve FER = 10^{-3} on a dicode channel.	35
2.11	The BP decoder for LDPC codes requires less than 50% of the memory required by BP decoder for polar codes with $N > 16$. This relative memory requirement decreases monotonically and goes very low for practical block lengths such as only 13% for a code of length 32768.	36
3.1	System model for Lemma: 3.1	38
3.2	At any depth $\lambda \in \{0, 1, \dots, n\}$, $\mathcal{L}_\lambda(\phi)$ for all $\phi \in \{0, \dots, 2^\lambda\}$ are stored in the memory for $\mathcal{L}_\lambda(0)$, which is shown in green.	44
3.3	Memory elements required to store B with corresponding ϕ displayed next to a particular $\mathcal{B}_\lambda(\phi)$. In any iteration, the SCAN decoder does not need $\{\mathcal{B}_\lambda(\phi) : \phi \text{ is even}\}$ for the next iteration, and we can overwrite $\mathcal{B}_\lambda(0)$ (shown with green rectangles) at any depth λ with $\{\mathcal{B}_\lambda(\phi) : \phi \text{ is even}, \phi \neq 0\}$ (shown with yellow rectangles). On the other hand, the SCAN decoder requires $\{\mathcal{B}_\lambda(\phi) : \phi \text{ is odd}\}$ (shown with white rectangles) for processing in the next iteration, and therefore it will keep these memory locations as they are. In this small example, we save five memory elements corresponding to $\mathcal{B}_2(2), \mathcal{B}_3(2), \mathcal{B}_3(4)$ and $\mathcal{B}_3(6)$	48
3.4	FER and BER performance of the SCAN decoder in the AWGN channel for $N = 32768$. We have optimized the polar code for $E_b/N_0 = 2.35$ dB using the method of [1].	53
3.5	FER performance of the SCAN decoder in partial response channels for $K = 4096$ and $N = 8192$. We have optimized the polar code for $E_b/N_0 = 1.4$ dB (dicode) and $E_b/N_0 = 1.55$ dB (EPR4) using the method of [1].	55
3.6	Memory efficiency improves with increasing block length.	56

4.1	Only P_0 , P_1 and P_2 are possible at depth n in the factor graph of the polar codes. The inputs on the right of these three protographs specify whether bit is free (in case of $\{0\}$) or fixed (in case of ∞). In case of P_0 , P_1 and P_2 , both of the output nodes have LLRs from the same set. For example for P_0 , the values in $B_0(0)$ corresponding to both the output nodes on the left have LLRs from the set $\{\infty\}$, i.e., the LLRs in both of these nodes are stuck to ∞ . On the other hand in P_6 , LLRs corresponding to output nodes come from the set $\{0, \infty\}$, i.e., both the values are different unlike other three protographs.	62
4.2	The notation used in the proof of Theorem 4.2 is explained.	65
4.3	An example design of a rate one-half polar code validates the properties. Only protographs P_0 , P_1 and P_2 appear at depth $\lambda = n$ (Special Prohibited Pairs Property). In the entire factor graph, P_6 , P_7 and P_8 do not occur (General Prohibited Pairs Property). All the node-groups have LLRs from either of the sets $\{\{0\}, \{\infty\}, \mathbb{R}\}$ (Corollary 4.1).	70
4.4	Every type of protograph has an equivalent reduced form.	71
4.5	The memory required for O is reduced by not storing the LLRs corresponding to rate-one and rate-zero subcodes.	77
4.6	The normalized number of computations, memory requirement and latency of the eSCAN decoder with LLR-skipping stays less than those of the SCAN decoder without LLR-skipping for a range of code rates.	79
4.7	The polar code with eSCAN decoding has approximately the same complexity/power trade-off trend as the LDPC code with BP decoding. However, polar codes require approximately 0.4 dB higher E_b/N_0 to achieve the same frame error rate on the dicode channel.	80
5.1	The factor graph of a parent polar code of length $N = 8$ is a concatenation of two outer codes of length four with an inner code of length eight.	84
5.2	The computation of EXIT chart of the BCJR decoder/equalizer boils down to computing three LLRs: a priori LLRs L_A , channel LLRs L_C and extrinsic LLRs L_E	86
5.3	The polar code of length N can be viewed as the concatenation of four outer codes \mathcal{C}_0 , \mathcal{C}_1 , \mathcal{C}_2 and \mathcal{C}_3 using an inner code.	87
5.4	The EXIT curve of polar codes follows a hill-like trajectory with two faces, two plateaus and one slope.	89
5.5	The inner code serves as the parity check and repetition code of degree three when the decoder for \mathcal{C}_1 is unsuccessful and the decoder for \mathcal{C}_0 is successful, respectively.	91
5.6	When decoders for outer codes \mathcal{C}_0 , \mathcal{C}_1 , \mathcal{C}_2 and \mathcal{C}_3 are unsuccessful, the inner code acts like a mixture of degree-five parity-check codes. The extrinsic mutual information at the output of the multistage decoder is zero, because all the decoders for \mathcal{C}_0 , \mathcal{C}_1 , \mathcal{C}_2 and \mathcal{C}_3 are unable to decode the message. . .	92

5.7	When the decoders for outer code \mathcal{C}_0 and \mathcal{C}_1 are successful and unsuccessful, respectively, the inner code becomes a code mixture of serially concatenated degree-three parity-check and degree-three variable nodes.	92
5.8	The EXIT curve of polar codes follows a hill-like trajectory for four-level codes.	94
5.9	The EXIT curve of polar codes calculated from Section 5.3 approximates that obtained through Monte Carlo simulations.	98
5.10	Polar codes constructed through the proposed method provide approximately 0.6 dB and 0.9 dB gain in FER performance on EPR4 and E2PR4 channels, respectively, relative to the ones optimized for AWGN.	101
6.1	In turbo decoding, the decoder decodes the combination of two codes by exchanging soft information between two decoders.	106

LIST OF SYMBOLS OR ABBREVIATIONS

APP	A Posteriori Probability.
AWGN	Additive White Gaussian Noise.
BCJR	Bahl, Cocke, Jelinek and Raviv.
BEC	Binary Erasure Channel.
BP	Belief Propagation.
CRC	Cyclic Redundancy Check.
DE	Desntiy Evolution.
E2PR4	Extended-Extended Partial Response Class-4.
EPR4	Extended Partial Response Class-4.
EXIT	Extrinsic Information Transfer.
HDD	Hard-Disk Drive.
ISI	Intersymbol Interference.
LDPC	Low-Density Parity-Check.
LLR	Log-Likelihood Ratio.
MAP	Maximum a Posteriori Probability.
RA	Repeat-Accumulate.
RS	Reed-Solomon.
SC	Successive Cancellation.
SCAN	Soft Cancellation.
SCL	Successive Cancellation List.
SNR	Signal-to-Noise Ratio.
SSC	Simplified Successive Cancellation.

SUMMARY

Powerful error-correcting codes have enabled a dramatic increase in the bit density on the recording medium of hard-disk drives (HDDs). Error-correcting codes in magnetic recording require a low-complexity decoder and a code design that delivers a target error-rate performance. This dissertation proposes an error-correcting system based on polar codes incorporating a fast, low-complexity, soft-output decoder and a design that is optimized for error-rate performance in the magnetic recording channel.

LDPC codes are the state-of-the-art in HDDs, providing the required error-rate performance on high densities at the cost of increased computational complexity of the decoder. Substantial research in LDPC codes has focused on reducing decoder complexity and has resulted in many variants such as quasi-cyclic and convolutional LDPC codes.

Polar codes are a recent and important breakthrough in coding theory, as they achieve capacity on a wide spectrum of channels using a low-complexity successive cancellation decoder. Polar codes make a strong case for magnetic recording, because they have low complexity decoders and adequate finite-length error-rate performance. In their current form, polar codes are not feasible for magnetic recording for two reasons. Firstly, there is no low-complexity soft-output decoder available for polar codes that is required for turbo-based equalization of the magnetic recording channel. The only soft-output decoder available to date is a message passing based belief propagation decoder that has very high computational complexity and is not suitable for practical implementations. Secondly, current polar codes are optimized for the AWGN channel only, and may not perform well under turbo-based detector for ISI channels.

This thesis delivers a powerful low-complexity error-correcting system based on polar codes for ISI channels. Specifically, we propose a low-complexity soft-output decoder for polar codes that achieves better error-rate performance than the belief propagation decoder for polar codes while drastically reducing the complexity. We further propose a technique

for polar code design over ISI channels that outperforms codes for the AWGN channel in terms of error rate under the proposed soft-output decoder.

Altogether, this thesis takes polar codes from the point of being infeasible for magnetic recording application and puts them at a competitive position with the state-of-the-art.

CHAPTER I

INTRODUCTION

Storage devices such as DVDs, hard-disks and flash drives are the backbone of modern data-driven life. Each of these devices is suitable for a specific application. DVDs suit applications where data is only read and is not written or erased such as software and movie distribution. Flash drives suit applications that require little storage with high read and write speed such as temporary personal data storage. Magnetic recording devices such as hard-disk drives cater for the bulk of today's data storage needs. Magnetic recording devices are popular, because they offer a non-volatile, high-speed, low-cost and physically manageable solution for data storage. For these reasons, the hard disk is an integral part of almost every computer system and data center.

A magnetic recording device consists of a magnetic recording medium and a read/write head, as shown in Figure 1.1. The magnetic recording medium is a circular disk, typically thin film. The disk is organized into concentric rings called tracks. The write head writes data bits by changing the polarization of tiny magnetized regions on each track. Figure 1.2 shows an example of the polarization of different magnetic regions in a track. The head and tail of the arrow represent north and south pole of the magnetized region, respectively. For reading the bits from the disk, a read head senses the transition in polarity of the magnetized regions.

For the magnetic recording industry, the challenge of handling more and more storage demand translates into packing more and more data bits per unit area of the recording medium, also called the areal density. Quite expectedly when we increase the areal density, the more difficult it gets for the device to read the data from the medium.

Over the course of time, two major research dimensions emerged to increase the areal density. One is to improve the write and read process by using better recording media and read head designs, and a second is to incorporate signal processing and

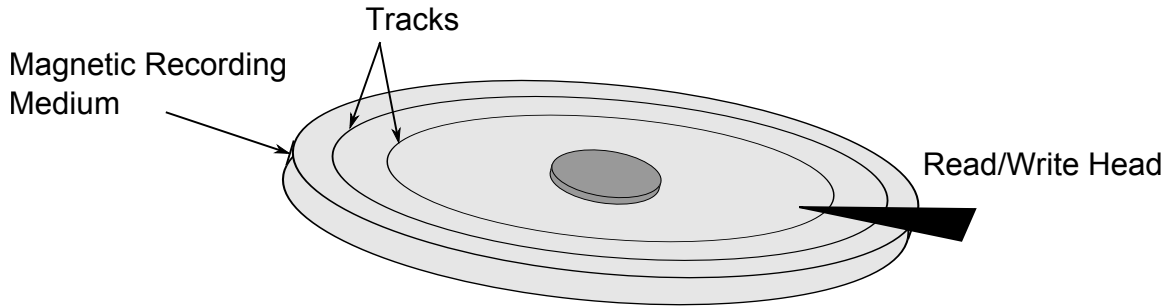


Figure 1.1: A magnetic recording device consists of a magnetic recording medium and a read/write head. The write head writes data bits on the magnetic recording medium in concentric rings called tracks.

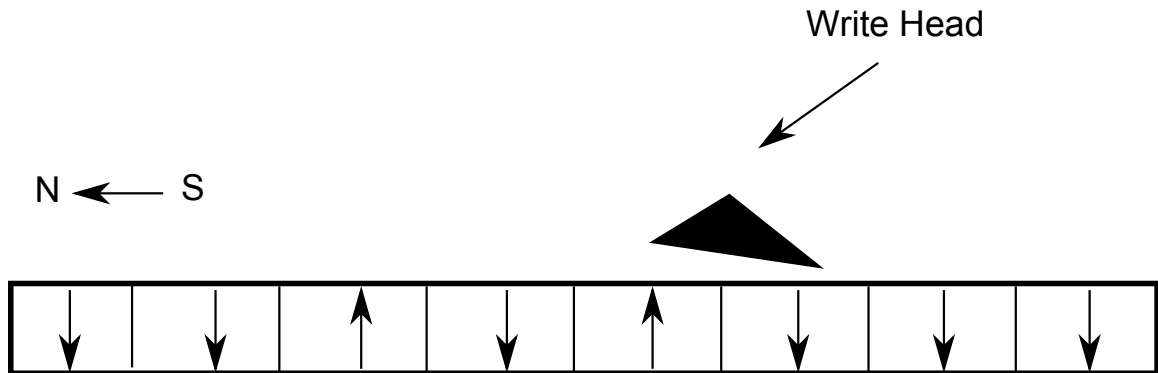


Figure 1.2: The write head writes data bits on a track by changing the polarity of small magnetized regions.

error-correcting techniques to make the read process robust against errors. This thesis extends research in the dimension of error-correcting techniques and proposes a new, competitive error-correcting system based on polar codes.

1.1 *Magnetic Recording Channel as a Communication Channel*

In error-control coding, a transmitter wishing to send a K -bit message will first encode it into a sequence of $N > K$ coded bits called the codeword before sending through a noisy channel. The set of all possible codewords is called the *code*. At the receiver, the decoder maps the noisy version of the transmitted codeword to a K -bit decision message. $N - K$ additional bits make the communication system more reliable. The price for this extra reliability is the reduction in useful data rate or storage capacity for the HDD, by a factor of $1 - K/N$.

A magnetic recording system is like a communication system. The read/write process

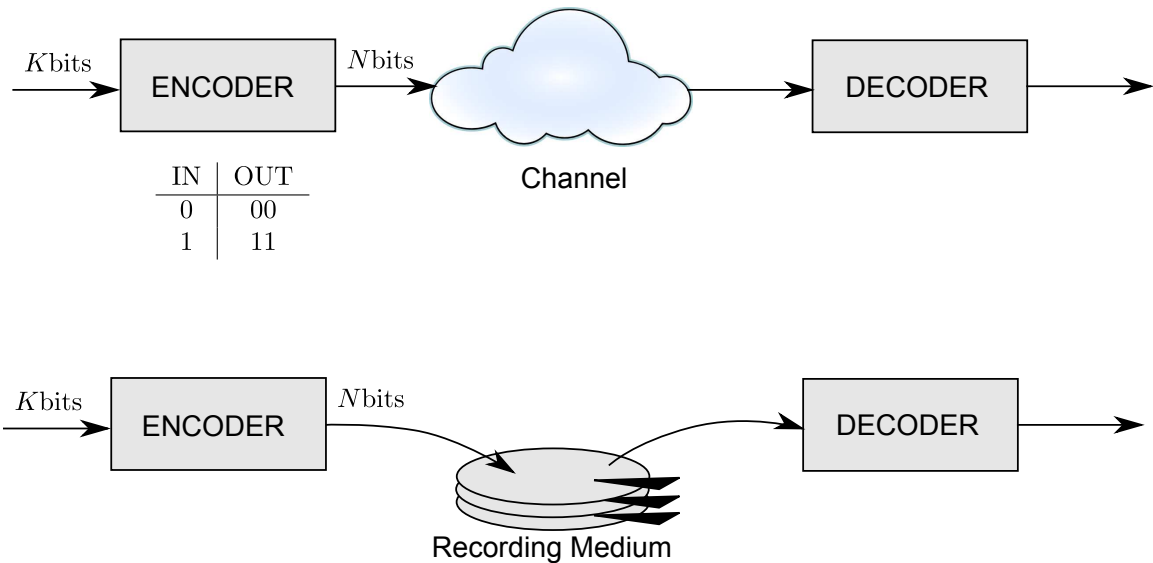


Figure 1.3: Hard-disk write/read process is similar to transmitting on a traditional communication channel except that instead of transmitting from one physical location to the other, hard-disk drives transmit data from one time instant (when the user writes the data) to the other (when the user reads the data). An example of mapping between message and coded bits is also shown below the encoder. In this example, the transmitter sends the message bit twice and for this repetition, the code is called the *repetition code*.

is similar to a communication system with the write process acting as the transmitter, the read process acting as the receiver, and the recording medium acting as the channel. Unlike communication systems, in which we transmit the data from one physical location to the other, the recording devices transmit data from one time instant to the other. Figure 1.3 compares the basic components of a communication system with those of a recording system.

The effectiveness of an error-correcting system broadly depends on both the encoder and the decoder. Often the code must be designed to match the specific characteristics of the channel being considered. For example, a code designed for the AWGN channel may not perform well on ISI channels. Secondly, the decoder should be optimal or near-optimal in error-rate performance for a specific channel and should also admit a memory-efficient, low-complexity, low-latency hardware implementation.

1.2 History of Error-Correcting Codes in Magnetic Recording

In 1990s, hard-disk drives employed Reed-Solomon (RS) codes for their error-correcting systems. At that time, the affordable computational power was very low, and the

error-correcting system was required to have ultra-low computational cost. RS codes fit the profile, because they are powerful as well as cyclic codes. In cyclic codes, a cyclic shift in a codeword produces another codeword of the same code. The cyclic nature of RS codes enables the implementation of good-performing decoders having low computational cost. RS codes are still one of the powerful codes available, but they are not capacity-achieving like LDPC codes.

Since late 2000s [2], hard-disk drives have switched to error-correcting systems based on LDPC codes. LDPC codes are powerful codes, and have near-optimal decoders for AWGN and ISI channels with relatively higher complexity than those of RS codes. Since affordable computational complexity has increased largely in past two decades, hard-disk drives can now support the computational complexity needed to decode LDPC codes. The high complexity of LDPC decoders is still an issue, and considerable research has been done to reduce this high complexity that resulted in many variants of LDPC codes such as repeat-accumulate (RA) codes and convolutional LDPC codes [3]. All in all, a powerful code with optimal or near-optimal, low-complexity decoder is always a top priority in these systems.

1.3 Polar Codes in Magnetic Recording

Polar codes are a type of linear block codes proposed by Arikan [4] and are considered to be one of the most important breakthroughs in coding theory in the past decade. Polar codes asymptotically achieve capacity on a wide array of channels using an encoder and decoder of complexity $O(N \log N)$. They also have the desirable property that the same decoder can be used to decode all polar codes of different rates and designs.

Polar codes achieve capacity for asymptotically large block lengths. For finite block lengths, however, the performance of polar codes is worse than the state-of-the-art, and the originally proposed successive cancellation decoder is not optimal. In past few years, construction as well as decoding algorithms of polar codes have improved significantly. Tal and Vardy [5] showed that at moderate block lengths, polar codes outperform state-of-the-art LDPC codes in terms of error rate on the AWGN channel when concatenated

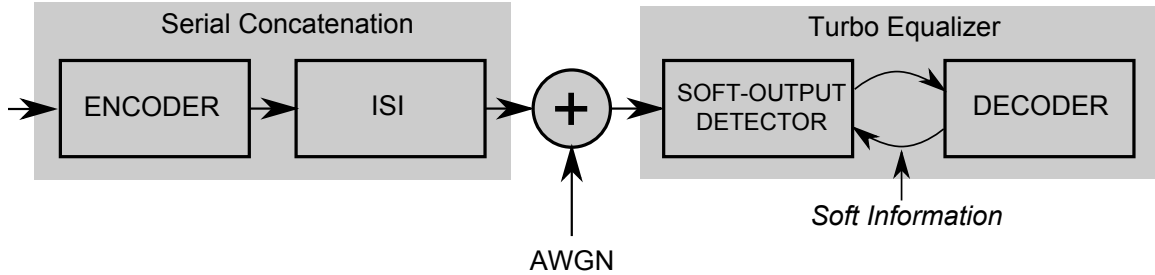


Figure 1.4: In turbo equalization, the receiver iteratively exchanges the soft information between the soft-output detector and the decoder for error-correcting code.

even with the simplest cyclic redundancy check (CRC) codes using a successive-cancellation list decoder [5]. The work of Tal and Vardy produced a powerful code with near-optimal performance and a relatively low-complexity decoder, but these results were limited to the AWGN channel only.

The magnetic recording channel is an intersymbol interference ISI channel. One famous detection strategy for intersymbol interference channels is turbo equalization [6], in which a detector for the ISI channel and the decoder for error-correcting code iteratively exchange reliability information known as *soft information* about the coded bits. A common way of representing soft information for binary symbols is the log-likelihood ratio (LLR), which is defined as

$$LLR = \log \left(\frac{\text{Likelihood of a bit being zero}}{\text{Likelihood of a bit being one}} \right).$$

The sign of the LLR describes the decision whether the bit is zero or one, whereas its magnitude corresponds to the reliability of this decision. The higher the magnitude is, the more confident the decoder is about its decision. For instance, if the LLR is positive, it means the decoder is more confident about the bit being zero than its being one. In the extreme case when this LLR is $+\infty$, the decoder is absolutely sure that the bit is zero. If the decoder decides only with absolute belief delivering only $+\infty$ and $-\infty$ LLRs, it is called a hard-output decoder. The iterative exchange of this soft information gradually reduces the error rate resulting in the improved reliability of a turbo-based communication system. Figure 1.4 shows the basic system diagram for a turbo-based equalizer.

For turbo-based receivers, polar codes need a soft-output decoder that can produce the reliability information to be exchanged. Additionally, polar codes are expected to

perform well in turbo-based receivers if codes are optimized for error-rate performance in ISI channels. Therefore, the goal of the thesis can be broadly defined as follows: to construct a turbo-based system for polar codes with error-rate performance close to state-of-the-art LDPC-based systems. We precisely describe this goal in the next section.

1.4 Thesis Goal: A Tale of Four Metrics

In the previous section, we established that the desirable properties of polar codes make them an excellent candidate for magnetic recording system, but to enable polar codes in this application, we need a soft-output decoder to decode these codes under turbo equalization framework. Furthermore, code designs matched to the characteristics of ISI channels often outperform the codes designed for the AWGN channel. Therefore, we expect better error-rate performance with the optimized code designs compared to the designs for the AWGN channel. This section further discusses these requirements.

1.4.1 Requirements from a Decoder

The requirements for a soft-output decoder stem from the fact that eventually it is realized on a hardware platform. The hardware has three important specifications, namely the power consumption, area utilization and the number of bits it can process per second, also called throughput. The following aspects of a decoder directly affect these three specifications:

1. *Computational Complexity:* Computational complexity relates to the number of computations (such as additions, multiplications and copy operations) required by a decoder. In general, higher computational complexity results in increased power consumption, higher area utilization and slower speed of operation of the device [7]. Therefore, an efficient decoder should minimize the number of operations while delivering a certain quality of service in terms of error rate.
2. *Memory Requirement:* A decoder requires not only computational hardware but also memory to store interval variables such as intermediate states. In general, a larger memory requirement translates to higher power and area utilization [7] on the hardware platform. Therefore, an efficient decoder should minimize the amount of

memory it uses as much as possible.

3. *Latency or Throughput:* Latency is usually defined in a normalized fashion as the number of clock cycles required to process one bit, and is inversely related to the throughput of the decoder [8]. A decoder with higher latency requires a higher clock than one with lower latency to achieve the same throughput. For example, consider two decoders A and B of normalized latency of 10 and 20 cycles per bit, respectively. To achieve a throughput of 1Mbps, the decoder A and B need a clock of 10 and 20 MHz, respectively. In general, the higher clock rate results in higher power consumption of hardware, and as decoder B requires a higher clock, it consumes more power than decoder A. Therefore, a decoder should minimize its latency as much as possible.

In short, power consumption, area utilization and latency are three key performance metrics for hardware implementation of any decoder. The two major contributors to power and area consumption are computational logic and memory. To elaborate this point further, Figure 1.5 shows the die micrograph of the LDPC decoder chip taken from [9]. The die shows that the majority of the area is taken up by the SISO engine corresponding to the computational unit and memory shown as Γ -SRAM and π -SRAM. The interconnect network connecting different parts of the chip shown as Ω -NETWORK, occupies most of the rest of the area.

Figure 1.6 summarizes this section and shows that a practically feasible decoder lies as close to the origin in three dimensional space of power, area and latency. This position directly corresponds to a region close to the origin in three dimensional space of computational complexity, memory required and the same latency.

1.4.2 Requirements from a Code/Encoder

Even if we have near-optimal performance by a decoder, the complete system may not deliver in terms of error rates if the underlying code itself is weak. Therefore, the requirement from the code is very straight forward – it should produce a lower error rate in a channel when decoded by a specific decoder. For example, early LDPC codes were not powerful enough to deliver better error rates on the AWGN channel, even though their decoder provided

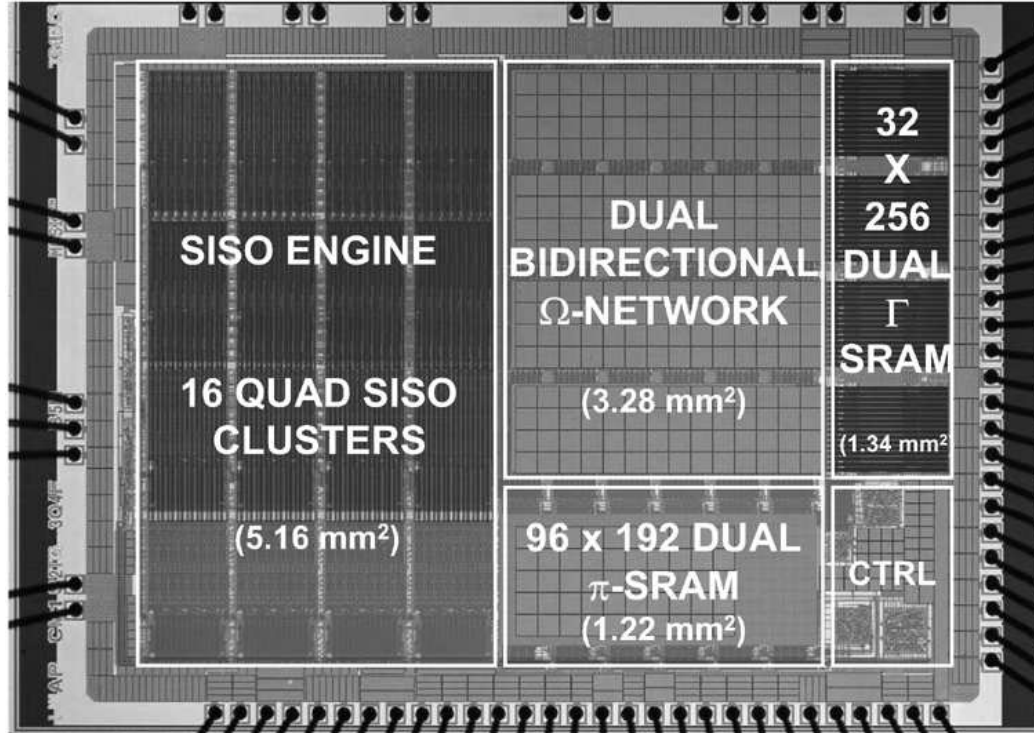


Figure 1.5: The majority of the area in the die micrograph of this LDPC decoder chip is occupied by computational and memory units shown as SISO engine and Γ -, π -SRAM, respectively. Most of the rest of the area is occupied by the wiring network connecting different parts of the chip shown as Ω -NETWORK. The image is taken from Mansour, M.M.; Shanbhag, N.R., "A 640-Mb/s 2048-bit programmable LDPC decoder chip," *Solid-State Circuits, IEEE Journal of*, vol.41, no.3, pp.684,698, March 2006 ©2006 IEEE.

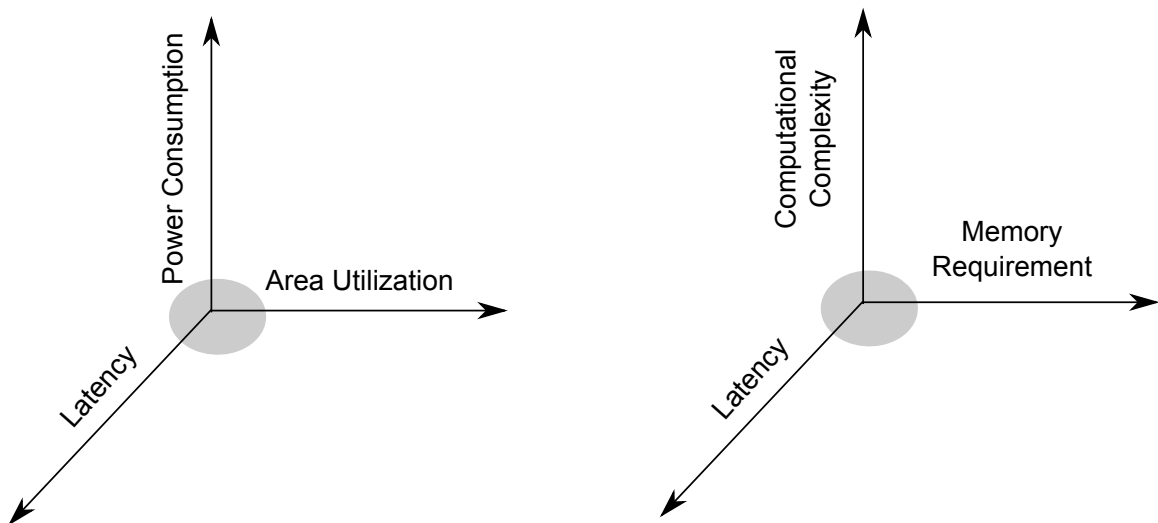


Figure 1.6: A good decoder lies in the region close to the origin in three dimensional space of power, area and latency. This region directly corresponds to a region close to the origin in three dimensional space of computational complexity, memory requirement and latency.

near-optimal performance. Later Richardson, Shokrollahi and Urbanke designed better LDPC codes that outperformed the state-of-the-art codes at that time for the AWGN channel [10]. In short, a code should be optimized for any required channel to deliver desired error rates using an optimal or near-optimal decoder.

1.4.3 Summary

Figure 1.7 summarizes all the requirements for a magnetic recording error-control system. In a four-dimensional space of these requirements, the ideal system (a code and its decoder) should lie as close to the origin in the highlighted region as possible, and this thesis primarily focuses on coming up with such a system for polar codes. In other words, this thesis produces both the optimized polar codes for ISI channels as well as a low-complexity, soft-output decoder for their decoding under the turbo framework, and delivers a powerful error-correcting system for magnetic recording application.

Figure 1.7 also describes the structure of the thesis. The thesis is structured as follows:

1. In Chapter 2, we provide a brief introduction to different concepts needed to explain rest of the thesis. We start with an introduction to block codes and then provide a tutorial on two examples block codes, namely parity-check codes and repetition codes. We then introduce polar codes with their factor graph description and show how parity-check and repetition codes combine to form polar codes. In the end, we discuss various soft-output and hard-output decoding algorithms.
2. In Chapter 3, we propose a low-complexity soft-output decoder called the *soft cancellation* (SCAN) decoder. The SCAN decoder is based on the SCAN schedule for message updates in the message passing decoder of polar codes. The SCAN schedule, in contrast with the original flooding schedule, drastically reduces the computational complexity of the message passing decoder. The reason for the substantial complexity reduction is better dissemination of information in the factor graph with the SCAN schedule compared to the flooding schedule. The SCAN schedule results in rapid convergence of message passing algorithm while providing soft outputs needed for turbo processing. Additionally, we propose a technique to reduce the memory

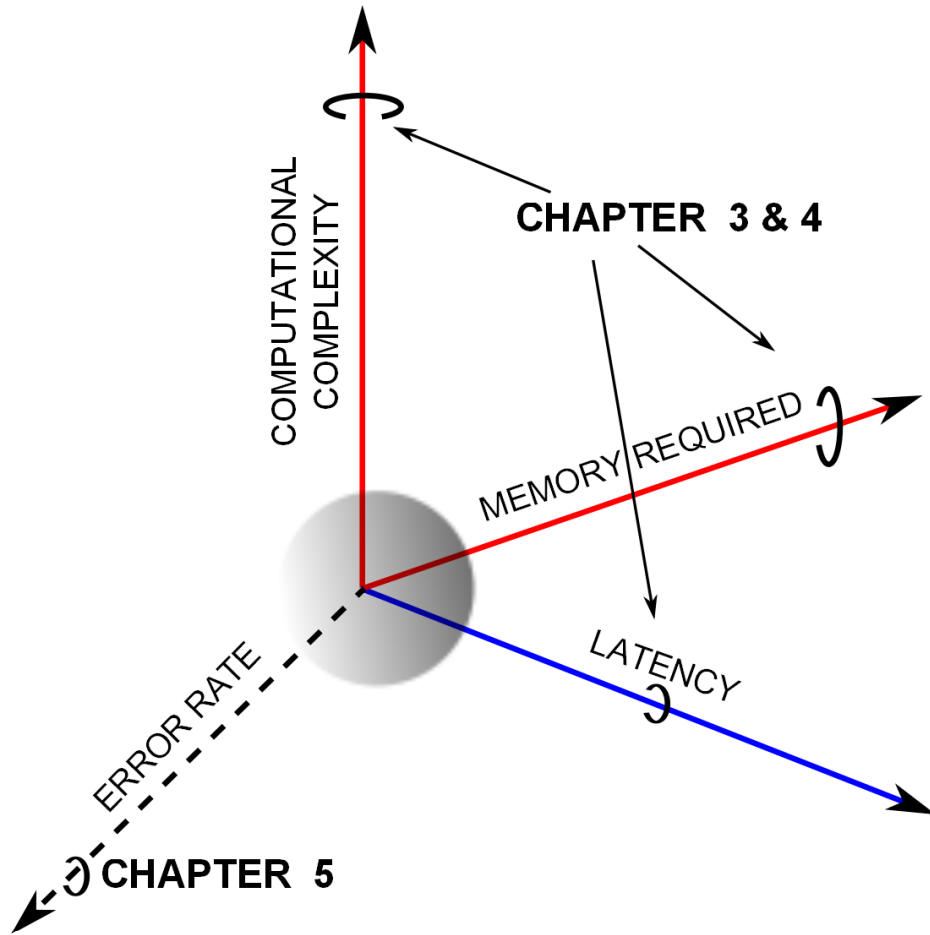


Figure 1.7: An ideal system consisting of polar codes and their soft-output decoder should lie in the highlighted region of the four-dimensional space.

requirement of the SCAN decoder based on the idea that the decoder can overwrite soft information corresponding to some of the nodes in the factor graph. We identify the nodes for which we can overwrite the soft information and reuse the memory to reduce the memory requirement of the decoder. We also provide error-rate curves for AWGN and ISI channels to show that the SCAN decoder outperforms the BP decoder for polar codes and performs close to the BP decoder of LDPC codes.

3. In Chapter 4, we have two major contributions. Firstly, we extend the simplified successive-cancellation (SSC) principle of Alamdar-Yazdi and Kschischang [11] to the SCAN decoder and reduce its latency and computational complexity. Secondly, we prove that the construction of polar codes exhibit two properties called the *special*

prohibited pair property and the *general prohibited pair property*. We apply these properties to the implementation of the SCAN decoder that reduces the memory requirement of the decoder even further. We call the resulting SCAN decoder with the improvements in latency, computational complexity and memory requirement the enhanced SCAN (eSCAN) decoder. The eSCAN has the same error-rate performance as the SCAN decoder but with reduced latency, computational complexity and memory requirement.

4. In Chapter 5, we propose a method to design polar codes for ISI channels. The method is based on the idea that the EXIT chart of an optimal code matches that of an ISI channel under iterative decoding. We show that in a multilevel description of polar codes, we can change the rates of polar codes in different levels in order to match the EXIT chart to that of an ISI channel. We demonstrate using simulations that polar codes designed using this method outperform the ones designed for the AWGN channel when decoded using the SCAN decoder, and perform close to the state-of-the-art LDPC codes with the belief propagation decoder.
5. In Chapter 6, we conclude the thesis by summarizing our contributions and outlining a few directions in which our work can be extended.

CHAPTER II

BACKGROUND

This chapter provides the necessary background required for the remainder of the thesis. We begin by an introduction to block codes along with description of two important types of these codes, namely the single parity-check and repetition codes. Next is an introduction of polar codes, their factor graph construction and how this factor graph relates to single parity-check and repetition codes. Later, we discuss the original successive cancellation (SC) decoder, and a method of constructing polar codes for this decoder. In the end, we present a brief overview of the state-of-the-art hard- and soft-output decoders for polar codes.

2.1 An Introduction to Block Codes

The basic purpose of a storage system is to reproduce a message from one time instant to another. A block code breaks the message into smaller blocks and encodes each block separately. The code is the set of all possible codewords. Figure 2.1 shows the typical diagram for block encoding. The large message is divided into chunks of K bits, and the encoder encodes each chunk separately into codewords of length N . We call the resulting set of 2^K codewords as the (N, K, R) block code, where $R = K/N$ is called the rate of the code and quantifies the fraction of information bits carried by each coded bit.

Two important block codes are single parity-check codes and repetition codes. Both of these codes are the building blocks of more powerful codes such as LDPC codes. We briefly explain single parity-check and repetition codes in the following section.

2.1.1 Single Parity-Check Codes

Single parity-check codes are $(N, N - 1, 1 - 1/N)$ codes that append a single extra bit to the message. The extra bit is called the parity bit, as its value is the binary XOR of all the message bits. Suppose we want to transmit a binary message $\mathbf{m} = [1\ 0]$ using a $(3, 2, 2/3)$

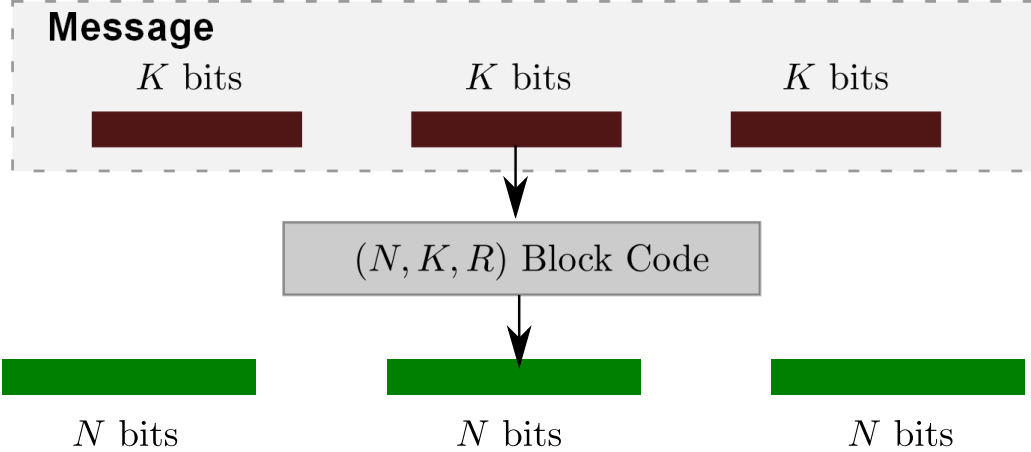


Figure 2.1: In a block code, the message is divided into blocks of K bits. Each block is then independently encoded to a block of N coded bits using an encoder.

single parity-check code. We first compute the parity-check bit $1 = 1 \oplus 0$ and append it to the message forming the codeword $\mathbf{c} = [1\ 0\ \boxed{1}]$, where the bit in the box is the parity bit.

Now, suppose we transmit codeword $\mathbf{c} = [1\ 0\ 1]$ on a binary-input discrete memoryless channel with conditional probability distribution $p(y | c)$. Let the channel observation be vector $\mathbf{y} = [y_0\ y_1\ y_2]$. The task of the decoder is to take this observation \mathbf{y} and decide what is transmitted. The decoder's decision depends on which parameter it optimizes, and one such parameter is the probability of error $\Pr(\hat{c}_i \neq c_i)$, where \hat{c}_i is the decoder's decision for the i -th coded bit. A common optimization metric is error probability, which can be lower bounded as follows:

$$\begin{aligned}
 \Pr(c_i \neq \hat{c}_i) &= 1 - \Pr(c_i = \hat{c}_i) \\
 &= 1 - \sum_{\mathbf{y}} p(c_i = \hat{c}_i, \mathbf{y}) \\
 &= 1 - \sum_{\mathbf{y}} p(c_i = \hat{c}_i | \mathbf{y}) p(\mathbf{y}) \\
 &\geq 1 - \sum_{\mathbf{y}} p(\mathbf{y}) \max_{\hat{c}_i \in \{0,1\}} p(c_i = \hat{c}_i | \mathbf{y}). \tag{2.1}
 \end{aligned}$$

(2.1) shows that the decoder that minimizes the error probability is the one that maximizes the probability $p(c_i | \mathbf{y})$ for all c_i . We call this probability the *a posteriori probability* (APP), the decoder the *maximum a posteriori* (MAP) decoder, and the decision the MAP decision.

The MAP decision \hat{c}_i is given by

$$\begin{aligned}
\hat{c}_i(\mathbf{y}) &= \arg \max_{c_i} p(c_i | \mathbf{y}) \\
&= \arg \max_{c_i} \frac{p(\mathbf{y} | c_i)p(c_i)}{p(\mathbf{y})} && \text{(Bayes' Rule)} \\
&= \arg \max_{c_i} p(\mathbf{y} | c_i)p(c_i), && (2.2)
\end{aligned}$$

where in the last step, we omitted $p(\mathbf{y})$, as it does not depend on c_i and does not take part in the optimization process.

Suppose we are interested in detecting bit c_2 . We calculate the MAP decision for c_2 by first computing the objective function in (2.2) for both the values $c_2 \in \{0, 1\}$ and then finding the value of c_i that maximizes it. We start by computing $p(\mathbf{y} | c_i = 0)\Pr(c_i = 0)$ as follows:

$$p(\mathbf{y} | c_2 = 0)\Pr(c_2 = 0) = \underbrace{p(y_0, y_1 | c_2 = 0)}_{\text{from } y_0, y_1} \underbrace{p(y_2 | c_2 = 0)}_{\text{from } y_2} \underbrace{\Pr(c_2 = 0)}_{\text{Message Source}}. \quad (2.3)$$

The right-hand side of (2.3) depends on the following:

1. $p(y_0, y_1 | c_2 = 0)$: This is likelihood of c_2 being zero given noisy observations y_0 and y_1 of c_0 and c_1 , respectively. This term carries the information that y_0 and y_1 convey about c_2 .
2. $p(y_2 | c_2 = 0)$: This is likelihood of c_2 being zero given noisy observation y_2 . This term carries the information that y_2 conveys about c_2 .
3. $\Pr(c_2 = 0)$: Assuming m_0 and m_1 are equally likely to be zero or one, c_2 is equally likely to be zero or one as well and $\Pr(c_2 = 0) = 1/2$.

Expanding $p(y_0, y_1 | c_2 = 0)$ term on the right-hand side of (2.3), we get

$$\begin{aligned}
p(y_0, y_1 | c_2 = 0) &= \sum_{c_0, c_1} p(y_0, y_1, c_0, c_1 | c_2 = 0) \\
&= \sum_{c_0, c_1} p(y_0, y_1 | c_0, c_1, c_2 = 0) p(c_0, c_1 | c_2 = 0) \\
&= p(y_0, y_1 | c_0 = 0, c_1 = 0, c_2 = 0) \Pr(c_0 = 0, c_1 = 0 | c_2 = 0) \\
&\quad + p(y_0, y_1 | c_0 = 1, c_1 = 0, c_2 = 0) \Pr(c_0 = 1, c_1 = 0 | c_2 = 0) \\
&\quad + p(y_0, y_1 | c_0 = 0, c_1 = 1, c_2 = 0) \Pr(c_0 = 0, c_1 = 1 | c_2 = 0) \\
&\quad + p(y_0, y_1 | c_0 = 1, c_1 = 1, c_2 = 0) \Pr(c_0 = 1, c_1 = 1 | c_2 = 0). \tag{2.4}
\end{aligned}$$

Since c_0 and c_1 must be identical when $c_2 = 0$, the middle two terms are zero, and (2.4) simplifies to:

$$\begin{aligned}
p(y_0, y_1 | c_2 = 0) &= p(y_0, y_1 | c_0 = 0, c_1 = 0, c_2 = 0) \Pr(c_0 = 0, c_1 = 0 | c_2 = 0) \\
&\quad + p(y_0, y_1 | c_0 = 1, c_1 = 1, c_2 = 0) \Pr(c_0 = 1, c_1 = 1 | c_2 = 0). \tag{2.5}
\end{aligned}$$

But since the message source is independently and uniformly distributed, we have

$$\Pr(c_0 = 1, c_1 = 1 | c_2 = 0) = \Pr(m_0 = 1, m_1 = 1 | c_2 = 0) = \frac{1}{2}.$$

Therefore, $p(y_0, y_1 | c_2 = 0)$ in (2.5) is simplified to

$$\begin{aligned}
p(y_0, y_1 | c_2 = 0) &= \frac{1}{2} \left(p(y_0, y_1 | c_0 = 0, c_1 = 0, c_2 = 0) + p(y_0, y_1 | c_0 = 1, c_1 = 1, c_2 = 0) \right) \\
&= \frac{1}{2} \left(p(y_0 | c_0 = 0) p(y_1 | c_1 = 0) + p(y_0 | c_0 = 1) p(y_1 | c_1 = 1) \right).
\end{aligned}$$

Using this value of $p(y_0, y_1 | c_2 = 0)$ in (2.3), we get

$$p(\mathbf{y} | c_2 = 0) \Pr(c_2 = 0) = \frac{1}{4} \left(p(y_0 | c_0 = 0) p(y_1 | c_1 = 0) + p(y_0 | c_0 = 1) p(y_1 | c_1 = 1) \right) p(y_2 | c_2 = 0),$$

where once again we have used the fact that the source is uniformly distributed, and $\Pr(c_2 = 0) = 1/2$. By following the same procedure we used for $p(\mathbf{y} | c_2 = 0) \Pr(c_2 = 0)$, we compute

$$p(\mathbf{y} | c_2 = 1) \Pr(c_2 = 1) = \frac{1}{4} \left(p(y_0 | c_0 = 0) p(y_1 | c_1 = 1) + p(y_0 | c_0 = 1) p(y_1 | c_1 = 0) \right) p(y_2 | c_2 = 1).$$

The last step of the decoder is to use these two probabilities to make a decision about i -th bit, according to

$$p(c_i = 0 | \mathbf{y}) \underset{1}{\overset{0}{\gtrless}} p(c_i = 1 | \mathbf{y})$$

or

$$p(\mathbf{y} | c_i = 0)\Pr(c_i = 0) \underset{1}{\overset{0}{\gtrless}} p(\mathbf{y} | c_i = 1)\Pr(c_i = 1).$$

In simple words, it means that decide the bit is zero if

$$p(\mathbf{y} | c_i = 0)\Pr(c_i = 0) > p(\mathbf{y} | c_i = 1)\Pr(c_i = 1)$$

and one otherwise. We can further simplify it by converting it into a ratio and taking natural logarithm of both sides as follows:

$$\begin{aligned} \frac{p(\mathbf{y} | c_i = 0)\Pr(c_i = 0)}{p(\mathbf{y} | c_i = 1)\Pr(c_i = 1)} &\underset{1}{\overset{0}{\gtrless}} 1 \\ \log \left(\frac{p(\mathbf{y} | c_i = 0)\Pr(c_i = 0)}{p(\mathbf{y} | c_i = 1)\Pr(c_i = 1)} \right) &\underset{1}{\overset{0}{\gtrless}} 0. \end{aligned} \quad (2.6)$$

The left-hand side of (2.6) can further be simplified as

$$\begin{aligned} \log \left(\frac{p(\mathbf{y} | c_i = 0)\Pr(c_i = 0)}{p(\mathbf{y} | c_i = 1)\Pr(c_i = 1)} \right) &= \log \left(\frac{p(y_0 | c_0 = 0)p(y_1 | c_1 = 0) + p(y_0 | c_0 = 1)p(y_1 | c_1 = 1)}{p(y_0 | c_0 = 0)p(y_1 | c_1 = 1) + p(y_0 | c_0 = 1)p(y_1 | c_1 = 0)} \right. \\ &\quad \left. \times \frac{p(y_2 | c_2 = 0)}{p(y_2 | c_2 = 1)} \right) \\ &= \log \left(\frac{\frac{p(y_0 | c_0 = 0)p(y_1 | c_1 = 0)}{p(y_0 | c_0 = 1)p(y_1 | c_1 = 1)} + 1}{\frac{p(y_0 | c_0 = 0)}{p(y_0 | c_0 = 1)} + \frac{p(y_1 | c_1 = 0)}{p(y_1 | c_1 = 1)}} \times \frac{p(y_2 | c_2 = 0)}{p(y_2 | c_2 = 1)} \right) \\ &= \log \left(\frac{(\ell_0 \ell_1 + 1)\ell_2}{\ell_0 + \ell_1} \right), \end{aligned} \quad (2.7)$$

where

$$\ell_j = \frac{p(y_j | c_j = 0)}{p(y_j | c_j = 1)}.$$

We can use trigonometric identities to reduce (2.7) to

$$\begin{aligned} \log \left(\frac{p(c_2 = 0 | \mathbf{y})}{p(c_2 = 1 | \mathbf{y})} \right) &= \underbrace{2 \tanh^{-1} \left(\tanh \left(\frac{L_0^{(i)}}{2} \right) \tanh \left(\frac{L_1^{(i)}}{2} \right) \right)}_{\text{Extrinsic LLR}} + \underbrace{L_2^{(i)}}_{\text{Intrinsic LLR}} \\ &= L_2^{(e)} + L_2^{(i)} \end{aligned}$$

where

$$L_j^{(i)} = \log \left(\frac{p(y_j | c_j = 0)}{p(y_j | c_j = 1)} \right).$$

Extrinsic LLRs provide the reliability information generated from code constraints, whereas intrinsic LLRs provide the reliability information directly gleaned from channel observations. To make a decision about bit c_2 , the decoder adds these two LLRs to compute the so-called *full* LLR and declares the bit zero if the sum is positive and one otherwise, as described by the rule (2.6).

We can follow a similar analysis for two other bits c_0 and c_1 to get the expression for their full LLRs. In general, for a $(N, N-1, 1-1/N)$ code the extrinsic LLR and full LLR of k th bit are given by

$$L_k^{(e)} = 2 \tanh^{-1} \left(\prod_{j \neq k} \tanh \left(\frac{L_j^{(i)}}{2} \right) \right),$$

and

$$L_k^{(full)} = L_k^{(e)} + L_k^{(i)},$$

respectively.

Figure 2.2 shows that the whole decision process as *message passing* along the edges on a graph. The rectangle represents a parity-check node, whereas the circles represent variable nodes. The parity-check node represents the constraint that all its inputs should sum to zero. The figure shows that to compute the extrinsic LLR for the parity bit, we send intrinsic LLRs observed from the channel on the edges corresponding to variable nodes c_0 to c_{N-2} . The parity-check node takes all these *messages* from different variable nodes and computes the outbound message $L_{N-1}^{(e)}$. The same process can be repeated for all other bits to compute their extrinsic LLRs and eventually their full LLRs for detection.

2.1.2 Repetition Codes

An $(N, 1, 1/N)$ repetition code repeats every message bit N times so that each message bit m_0 gets mapped to the codeword $\mathbf{c} = [m_0, m_1, \dots, m_{N-1}]$.

Suppose we want to transmit a zero bit using a $(N, 1, 1/N)$ repetition code. This code takes the message bit and transmits it N times producing the following equality constraint

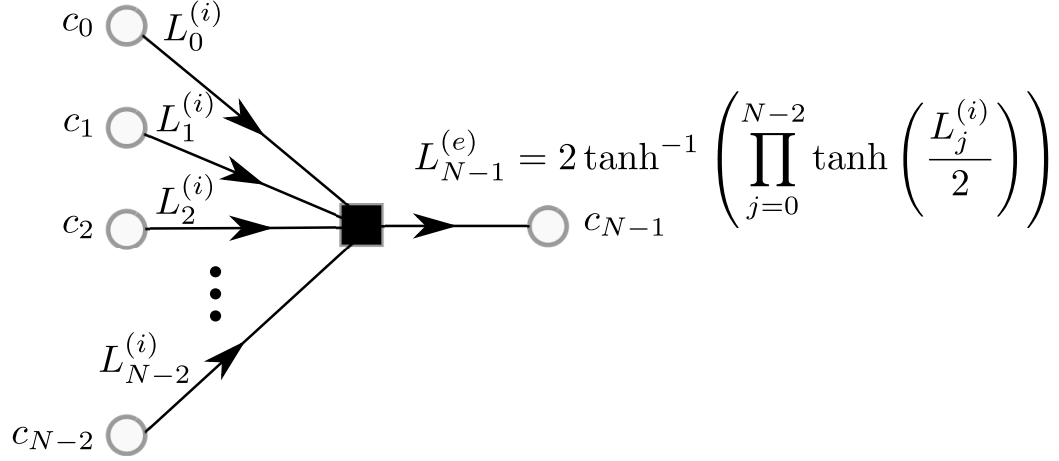


Figure 2.2: The parity-check node takes all the input *messages* in the form of intrinsic LLRs and produces the outbound *message* $L_{N-1}^{(e)}$.

between all these transmitted bits:

$$c_0 = c_1 = \dots = c_{N-1}.$$

Following a similar analysis as in Section 2.1.1, the MAP decision for k th coded bit is given by

$$\begin{aligned} \log \left(\frac{p(c_k = 0 | \mathbf{y})}{p(c_k = 1 | \mathbf{y})} \right) &= \underbrace{\sum_{j \neq k} L_j^{(i)}}_{\text{Extrinsic LLR}} + \underbrace{L_k^{(i)}}_{\text{Intrinsic LLR}} \\ &= L_k^{(e)} + L_k^{(i)}. \end{aligned} \quad (2.8)$$

Figure 2.3 shows that the decoding process for a repetition code can also be viewed as message passing on a graph like parity-check codes. The circle represents the variable node that puts the constraint that the bits corresponding to all the edges connected to it should be equal to each other. The left-hand image shows the trivial parity-check constraints of two edges. This two-edge parity-check is equivalent to an equality-check constraint meaning that the bits corresponding to the edges connected to it should be equal. The right-hand image is a rearranged form of the left-hand image and resembles the parity-check code graph.

In Figure 2.3, we detect bit c_0 as all transmitted bits are equal, and detecting this bit is enough to decode the message. To detect c_0 , we send all the intrinsic LLRs for

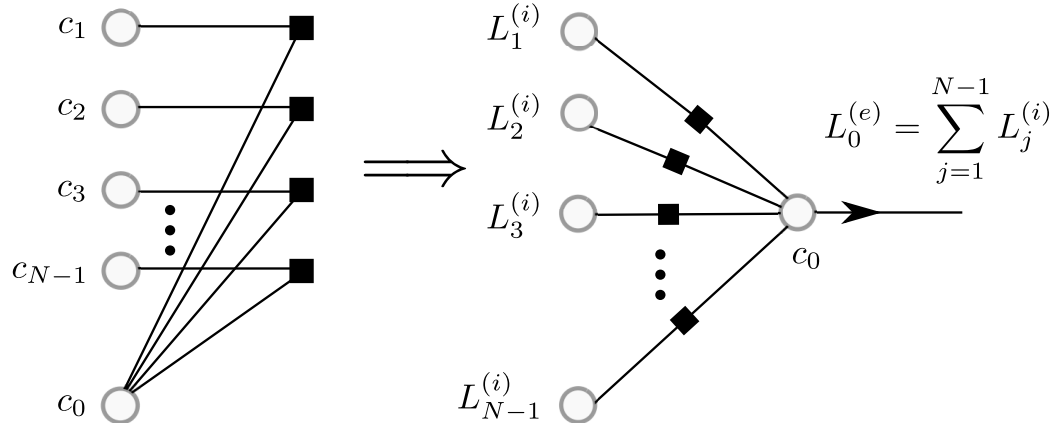


Figure 2.3: A $(N, 1, 1/N)$ repetition code repeats the message bit N times giving rise to $N - 1$ trivial parity-check nodes with two edges as shown on the left. The right-hand side image is the rearranged version of the left-hand side image with the equality-check node corresponding to c_0 summing all incoming LLRs to produce an outgoing extrinsic LLR for c_0 .

c_1, c_2, \dots, c_{N-1} to the variable node of c_0 . The variable node sums all the incoming messages and produce the extrinsic LLR $L_0^{(e)}$ that we add to intrinsic LLR $L_0^{(i)}$ calculating the full LLR. The sign of this full LLR decides about the message bit. It is easy to see that the full LLR for all the bits is equal to $\sum_{j=0}^{N-1} L_j^{(i)}$, highlighting once again that no matter which bit we decode, the resulting decision for the message bit stays the same. However, note that extrinsic LLRs corresponding to different bits will generally be different.

2.2 An Introduction to Polar Codes

In the previous section, we discussed block codes and their two important examples. This section builds on this discussion and introduces polar codes that are complex combination of the basic parity-check and repetition codes.

2.2.1 Generator Matrix and Encoding

Like all other linear binary block codes, polar codes encode a block of K bits to a block of N bits using a generator matrix \mathbf{G} . The difference is in the construction of this generator matrix.

Consider a (N, K, R) polar code of length N , dimension K and rate $R = K/N$. The generator matrix \mathbf{G} for this polar code can be constructed in four steps:

1. Construct \mathbf{F}_N using $\mathbf{F}_N = \mathbf{F}_2^{\otimes n}$, where $n = \log_2(N)$, $(\cdot)^{\otimes}$ denotes the n th Kronecker power and

$$\mathbf{F}_2 := \begin{bmatrix} 1 & 0 \\ 1 & 1 \end{bmatrix}.$$

2. Construct \mathbf{G}_N using $\mathbf{G}_N = \mathbf{B}\mathbf{F}_N$, where \mathbf{B} is called the bit-reversal matrix. \mathbf{B} is a permutation matrix ensuring that

$$\mathbf{x} = \mathbf{y}\mathbf{B} \implies x_{b_{n-1}, b_{n-2}, \dots, b_0} = y_{b_0, b_1, \dots, b_{n-1}},$$

where $b_1, \dots, b_n \in \{0, 1\}$ represent the binary expansion of the index of an element in row vectors \mathbf{x} and \mathbf{y} [4]. For example, $x_1 = x_{0,0,1}$ for $n = 3$. The significance of this permutation operation will be explained in Section 2.2.2.

3. Remove $N - K$ rows with indices from the set $\mathcal{S}^c \subset \{0, 1, \dots, N - 1\}$ from \mathbf{G}_N to obtain a $K \times N$ matrix \mathbf{G} . The codeword \mathbf{v} is given by

$$\mathbf{v} = \mathbf{m}\mathbf{G}.$$

4. An alternative to the last step is to take the message vector $\mathbf{m} = [m_0 \ m_1, \dots, m_{(K-1)}]$ of length K and form another vector $\mathbf{u} = [u_0 \ u_1, \dots, u_{(N-1)}]$ such that \mathbf{m} appears in \mathbf{u} on the index set $\mathcal{S} \subseteq \{0, 1, 2, \dots, N - 1\}$ and zero bit appears on \mathcal{S}^c . In this case, $\mathbf{v} = \mathbf{u}\mathbf{G}_N$.

In literature, the set \mathcal{S} is usually referred to as the set of 'free indices' and the complement \mathcal{S}^c as the set of 'frozen indices'. The construction of polar codes is equivalent to constructing \mathcal{S} and is discussed in Section 2.3.

Example 2.1. Suppose we want to generate a $(8, 4, 0.5)$ polar code with frozen indices

$\mathcal{I}^c = \{0, 1, 2, 4\}$. Taking 3rd Kronecker product (because $\log_2 N = 3$) of \mathbf{F}_2 , we get

$$\mathbf{F}_8 = \begin{bmatrix} 1 & 0 & 0 & 0 & 0 & 0 & 0 & 0 \\ 1 & 1 & 0 & 0 & 0 & 0 & 0 & 0 \\ 1 & 0 & 1 & 0 & 0 & 0 & 0 & 0 \\ 1 & 1 & 1 & 1 & 0 & 0 & 0 & 0 \\ 1 & 0 & 0 & 0 & 1 & 0 & 0 & 0 \\ 1 & 1 & 0 & 0 & 1 & 1 & 0 & 0 \\ 1 & 0 & 1 & 0 & 1 & 0 & 1 & 0 \\ 1 & 1 & 1 & 1 & 1 & 1 & 1 & 1 \end{bmatrix} \quad \text{with} \quad \mathbf{B}_8 = \begin{bmatrix} 1 & 0 & 0 & 0 & 0 & 0 & 0 & 0 \\ 0 & 0 & 0 & 0 & 1 & 0 & 0 & 0 \\ 0 & 0 & 1 & 0 & 0 & 0 & 0 & 0 \\ 0 & 0 & 0 & 0 & 0 & 0 & 1 & 0 \\ 0 & 1 & 0 & 0 & 0 & 0 & 0 & 0 \\ 0 & 0 & 0 & 0 & 0 & 1 & 0 & 0 \\ 0 & 0 & 0 & 1 & 0 & 0 & 0 & 0 \\ 0 & 0 & 0 & 0 & 0 & 0 & 0 & 1 \end{bmatrix}. \quad (2.9)$$

Therefore, G_8 matrix is given by

$$\mathbf{G}_8 = \begin{bmatrix} 1 & 0 & 0 & 0 & 0 & 0 & 0 & 0 \\ 1 & 0 & 0 & 0 & 1 & 0 & 0 & 0 \\ 1 & 0 & 1 & 0 & 0 & 0 & 0 & 0 \\ 1 & 0 & 1 & 0 & 1 & 0 & 1 & 0 \\ 1 & 1 & 0 & 0 & 0 & 0 & 0 & 0 \\ 1 & 1 & 0 & 0 & 1 & 1 & 0 & 0 \\ 1 & 1 & 1 & 1 & 0 & 0 & 0 & 0 \\ 1 & 1 & 1 & 1 & 1 & 1 & 1 & 1 \end{bmatrix}.$$

Removing four rows corresponding to the set of frozen indices gives us a 4×8 generator matrix

$$\mathbf{G} = \begin{bmatrix} 1 & 0 & 1 & 0 & 1 & 0 & 1 & 0 \\ 1 & 1 & 0 & 0 & 1 & 1 & 0 & 0 \\ 1 & 1 & 1 & 1 & 0 & 0 & 0 & 0 \\ 1 & 1 & 1 & 1 & 1 & 1 & 1 & 1 \end{bmatrix}.$$

The encoder for Example 2.1 is shown in Figure 2.4. Note that the encoder corresponds to G_8 and not F_8 . Since, B_8 is only a permutation matrix, the same encoder diagram can be used to represent F_8 by permuting the positions of \mathbf{u} .

Reed-Muller codes are similar to polar codes in the sense that we can construct both the codes using the same \mathbf{F}_N or \mathbf{G}_N matrix. The difference is in the choice of rows to be

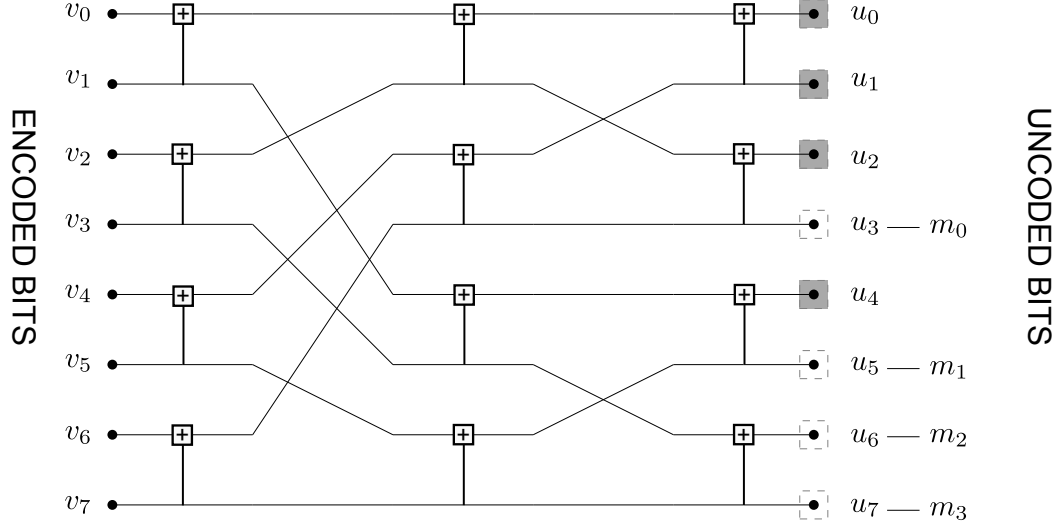


Figure 2.4: The encoder represents the relationship between encoded and uncoded bits of a rate one-half polar code with $\mathcal{S} = \{3, 5, 6, 7\}$. The rectangles with '+' sign represents binary XOR operation.

removed. We can construct a (r, m) Reed-Muller code by keeping all the rows in \mathbf{F}_N with Hamming weight greater than or equal to 2^{m-r} [12]. In other words, in Reed-Muller codes the rows with low Hamming weights are removed. In polar codes, a channel-specific rule determines the rows to be removed and will be discussed in Section 2.3.

The polar code in Example 2.1 with generator matrix \mathbf{G} is also a $(1, 3)$ Reed-Muller code [12]. Note that \mathbf{G} is obtained by removing all the rows with Hamming weight less than $2^{3-1} = 4$ in G_8 . Example 2.1 is a special case in which the choice of the rows to be removed happens to be the same for Reed-Muller and polar codes, and in general, both codes will be different.

2.2.2 The Factor Graph Representation of Polar Codes

Factor graphs are a graphical way of representing relationship between two set of variables [13]. This graphical representation is specially beneficial when the relationship to be represented can be factored into relationships between subsets of these variables. The factor graph for polar codes can be understood with the help of parity-check and repetition codes discussed in Section 2.1.

Figure 2.5 shows the basic structure in the encoder of polar codes that is also the

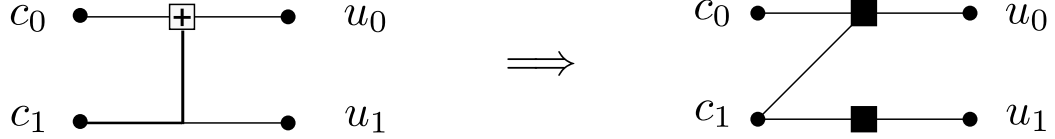


Figure 2.5: The basic structure in the encoder of polar code represents polar codes of length two. This basic encoder correspond to a parity-check and an equality-check constraint.

encoder of a length-two polar code. Two bits u_0 and u_1 add to produce the first codeword bit c_0 , whereas the second codeword bit c_1 is simply u_1 . As discussed in Section 2.1.1, we can decode u_0 using the parity-check node, whereas a variable node can represent the equality constraint of c_1 and u_1 as discussed in Section 2.1.2. Therefore, we can convert the constraints between message bits and codeword bits using a parity-check and variable node, as shown in Figure 2.5.

Note that the bottom parity-check node is essentially an equality check node and can be removed as well. The reason for this additional parity-check node is to make the decoder's graph a bipartite one. A bipartite graph consists of two disjoint set of vertices with the restriction that the every edge of this graph connects a vertex from one set to the other. In our example, variable nodes and parity-check nodes constitute two disjoint sets, and the additional bottom parity-check ensures that every edge of this graph connects a variable node to a check node instead of connecting two variable or two parity-check nodes.

We can repeat the process of converting the basic encoding structure of length two to two parity-check codes on the entire encoder to build constraints between message bits and codeword bits of polar code of arbitrary length. This collection of constraints give rise to a factor graph, as shown in Figure 2.6.

The factor graph representation of polar codes consists of $N(n+1)$ unique nodes, divided into $n+1$ columns indexed by $\lambda \in \{0, \dots, n\}$. Each column consists of 2^λ groups indexed by $\phi \in \{0, \dots, 2^\lambda - 1\}$, and each group consists of $2^{n-\lambda}$ nodes, represented by $\omega \in \{0, \dots, 2^{n-\lambda} - 1\}$. Each of these groups, denoted by $\Phi_\lambda(\phi)$, are defined as the set of nodes at a depth λ in the group ϕ . The factor graph of polar codes contains a total of $2N - 1$ such groups.

The factor graph of a rate-0.5 polar code of length $N = 8$ is shown in Figure 2.6. The dashed rectangles group the nodes in a $\Phi_\lambda(\phi)$ at any depth λ along with corresponding

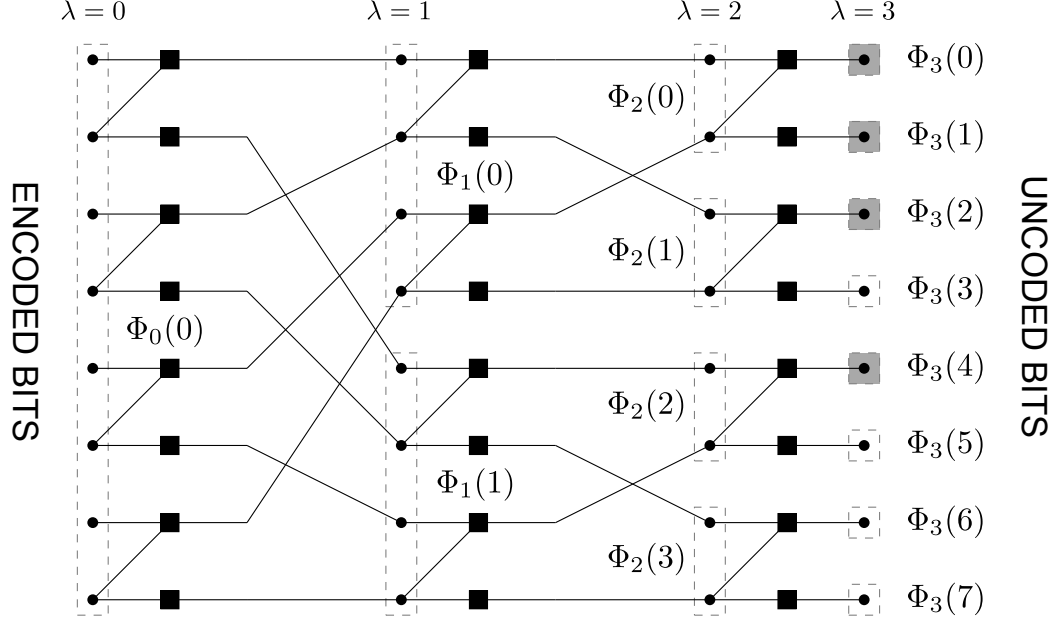


Figure 2.6: The factor graph represents the relationship between encoded and uncoded bits of a rate one-half polar code with $\mathcal{S} = \{3, 5, 6, 7\}$.

notation.

The trio (λ, ϕ, ω) can pinpoint any node in the factor graph of polar codes. Figure 2.7 shows indexing of different nodes in the column with $\lambda = 1$ of the factor graph in Figure 2.6. All the nodes in the same column have the same $\lambda = 1$ value. The column at $\lambda = 1$ has an upper node group and a lower node group indexed by $\phi = 0$ and $\phi = 1$, respectively. All the nodes in a group share the same value of second index variable ϕ . Each node group contains four nodes, and the value of ω points to a node within a group. For example, the second node in the upper and lower group of nodes in Figure 2.7 share the same value of $\omega = 1$ and are indexed by $(1, 0, 1)$ and $(1, 1, 1)$, respectively.

2.2.3 Hard-Output Successive Cancellation Decoder

In his seminal paper [4], Arikan proposed a successive cancellation (SC) decoder for polar codes. Polar codes with the SC decoder approach capacity of the DMC in the asymptotic region of large N .

Let $L_\lambda(\phi, \omega)$ denote the LLR corresponding to the node indexed by the trio (λ, ϕ, ω) . Recall from Section 2.2.2 that the trio (λ, ϕ, ω) can index any node in the factor graph of

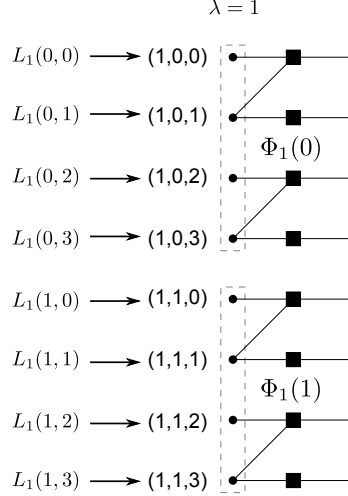


Figure 2.7: The trio (λ, ϕ, ω) can index all the nodes in the factor graph of polar codes.

polar codes.

Figure 2.7 explains $L_\lambda(\phi, \omega)$ notation for LLRs corresponding to the nodes in the factor graph of polar codes. Figure 2.7 shows only the nodes for the column with $\lambda = 1$ of the factor graph in Figure 2.6. Since all the LLRs belong to the same column, their notation has the same form $L_1(\cdot, \cdot)$. As explained in Section 2.2.2, ϕ corresponds to the node group and ω corresponds to the node within the node group $\Phi_\lambda(\phi)$. All the LLRs of the upper node group $\Phi_1(0)$ have the same form $L_1(0, \cdot)$, as all of them have the same $\phi = 0$ value. Similarly, all the LLRs of the lower node group $\Phi_1(1)$ have the same form $L_1(1, \cdot)$. Within a node group, the LLR of an individual node is denoted using ω . For example in Figure 2.7, $L_1(1, 2)$ denotes the LLR of the third node from the top in the lower group of nodes $\Phi_1(1)$.

Let $B_\lambda(\phi, \omega)$ denote the bit decision corresponding to the node indexed by the trio (λ, ϕ, ω) .

Let us denote the memory used to store LLRs and bit decisions corresponding to all the nodes in the factor graph as L and B , respectively.

The SC decoder detects the message bits using Algorithms 2.1, 2.2 and 2.3. Algorithm 2.1 wraps up the SC decoder initializing $\{L_0(0, i)\}_{i=0}^{(N-1)}$ with LLRs received from the channel and iterates through all the message bits \mathbf{u} in the outer loop. If the message bit corresponds to the frozen bit, the algorithm sets message decision $B_n(i, 0)$ to zero. Otherwise, Algorithm 2.1 calls Algorithm 2.2 to compute LLR $L_n(i, 0)$ of u_i and decides about $B_n(i, 0)$ based

Algorithm 2.1: The SC decoder

Data: LLRs from channel
Result: Message Estimates in $\{B_n(i, 0)\}_{i=0}^{(N-1)}$
1 $\{L_0(0, i)\}_{i=0}^{(N-1)} \leftarrow$ LLRs from channel
2 **for** $i = 0 \rightarrow (N - 1)$ **do**
3 **if** $i \in \mathcal{S}^c$ **then**
4 $B_n(i, 0) \leftarrow 0$
5 **end**
6 **else**
7 $\text{updatellrmap}(n, i)$
8 $B_n(i, 0) \leftarrow \begin{cases} 0 & \text{if } L_n(i, 0) > 0, \\ 1 & \text{otherwise.} \end{cases}$ (2.11)
9 **end**
10 **if** i *is odd* **then** $\text{updatebitmap}(n, i)$
11 **end**

on $L_n(i, 0)$. Algorithm 2.2 calculates LLR $L_n(i, 0)$ for u_i using the estimates for already detected bits. For all message bits, Algorithm 2.1 calls Algorithm 2.3 if the message bit being detected has an odd index, e.g., u_3, u_5 etc. Algorithm 2.3 keeps on updating the decisions for all nodes in the factor graph recursively as the decoder detects the message bits.

In these algorithms, \boxplus is defined as

$$a \boxplus b \triangleq 2 \tanh^{-1} \left[\tanh \left(\frac{a}{2} \right) \times \tanh \left(\frac{b}{2} \right) \right]. \quad (2.10)$$

2.3 The Construction of Polar Codes

The basic principle of the construction of polar codes is to find a set \mathcal{S} such that the block error probability of the polar code is minimum when decoded using the SC decoder. Arikan provided an upper bound on the block error probability of polar codes under the SC decoder [4] as follows:

$$P_e \leq \sum_{i \in \mathcal{S}} P_e(i), \quad (2.17)$$

where $P_e(i)$ is the error probability in detecting u_i given the perfect knowledge of all the previous bits u_0 to u_{i-1} and no information about u_{i+1} to u_{N-1} – the bits yet to be detected.

Algorithm 2.2: updatellrmap(λ, ϕ)

```
1 if  $\lambda = 0$  then return
2  $\psi \leftarrow \lfloor \frac{\phi}{2} \rfloor$ 
3 if  $\phi$  is even then updatellrmap( $\lambda - 1, \psi$ )
4 for  $\omega = 0 \rightarrow (2^{n-\lambda} - 1)$  do
5   if  $\phi$  is even then
6      $L_\lambda(\phi, \omega) \leftarrow L_{\lambda-1}(\psi, 2\omega) \boxplus L_{\lambda-1}(\psi, 2\omega + 1)$  (2.12)
7   end
8   else
9     if  $B_\lambda(\phi - 1, \omega)$  is 0 then
10       $L_\lambda(\phi, \omega) \leftarrow L_{\lambda-1}(\psi, 2\omega + 1) + L_{\lambda-1}(\psi, 2\omega)$  (2.13)
11      end
12      else
13         $L_\lambda(\phi, \omega) \leftarrow L_{\lambda-1}(\psi, 2\omega + 1) - L_{\lambda-1}(\psi, 2\omega)$  (2.14)
14      end
15    end
16 end
```

Algorithm 2.3: updatebitmap(λ, ϕ)

```
1 if  $\phi$  is odd then
2   for  $\omega = 0 \rightarrow (2^{n-\lambda} - 1)$  do
3      $B_{\lambda-1}(\psi, 2\omega) \leftarrow B_\lambda(\phi - 1, \omega) \oplus B_\lambda(\phi, \omega)$  (2.15)
4      $B_{\lambda-1}(\psi, 2\omega + 1) \leftarrow B_\lambda(\phi, \omega)$  (2.16)
5   end
6   if  $\psi$  is odd then updatebitmap( $\lambda - 1, \psi$ )
7 end
```

Therefore, the task of constructing \mathcal{S} boils down to efficiently estimating $P_e(i)$ and finding a set \mathcal{S} that minimizes the right-hand side of (2.17). The estimation of $P_e(i)$ is specific to the underlying channel, and therefore, we discuss the construction method for two famous

channels; namely, the binary erasure channel (BEC) and the added white Gaussian noise (AWGN) channel.

2.3.1 Construction for the BEC

Suppose we want to construct a polar code for a BEC with erasure probability ϵ . Arikan showed in [4] that we can calculate $P_e(i) = \epsilon_n(i)$ using the following recursions:

$$\begin{aligned}\epsilon_k(2j) &= 2\epsilon_{k-1}(j) - \epsilon_{k-1}^2(j), \\ \epsilon_k(2j+1) &= \epsilon_{k-1}^2(j),\end{aligned}$$

where $\epsilon_\lambda(\phi)$ represents the erasure probability for the bits corresponding to $\Phi_\lambda(\phi)$ and $\epsilon_0(0) = \epsilon$. The last step of the code construction is to choose a set \mathcal{J} such that $\sum_{i \in \mathcal{J}} P_e(i)$ is minimum.

2.3.2 Construction for the AWGN Channel

For more general channels (including the AWGN channel), [4], [1], [14], and [15] constitute a list for the methods to estimate $P_e(i)$. In this thesis, we choose the method reported in [1] because of its accuracy and implementation ease.

The method of [1] is an extension of the full-blown density evolution-based construction [14] and assumes Gaussian distribution for the LLRs exchanged. In this method, we suppose that the transmitter sends all-zeros codeword. In the case of all-zeros codeword transmission, it is easy to show that the log-likelihoods (LLRs) $2r_i/\sigma^2$ are distributed according to a Gaussian distribution with mean $2/\sigma^2$ and variance $4/\sigma^2$, i.e., $2r_i/\sigma^2 \sim \mathcal{N}(2/\sigma^2, 4/\sigma^2)$. Since the decoder uses the same equations to compute all the LLRs in a $\Phi_\lambda(\phi)$, all these LLRs follow the same distribution $\mathcal{N}(m_\lambda(\phi), 2m_\lambda(\phi))$, where $m_\lambda(\phi)$ is the mean of this distribution. In this notation, the LLRs corresponding to message bits u_i have mean $m_n(i)$, and the probability of error $P_e(i)$ (the probability that the LLR is negative) is given by:

$$P_e(i) = Q\left(\sqrt{\frac{m_n(i)}{2}}\right). \quad (2.18)$$

Trifonov and Semenov showed in [1] that $m_n(i)$ in (2.18) can be approximated using the

initial value of $m_0(0) = 2/\sigma^2$ in the following recursions:

$$\begin{aligned} m_k(2j) &= g(m_{k-1}(j)), \\ m_k(2j+1) &= 2m_{k-1}(j), \end{aligned} \tag{2.19}$$

where

$$\begin{aligned} g(x) &= h^{-1} \left(1 - (1 - h(x))^2 \right), \\ h(x) &= \begin{cases} e^{-0.4527x^{0.86} + 0.0218} & x > 10, \\ \sqrt{\frac{\pi}{x}} e^{-\frac{x}{4}} \left[1 - \frac{10}{7x} \right] & \text{otherwise.} \end{cases} \end{aligned} \tag{2.20}$$

Once we have $P_e(i)$ for all $i \in \{0, 1, \dots, N-1\}$, we can choose a set \mathcal{J} that minimizes $\sum_{i \in \mathcal{J}} P_e(i)$ in (2.17).

2.4 System Model

The binary codeword \mathbf{v} is interleaved and mapped to $\mathbf{x} \in \{1, -1\}^N$. \mathbf{x} is passed through an ISI channel with impulse response $\mathbf{h} = [h_0 h_1, \dots, h_{\mu-1}]$ followed by the AWGN channel with noise variance $\sigma^2 = N_0/2$, so that k th element of observation \mathbf{r} at the output of the channel is

$$r_k = \sum_{i=0}^{\mu-1} h_i x_{k-i} + n_k, \tag{2.21}$$

where $n_k \sim \mathcal{N}(0, \sigma^2)$ is a Gaussian random variable with mean zero and variance σ^2 . The per-bit signal-to-noise ratio is thus $E_b/N_0 = \sum_i h_i^2 / (2R\sigma^2)$, where $R = K/N$.

The receiver uses a standard turbo equalization architecture. It equalizes the channel using the Bahl, Cocke, Jelinek and Raviv (BCJR) algorithm [16], computes extrinsic log-likelihoods (LLRs) \mathbf{e}_b using BCJR, deinterleaves \mathbf{e}_b to \mathbf{a}_b and passes the result to the polar decoder that estimates the message vector $\hat{\mathbf{m}}$ as well as the extrinsic LLRs \mathbf{e}_d . Extrinsic LLRs \mathbf{e}_d are interleaved again and are passed to the BCJR equalizer which uses these LLRs as prior information to once again compute \mathbf{e}_b . This information/LLR exchange continues for T number of iterations and at the end of the last iteration, the message vector $\hat{\mathbf{m}}$ is estimated.

2.5 Advanced Decoders for Polar Codes

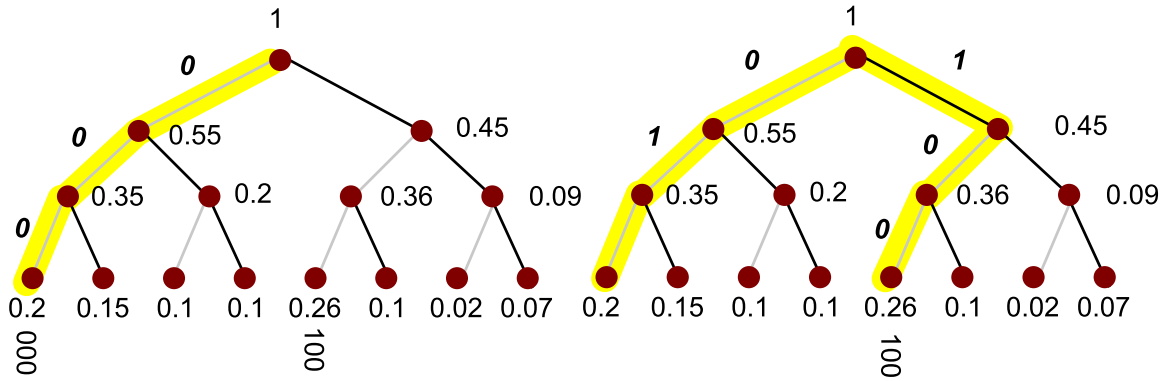
Arikan showed that polar codes achieve capacity with the SC decoder in the asymptotic region of very large block length [4]. For finite block lengths, the SC decoder is not an optimal decoder for polar codes, and since [4], many advanced decoders have been proposed, most of which are hard-output decoders. In this section, we review three most important of the advanced decoders for polar codes that outperformed the SC decoder.

2.5.1 Hard-Output Successive Cancellation List Decoder

The SC decoder is a greedy algorithm that estimates bit u_i in ascending order, and once the decoder decides about a bit, it does not go back to correct the bit in case of an incorrect decision. The SC decoder uses the bit's decision for the decision of all subsequent bits, and as a result, the effect of an incorrect decision propagates to all the subsequent decisions.

Tal and Vardy proposed a successive cancellation list (SCL) decoder that alleviates the error propagation problem of the SC decoder by keeping both the options of u_i being zero and u_i being one. The two options for every bit being detected results in a list of possible sequences of the size exponential in the number of bits detected instead of only one sequence as in the case of the SC decoder. Since, this exponential increase in the number of sequences require a large amount of memory, the decoder uses a *pruning* technique. In the pruning technique, when the number of possible sequences in the list increases beyond a preset size L , the least probable sequences are dropped from the list, and in the end, the SCL decoder chooses the sequence with the largest likelihood as the estimated sequence.

The difference between the SC decoder and the SCL decoder is explained in Figure 2.8. Both of these decoders can be described with the help of a tree diagram. In this tree diagram, each node represents a sequence of decisions, and the number next to each node represents its probability. The root node represents an empty sequence with probability one, as it points to the start of the decoding process. As the decoding proceeds, the tree starts building up from root node to leaf nodes. The first bit to decide is u_0 . A branch to the left represents a $u_0 = 0$ decision, while a branch to the right represents a $u_0 = 1$ decision. The task of any sequential decoder, starting from the detection of u_0 to that of



(a) The SC decoder keeps only one path while detecting any message bit. (b) The SCL decoder keeps L paths while detecting any message bit. The example shows the operation of the SCL decoder for list size $L = 2$.

Figure 2.8: The difference between the SC and the SCL decoder lies in the number of paths they keep while detecting any message bit.

u_{N-1} , is to find the most likely leaf node of the tree.

The SC decoder is a greedy algorithm that tries to keep the most likely node at every level of the tree. As shown in the Figure 2.8a, on the first level of the tree (below the root node), the SC decoder chooses the maximum of the two available options: the node belonging to the the sequence $\mathbf{0}$ on the left with probability 0.55. On the second and third level, it once again chooses the nodes corresponding to $\mathbf{0}$ decision with probabilities 0.35 and 0.2, respectively and outputs $\mathbf{000}$ as the estimated message.

The SCL decoder keeps a list of partial message estimates on every decoding stage. An example of the operation of the SCL decoder with a list size $L = 2$ is described in Figure 2.8b. On the first level, the decoder keeps both the nodes corresponding to $u_0 = 0$ and $u_0 = 1$ with probabilities 0.55 and 0.45, respectively. On the second stage, it extends the two available paths to four paths, but since the maximum list size is two, it keeps the two paths with the larger probabilities than the other two. The two paths with larger probabilities further extend to four paths again on the third level. Since the decoder has reached the leaf nodes, it selects the node with the largest probability of 0.26. In this way, the SCL decoder is able to find the most likely message $\mathbf{100}$ with the largest probability of 0.26 among all the leaf nodes instead of picking up the less likely message estimate $\mathbf{000}$ with probability 0.20 in the case of the SC decoder.

Polar codes outperform LDPC codes if concatenated with a CRC code and decoded by the SCL decoder with a minute difference from above-mentioned algorithm [5]. The difference is that at the end of the decoding operation, the sequence that passes CRC check is picked up instead of picking up the sequence with largest probability.

2.5.2 Hard-Output Simplified Successive Cancellation Decoder

One of the drawbacks of the SC decoder is its very high latency: approximately $0.5fR$ [8], where f is the clock frequency. To overcome this problem, Alamdar-Yazdi and Kschischang proposed the SSC decoder that exploited the rate-zero and rate-one subcodes in a polar code [11]. A rate-zero subcode is the one that does not transmit any information, and all its message bits are fixed to zero. On the other hand, a rate-one subcode is the one that does not provide any error-correcting capability, and all its message bits are free bits. For example, in Figure 2.6 the subgraph consisting of $\Phi_3(0), \Phi_3(1)$ and $\Phi_2(0)$ correspond to a rate-zero subcode, because no information is transmitted using this subcode as all the nodes belonging to this subcode are fixed to zero. Similarly, the subgraph consisting of $\Phi_3(6), \Phi_3(7)$ and $\Phi_2(3)$ correspond to a rate-one subcode, because both $\Phi_3(6)$ and $\Phi_3(7)$ correspond to free bits.

The SSC decoder skips the computations for rate-zero subcodes (corresponding to frozen bits), and decodes rate-one subcodes (corresponding to free bits) in one clock cycle using the thresholding operation. In this way, the decoder avoids unnecessary computations and reduces the computational complexity as well as decoding latency.

For example, consider the SSC decoder operation to decode a polar code of $N = 8$ and $\mathcal{S} = \{3, 5, 6, 7\}$ as shown in Figure 2.6. The SSC decoder starts with the computation of $\mathcal{L}_3(0)$, i.e., the top node at the depth $\lambda = 3$, but the decoder knows a-priori that the nodes at $(3, 0, 0)$ and $(3, 1, 0)$ correspond to fixed bits and fixes $\mathcal{B}_2(0)$ to zero. Therefore, the decoder can skip the calculation of $\mathcal{L}_3(0), \mathcal{L}(1)$ and $\mathcal{L}_2(0)$ and directly assign bit decisions in $\mathcal{B}_2(0)$ to zero. The decoder computes $\mathcal{L}_1(0)$ and proceeds to the calculation of $\mathcal{L}_3(2), \mathcal{L}_3(3)$ as usual. In a similar way to rate-zero subcodes, the nodes $\{(3, i, 0)\}_{i=6}^7$ form a rate-one sub-code. In [11], the authors proposed skipping the calculation of $\{\mathcal{L}_3(i)\}_{i=6}^7$

and computing $\mathcal{B}_2(3)$ by thresholding the LLRs in $\mathcal{L}_2(3)$ using an operation like (2.11) in Algorithm 2.1. In this way, the SSC decoder reduces the number of operations, and therefore, reduces the latency in the decoder.

2.5.3 Soft-Output Belief Propagation Decoder

The factor graph description of Figure 2.6 enables the message passing based BP algorithm to be used for polar codes [17], [18]. One advantage of this decoder is that it provides soft outputs for the coded bits. The pitfall, however, is that it requires a large number of iterations over the factor graph of the polar code resulting in a larger processing and memory requirement. Additionally, a large number of iterations hinders high-throughput (low-latency) implementations. Therefore, this high processing, memory and latency requirement of the BP decoder makes it practically infeasible for many applications. We briefly describe the operation of the decoder here.

The decoder works locally on protographs of length two by computing extrinsic LLRs corresponding to all the four nodes of the protograph. Figure 2.9 explains the LLR updates in a single protograph, which is the factor graph of a polar code of length two. The decoder first updates $L_1(0,0)$ using $L_0(0,0)$ and $L_0(0,1)$ from L and $B_1(1,0)$ from B , and then updates $B_1(1,0)$ using the same $L_0(0,0)$ and $L_0(0,1)$ from L but $B_1(0,0)$ from B , completing the left-to-right update on the protograph. The decoder then starts to update the LLRs from right to left by updating $B_0(0,0)$ and $B_0(0,1)$. The four steps shown in Figure 2.9 complete the updates on this single protograph. The LLRs in red represent the LLRs that are used to update the LLRs in green.

The BP decoder updates messages on the top-right protograph of the factor graph and then moves down updating all the protograph at $\lambda = n$. Once the BP decoder has updated all the protographs at depth $\lambda = n$, it moves from right to left updating all the protographs at depth $0 \leq \lambda < n$ in a similar fashion until it reaches the bottom-left corner of the factor graph, completing the first iteration of the BP decoder. The decoder repeats this process for a fixed number of iterations and at the end of last iteration, produces the message estimate.

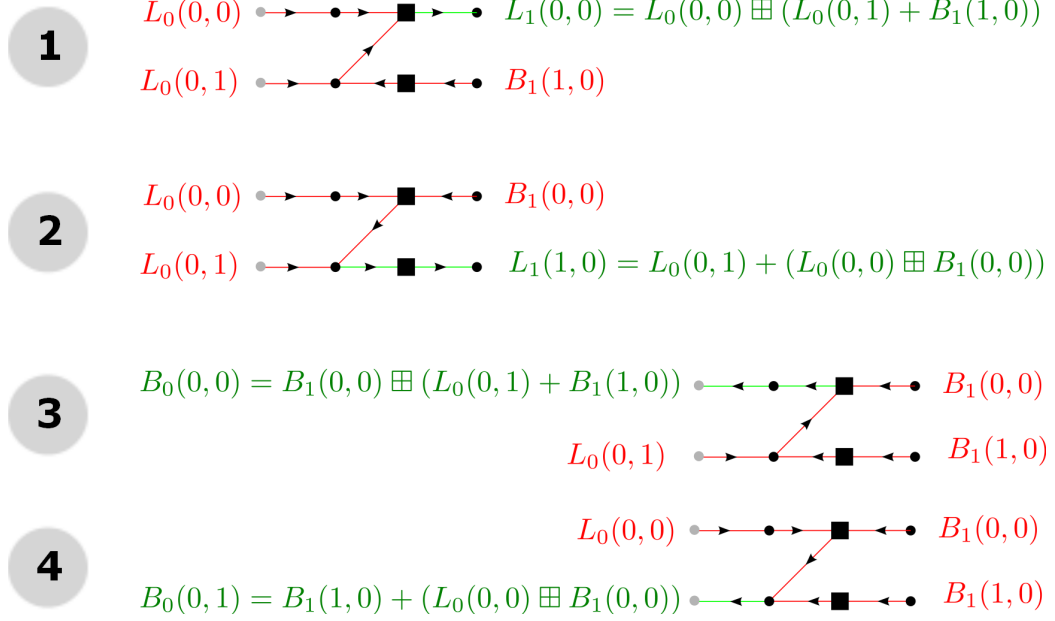


Figure 2.9: The BP decoder updates LLRs on a protograph-by-protograph basis. In a single protograph, it updates four LLRs with two LLRs in both L and B .

Since the BP decoder is the only soft-output decoder available for polar codes, we compare its performance metrics with those of the BP decoder for LDPC codes. Figure 2.10 compares the trade-off between the complexity and the E_b/N_0 required to achieve FER = 10^{-3} on a dicode channel with impulse response $h = [1 \ -1]$. The total number of turbo iterations between the channel detector and the decoder is 15. The number next to an individual performance point refers to the number of iterations used in the respective decoder. The LDPC code used is an irregular LDPC code of the variable node distribution $\lambda(x) = 0.2184x + 0.163x^2 + 0.6186x^3$, check node distribution $\rho(x) = 0.6821x^4 + 0.3173x^5 + 0.0006x^6$, average column weight $d_v = 3.4$ and row weight $d_c = 5.31$. Clearly, the BP decoder for polar codes requires a larger number of computations and E_b/N_0 to achieve the required FER than that for LDPC codes. The BP decoder for polar codes with 60 iterations require approximately 11 times more iterations than the BP decoder for LDPC codes with 60 iterations. The huge computational complexity overshadows any benefits polar codes have and makes polar codes with BP decoder infeasible for practical applications.

The BP decoder for polar codes requires $2N(\log_2(N) + 1)$ real values to store, whereas full parallel implementation of the BP decoder for LDPC codes requires storage of $N(d_v + 1)$

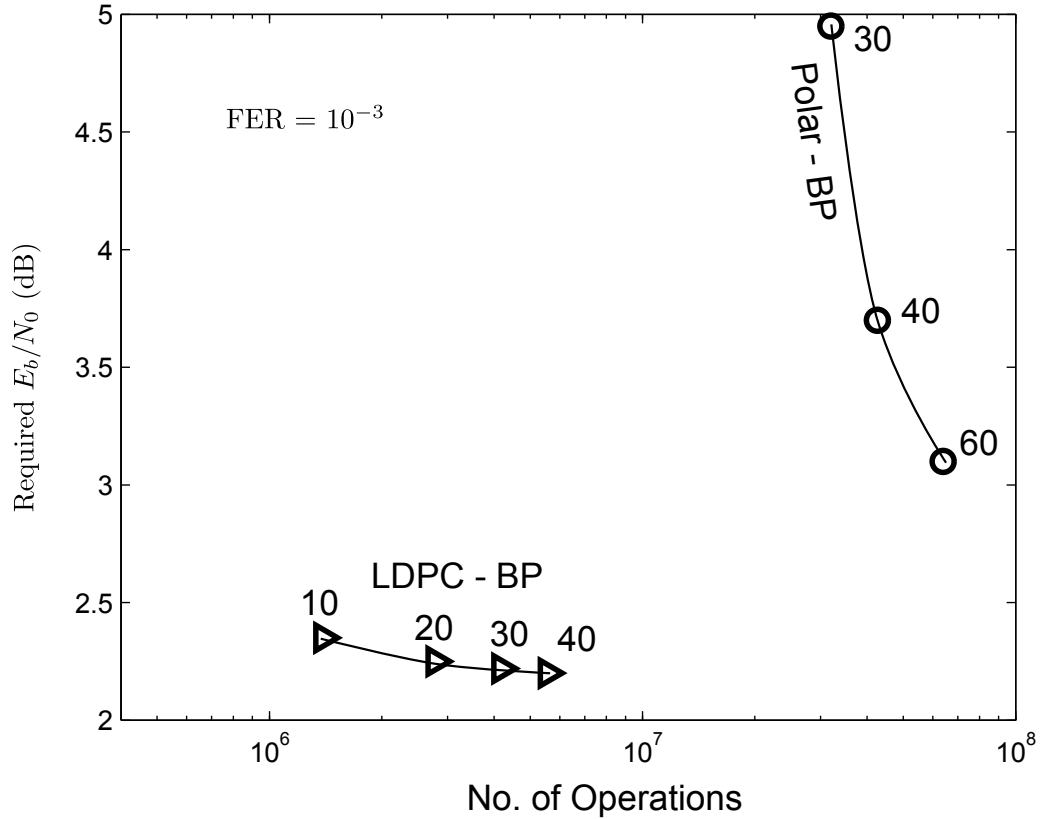


Figure 2.10: The polar code with BP decoding performs worse than the LDPC code with BP decoding on both the fronts: it requires a larger number of computations while requiring a larger E_b/N_0 to achieve $\text{FER} = 10^{-3}$ on a dicode channel.

[19] real values. Figure 2.11 shows the relative memory required for the BP decoder for LDPC codes with respect to the one required for that for polar codes, and for block lengths of practical importance ($N > 2048$) is well below 15%.

Unlike the computational complexity and memory requirement, latency is highly related to the hardware implementation of a decoder, and it is hard to compare two decoders until they are realized in hardware. The hardware implementation of a decoder is beyond the scope of this thesis, but if we are able to reduce the number of operations required to be performed in a sequential fashion, we can guarantee latency reduction by reducing the clock cycles required to perform these operations without any hardware implementation. An excellent example is the SSC decoder we described in Section 2.5.2 in which the decoder skips the detection of a few bits that used to occur in a sequential order in the SC decoder,

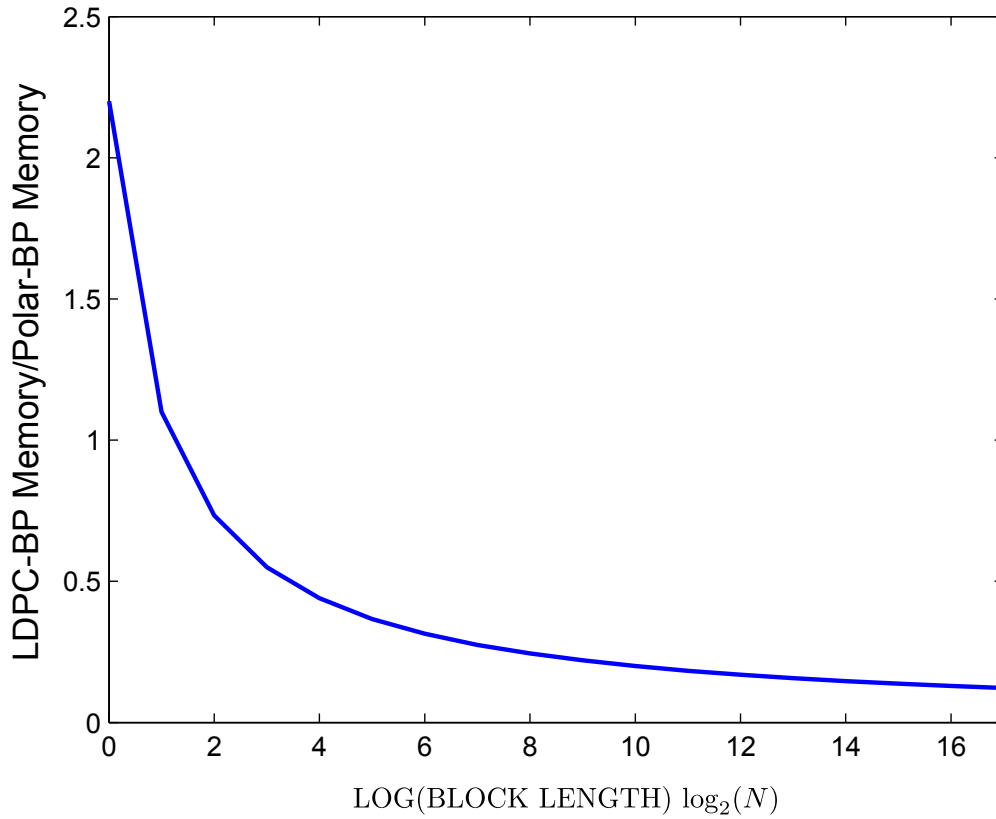


Figure 2.11: The BP decoder for LDPC codes requires less than 50% of the memory required by BP decoder for polar codes with $N > 16$. This relative memory requirement decreases monotonically and goes very low for practical block lengths such as only 13% for a code of length 32768.

resulting in a lower number of clock cycles required. In this thesis, we will be concerned with the latency improvement resulting from these methods based on reducing the number of sequential operations required instead of hardware implementation.

CHAPTER III

IMPROVED BELIEF-PROPAGATION SCHEDULE FOR POLAR CODES

Chapter 2 briefly discussed the BP decoder, which provides the soft outputs needed for turbo-based receivers as well as better performance than the SC decoder. However, these gains come at the price of high complexity and latency of the decoder that render it infeasible for practical applications. In this chapter, we take the first step toward the ideal system by proposing a decoder based on a new schedule that targets this high complexity issue.

In the original BP decoder, the message updates follow a flooding schedule, in which it updates messages on a protograph-by-protograph basis starting from the top-right protograph and coming down till the bottom-right one. The decoder repeats the same process for all the depths of the factor graph completing its first iteration. After the first iteration, the decoder repeats the same process for a fixed number of iterations. As explained later in detail, the flooding schedule is unable to disseminate the information efficiently throughout the factor graph and requires many iterations to reach acceptable error rates.

We propose a new serial schedule based on the successive cancellation schedule of the SC decoder and call it the soft-cancellation schedule. We call the message-passing decoder with the proposed schedule the soft-cancellation SCAN decoder. The proposed schedule reduces the complexity of the decoder immensely compared to the flooding schedule of the BP decoder and is similar to the schedule of message updates in the SC decoder. Therefore, the ideas used in the improvement of the SC decoder can be extended to the SCAN decoder in many cases. Furthermore, we propose a technique to reduce memory utilization of the decoder based on the proposed schedule.

We now explain the key idea behind the proposed schedule.

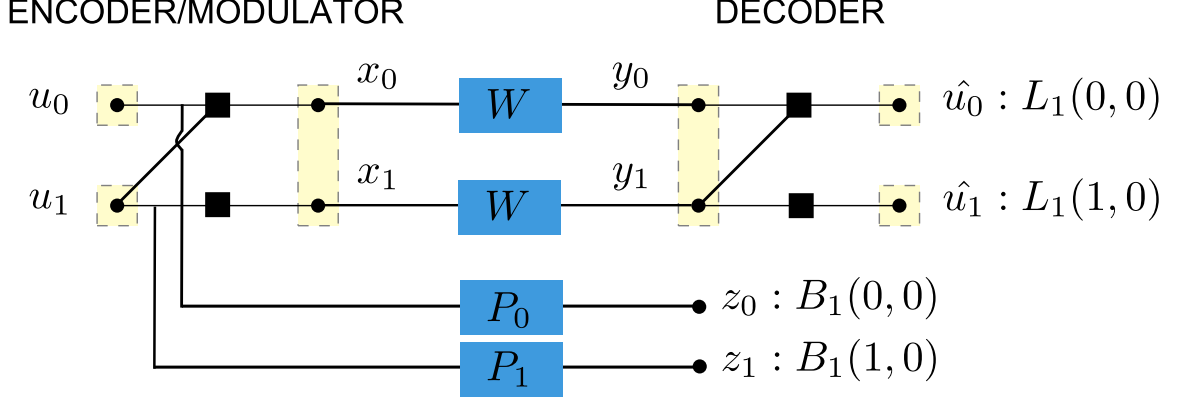


Figure 3.1: System model for Lemma: 3.1

3.1 The Soft-Cancellation (SCAN) Schedule and Decoder

Consider the factor graph of a polar code of length two as shown in Figure 3.1. We call the small factor graph the *basic decision element*, as in the SC decoder, all the processing on the factor graph of any polar code of length more than two occurs locally on this basic decision element. Therefore, we can build our intuition and analysis of the proposed schedule on the basic decision element and then extend it to the general case of the factor graph of polar codes with length larger than two.

Suppose we encode the bits u_0, u_1 using a polar code of length two and map the resulting coded bits to $x_0, x_1 \in \{+1, -1\}$. We then send x_0 and x_1 on a binary-input DMC W with transition probabilities $W(y|x)$. The SC decoder first calculates the log-likelihood ratio for the bit u_0 using (2.12) with channel observations y_0, y_1 while assuming that u_1 is equally likely to be 0 or 1. The SC decoder assumes this about u_1 , because it does not have an estimate of u_1 yet. Once it has an estimate for the bit u_0 , it assigns the estimate to $B_1(0, 0)$ using (2.11) and calculates the log-likelihood ratio for the bit u_1 using (2.13) with the assumption that u_0 has been decoded with no error. After the calculation of m_1 using $L_1(1, 0)$ in (2.11), it assigns m_1 to $B_1(1, 0)$ and use (2.12) to estimate the values of x_0, x_1 . The final operation of assigning m_1 completes the SC decoding on this polar code of length two.

The aforementioned process transforms the vector channel $W_2(y_0, y_1|u_0, u_1)$ into two separate channels W_{SC}^- and W_{SC}^+ defined by the transition probabilities $W_{SC}^-(y_0, y_1|u_0)$ and

$W_{SC}^+(y_0, y_1, u_0|u_1)$, respectively. We reiterate the assumptions used in the SC decoder as follows:

1. u_1 is equally likely to be 0 or 1 for the computation of likelihood $W_{SC}^-(y_0, y_1, u_1|u_0)$.
2. u_0 has been decoded with no error for the computation of likelihood $W_{SC}^+(y_0, y_1, u_0|u_1)$.

The first assumption is an oversimplification given the channel observations y_0 and y_1 contain information about u_0 that the decoder is not using, whereas the second assumption is true only for very high E_b/N_0 . Both assumptions degrade the LLR estimates, and we expect improved LLR estimates if we can incorporate soft information about u_0 and u_1 in the decoder instead of hard decision and no information, respectively. We first show in the following lemma how the likelihood computation changes if we have access to such soft information, and then we show how we provide this soft information in the SCAN decoder.

Figure 3.1 explains the system model used in this lemma. We encode bits u_0 and u_1 to x_0 and x_1 and transmit on channel W . At the receiver, the SC decoder has y_0 and y_1 as channel observations to estimate the transmitted bits. Now assume that we have information about u_0 and u_1 through other channels P_0 and P_1 in the form of z_0 and z_1 , respectively. Lemma 3.1 describes the likelihood calculations for u_0 and u_1 given access to y_0, y_1, z_0 and z_1 .

Lemma 3.1. *Let z_0 and z_1 be the output of DMCs P_0 and P_1 , defined by the transition probabilities $P_0(z_0|u_0)$ and $P_1(z_1|u_1)$, respectively. Suppose z_0 and z_1 are conditionally independent given u_0 and u_1 , respectively implying $P(z_0, z_1|u_0, u_1) = P_0(z_0|u_0)P_1(z_1|u_1)$. If we have access to z_0 or z_1 instead of perfect or no knowledge of u_0 and u_1 , respectively the log-likelihood ratios of u_0 and u_1 are given by*

$$L_1(0, 0) = L_0(0, 0) \boxplus [B_1(1, 0) + L_0(0, 1)], \quad (3.1)$$

$$L_1(1, 0) = L_0(0, 1) + [B_1(0, 0) \boxplus L_0(0, 0)]. \quad (3.2)$$

Proof. The proof is provided in the Appendix A. □

One problem that remains now is to show how we can provide additional LLRs $B_1(0,0), B_1(1,0)$ in all decision elements in a factor graph for any N . In the start of a decoding cycle, we compute $\{L_0(0,k)\}_{k=0}^{(N-1)}$ as we receive symbols \mathbf{r} from the channel. We inform the decoder about the location of fixed bits by initializing $\{B_n(k,0)\}_{k \in \mathcal{J}^c}$ to ∞ . Suppose we are interested in finding the LLR $L_n(i,0)$ with $\{L_n(k,0)\}_{k=0}^{(i-1)}$ already computed and no information about $\{u_k\}_{k=(i+1)}^{N-1}$. Since we cannot have any information about $\{u_k\}_{k=(i+1)}^{N-1}$ in the first iteration, we will keep the assumption that they are equally likely, i.e., $B_n(k,0) = 0, \forall (i+1) \leq k \leq (N-1)$. It is noteworthy that we have already populated L partially from left to right while calculating $\{L_n(k,0)\}_{k=0}^{(i-1)}$. Therefore, as we calculate $\{L_n(k,0)\}_{k=0}^{(i-1)}$, we can use the partially calculated L as a-priori information to update B from right to left using (3.1) and (3.2) on all the decision elements involved. When $i = N-1$, we have B with extrinsic LLRs corresponding to all the nodes in the decoder's factor graph.

We once again start computing LLRs $\{L_n(i,0)\}_{i=1}^{N-1}$, but this time we have soft information in B for $\{u_k\}_{k=(i+1)}^{N-1}$ unlike the first iteration. Therefore, we can use B to supply a-priori information to all decision elements in subsequent iterations. We use this iterative process I times and use the extrinsic LLRs $\{L_n(i,0)\}_{i=0}^{N-1}$ and $\{B_0(0,i)\}_{i=0}^{N-1}$ calculated in the last iteration corresponding to message and coded bits, respectively. We explain all the necessary implementation details in Algorithms 3.1, 3.3 and 3.2.

Algorithm 3.1 provides the decoder's wrapper and calls Algorithm 3.2 to calculate $\{L_n(\phi,0)\}_{\phi=0}^{(N-1)}$. Algorithm 3.2 updates L from left to right using B as prior information. Since B is initialized to zero except $\{B_n(i,0)\}_{i=0}^{(N-1)}$, $B_\lambda(\phi+1,\omega)$ in Algorithm 3.1 has zero value in the first iteration, just like the SC decoder. On the other hand, the SCAN decoder in the first iteration uses soft information in $B_\lambda(\phi-1,\omega)$ in contrast to the SC decoder which uses hard information about $B_\lambda(\phi-1,\omega)$ in (2.13). As we iterate through ϕ in the inner loop of Algorithm 3.1, for the odd values of ϕ the wrapper calls Algorithm 3.3 to update B from right to left. Algorithm 3.3 populates B using L as prior information, and by the end of the first iteration, $\{B_0(0,\phi)\}_{\phi=0}^{(N-1)}$ contains extrinsic LLRs for the coded bits. In the second iteration, (3.3) uses the values of $B_\lambda(\phi+1,\omega)$ from the first iteration, unlike

the first iteration in which $B_\lambda(\phi + 1, \omega)$ were initialized to zero. Algorithm 3.1 repeats this process for I times using the outer loop and estimates message bits at the end of I th iteration.

One of the important parameters of polar codes under any decoding scheme is the rate of channel polarization, which describes how fast the capacity of the transformed bit channels approaches 1 and 0, respectively as $N \rightarrow \infty$. We refer the interested readers to [4] for further details about this parameter, and mention here the advantage of using the SC decoder in place of the SCAN decoder with $I = 1$ for the AWGN channel. We observe that by clipping the LLRs of already detected bits to $+\infty, -\infty$ we can increase the convergence and polarization rate. Zimmermann et al. [20] observed the same phenomenon in belief propagation decoder for LDPC codes and called it '*belief pushing*'. It is noteworthy here that the SCAN decoder with $I = 1$ is different from the SC decoder, because the SC decoder clips the LLRs of already detected bits in the factor graph to either $+\infty$ or $-\infty$, whereas the SCAN decoder uses soft information about these bits. However, both of these decoders do not use information about the bits yet to be detected and are similar in this respect. With this in mind, one can convert the SCAN decoder with $I = 1$ into the SC decoder by assigning $B_n(k, 0) = \infty \times \text{sgn}(B_n(k, 0) + L_n(k, 0))$ as we calculate $\{L_n(k, 0)\}_{k=0}^{N-1}$, where $\text{sgn}(\cdot)$ is the sign function. Therefore, we can consider the SC decoder as a modified version of the more general SCAN decoder. We conclude this section by presenting the following proposition.

Proposition 3.1. *The rate of channel polarization is higher under the SC decoder than the SCAN decoder with $I = 1$.*

Proof. The proof is provided in the appendix. □

3.2 Reducing the Memory of the SCAN Decoder

One of the two contributors to the area and power consumption on a chip is memory as explained in Section 1.4. A larger memory requirement translates into a higher power and area utilization, and therefore, the memory requirement of a decoder should be minimized as

Algorithm 3.1: The SCAN decoder

```

1 initialization
2  $\{L_0(0, i)\}_{i=0}^{(N-1)} \leftarrow$  LLRs from channel
3  $\{B_n(i, 0)\}_{i \in \mathcal{I}^c} \leftarrow \infty$ 
4  $\{B_n(i, 0)\}_{i \in \mathcal{I}} \leftarrow 0$ 
5  $\{\mathcal{B}_\lambda(\phi)\}_{\lambda=0}^{n-1} \leftarrow 0, \forall \phi \in \{0, \dots, 2^\lambda - 1\}$ 
6
7 for  $i = 1 \rightarrow I$  do
8   for  $\phi = 0 \rightarrow (N - 1)$  do
9     updatellrmap( $n, \phi$ )
10    if  $\phi$  is odd then updatebitmap( $n, \phi$ )
11  end
12 end
13 for  $i = 0 \rightarrow (N - 1)$  do
14   if  $(B_n(i, 0) + L_n(i, 0)) \geq 0$  then  $\hat{m}_i \leftarrow 0$ 
15   else  $\hat{m}_i \leftarrow 1$ 
16 end

```

Algorithm 3.2: updatellrmap(λ, ϕ)

```

1 if  $\lambda = 0$  then return
2  $\psi \leftarrow \lfloor \frac{\phi}{2} \rfloor$ 
3 if  $\phi$  is even then updatellrmap( $\lambda - 1, \psi$ )
4 for  $\omega = 0 \rightarrow (2^{n-\lambda} - 1)$  do
5   if  $\phi$  is even then
6     
$$L_\lambda(\phi, \omega) \leftarrow L_{\lambda-1}(\psi, 2\omega) \boxplus [L_{\lambda-1}(\psi, 2\omega + 1) + B_\lambda(\phi + 1, \omega)] \quad (3.3)$$

7   end
8   else
9     
$$L_\lambda(\phi, \omega) \leftarrow L_{\lambda-1}(\psi, 2\omega + 1) + [L_{\lambda-1}(\psi, 2\omega) \boxplus B_\lambda(\phi - 1, \omega)] \quad (3.4)$$

10  end
11 end

```

much as possible. In this section, we propose a technique to reduce the memory requirement of the SCAN decoder.

In [5] and [8], a memory-efficient version of the SC decoder has been proposed by modifying L and B memory indexing. The proposed modifications reduced the memory requirement for L and B to $2N - 1$ and $4N - 2$, respectively. We show that the modification

Algorithm 3.3: updatebitmap(λ, ϕ)

```

1 if  $\phi$  is odd then
2   for  $\omega = 0 \rightarrow (2^{n-\lambda} - 1)$  do
3      $B_{\lambda-1}(\psi, 2\omega) \leftarrow B_{\lambda}(\phi - 1, \omega) \boxplus [B_{\lambda}(\phi, \omega) + L_{\lambda-1}(\psi, 2\omega + 1)]$       (3.5)
      $B_{\lambda-1}(\psi, 2\omega + 1) \leftarrow B_{\lambda}(\phi, \omega) + [B_{\lambda}(\phi - 1, \omega) \boxplus L_{\lambda-1}(\psi, 2\omega)]$       (3.6)
4   end
5   if  $\psi$  is odd then updatebitmap( $\lambda - 1, \psi$ )
6 end

```

that [5] proposed for L can be directly applied to the SCAN decoder, and the memory requirement for L can be reduced to $2N - 1$ from $N(n + 1)$. On the other hand, the modification that [5] proposed for B is not directly applicable for the reasons explained later. This section introduces a partitioning method for B that reduces its memory requirement to $4N - 2 + Nn/2$ from $N(n + 1)$.

We first briefly describe the modification proposed for L and apply it directly to the SCAN decoder. Looking at the factor graph in Figure 3.2, it is clear that all the Φ -groups on a single λ depth has the same number of nodes $2^{n-\lambda}$. Let us denote L and B values corresponding to $\Phi_{\lambda}(\phi)$ as $\mathcal{L}_{\lambda}(\phi)$ and $\mathcal{B}_{\lambda}(\phi)$, respectively. As we calculate $\{L_n(i, 0)\}_{i=0}^{N-1}$, traversing i in ascending order, we use the Φ -groups at different depths in ascending order as well. With this schedule of LLR update, when we are updating $\mathcal{L}_{\lambda}(i)$, we do not need any of the $\{\mathcal{L}_{\lambda}(\phi) : \phi < i\}$. Therefore, we can overwrite the values of previously calculated $\{\mathcal{L}_{\lambda}(\phi) : \phi < i\}$ and only need $2^{n-\lambda}$ memory locations for a depth λ . Figure 3.2 shows that the memory for $\mathcal{L}_{\lambda}(0)$ of size $2^{n-\lambda}$ can be used to store all $\mathcal{L}_{\lambda}(\phi)$ at the depth λ . Hence, the total number of memory elements required by L is $\sum_{\lambda=0}^n N/2^{\lambda} = 2N - 1$.

The SCAN decoder updates L with a similar schedule to the schedule of updates in the SC decoder, and therefore, the above-mentioned modification can be directly applied to L in the SCAN decoder, reducing the memory requirement of L from $N(n + 1)$ to $2N - 1$. It is noteworthy that this modification is not possible in the similar fashion to the originally proposed belief propagation decoder of [17] because of the flooding schedule of LLR updates in L and B .

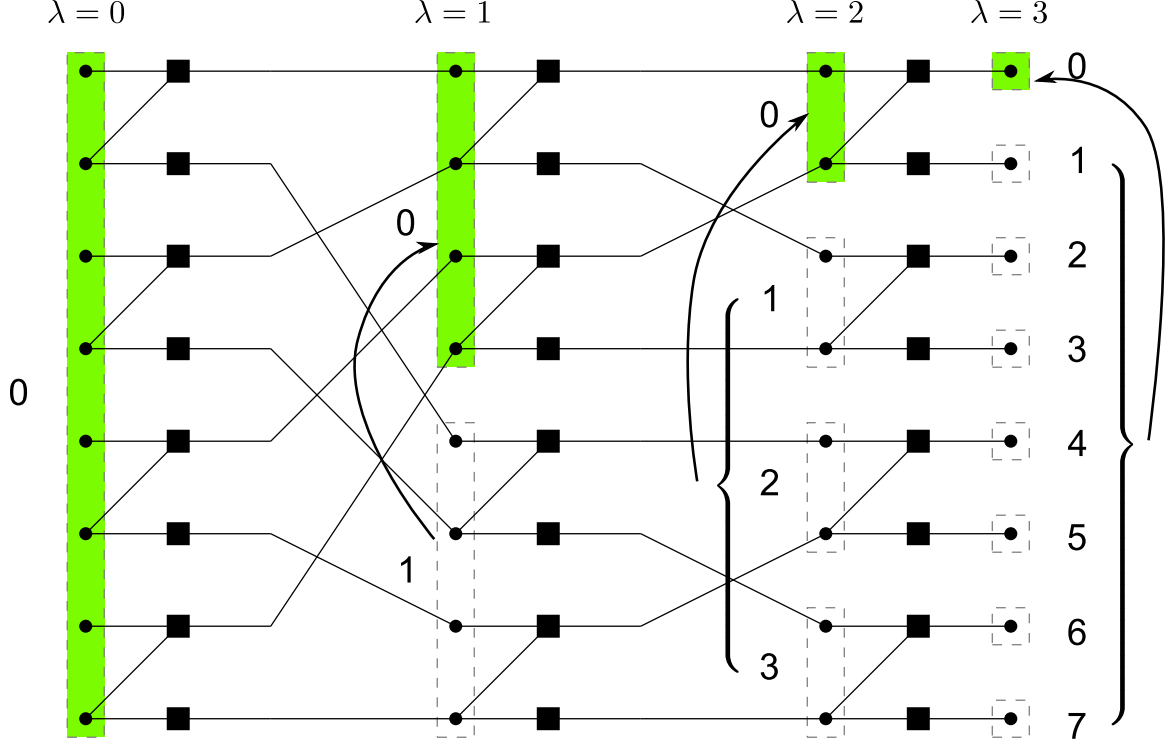


Figure 3.2: At any depth $\lambda \in \{0, 1, \dots, n\}$, $\mathcal{L}_\lambda(\phi)$ for all $\phi \in \{0, \dots, 2^\lambda\}$ are stored in the memory for $\mathcal{L}_\lambda(0)$, which is shown in green.

The modification for B in [5] (where B used binary values) that is similar to the modification for L described above, is not applicable to the SCAN decoder, because now not only do we need to calculate LLRs in B , but we also need to pass them onto the next iteration. Therefore, as [5] suggested for the SC decoder, we cannot overwrite the values of B .

To see how we might reduce the memory requirement for B in the SCAN decoder, we first present the following notation and lemmas. Consider $\mathcal{L}_\lambda(\phi)$ and $\mathcal{L}_\lambda(\delta)$ at any depth $\lambda, \forall \phi \neq \delta$ and $\phi, \delta \in \{0, \dots, 2^\lambda - 1\}$.

We denote

$$\mathcal{L}_\lambda(\phi) \prec \mathcal{L}_\lambda(\delta)$$

to show that the decoder updates $\mathcal{L}_\lambda(\phi)$ before $\mathcal{L}_\lambda(\delta)$.

Lemma 3.2. *At any depth $\lambda \in \{0, \dots, n\}$, the SCAN decoder updates Φ -groups for both L*

and B in ascending order from $\phi = 0 \rightarrow N - 1$, i.e.,

$$\mathcal{L}_\lambda(\phi) \prec \mathcal{L}_\lambda(\phi + 1)$$

$$\mathcal{B}_\lambda(\phi) \prec \mathcal{B}_\lambda(\phi + 1)$$

for all $\phi \in \{0, \dots, 2^\lambda - 2\}$.

Proof. We prove this lemma using mathematical induction. First we note the following trivial cases:

1. The SCAN decoder does not update B and L for $\lambda = n$ and $\lambda = 0$.
2. The SCAN decoder trivially updates B in ascending order for $\lambda = 0$, because there is only one Φ -group.
3. The SCAN decoder trivially updates L in ascending order for $\lambda = n$ because of the schedule of the decoder on this depth.

First we prove this Lemma for L only. Let us denote $\{\phi_i^\lambda\}_{i=0}^{2^\lambda}$ as the sequence in which we update L at any depth λ . From the schedule of the SCAN decoder, we know that $\{\phi_i^n = i\}_{i=0}^{2^n}$. Suppose that $\{\phi_i^k = i\}_{i=0}^{2^k}$ is true. From (3.3) and (3.4), we know that the update in $\mathcal{L}_\lambda(\phi)$ requires the update in $\mathcal{L}_{\lambda-1}(\lfloor \phi/2 \rfloor)$. Therefore, $\{\phi_i^{(k-1)} = i\}_{i=0}^{2^{k-1}}$ is also true from the definition of the 'floor' function. We can use the same argument for both the base and induction step of the proof.

Similarly, with (3.5) and (3.6), we can prove the same results for B . □

Lemma 3.3. *At any depth $\lambda \in \{1, \dots, n - 1\}$,*

$$\mathcal{L}_\lambda(\phi) \prec \mathcal{B}_\lambda(\phi) \prec \mathcal{L}_\lambda(\phi + 1), \tag{3.7}$$

where $\phi \in \{0, \dots, 2^\lambda - 2\}$.

Proof. Without loss of generality, consider the calculation of $\mathcal{L}_\lambda(\phi)$ and $\mathcal{L}_\lambda(\phi + 1)$ for ϕ even, and $\lambda \in \{2, \dots, n\}$. From Lemma 3.2, (3.3) and (3.4) we know that

$$\mathcal{L}_{\lambda-1}(\psi) \prec \mathcal{L}_\lambda(\phi) \prec \mathcal{L}_\lambda(\phi + 1),$$

where $\psi = \lfloor \phi/2 \rfloor$. Also from (3.5) and (3.6),

$$\mathcal{L}_\lambda(\phi + 1) \prec \mathcal{B}_{\lambda-1}(\psi).$$

Therefore, using these two relationships we get

$$\mathcal{L}_{\lambda-1}(\psi) \prec \mathcal{B}_{\lambda-1}(\psi).$$

Now considering the calculation of $\mathcal{L}_\lambda(\phi + 2)$ and $\mathcal{L}_\lambda(\phi + 3)$, we get

$$\mathcal{L}_{\lambda-1}(\psi + 1) \prec \mathcal{B}_{\lambda-1}(\psi + 1).$$

From Lemma 3.2, we know that at any λ , the decoder updates both L and B in ascending order, we conclude

$$\mathcal{L}_{\lambda-1}(\psi) \prec \mathcal{B}_{\lambda-1}(\psi) \prec \mathcal{L}_{\lambda-1}(\psi + 1),$$

for all $\lambda \in \{2, \dots, n\}$, and $\psi \in \{0, \dots, 2^{\lambda-1} - 2\}$. We complete the proof by changing variables. \square

Theorem 3.1. *In any iteration i and for any depth λ , the SCAN decoder requires only $\{\mathcal{B}_\lambda(\phi) : \phi \text{ is odd}\}$ from iteration $(i - 1)$ to update L .*

Proof. Consider (3.3) for iteration i . From Lemma 3.3, we know that

$$\mathcal{L}_\lambda(\phi) \prec \mathcal{B}_\lambda(\phi).$$

Therefore, when the decoder is updating $\mathcal{L}_\lambda(\phi)$, $\mathcal{B}_\lambda(\phi+1)$ is holding the value from iteration $(i - 1)$. Since it is true for ϕ even only, $(\phi + 1)$ is odd and we use $\{\mathcal{B}_\lambda(i) : i \text{ is odd}\}$ from $(i - 1)$. Similarly, (3.4) shows that to update $\mathcal{L}_\lambda(\phi)$ for odd ϕ , we need $\mathcal{B}_\lambda(\phi - 1)$ that, by Lemma 3.3, the decoder has already updated. Therefore, $\mathcal{B}_\lambda(\phi - 1)$ contains the values calculated in the current iteration i . \square

Suppose we reserve two separate memory locations for B : one to hold $\{\mathcal{B}_\lambda(\phi) : \phi \text{ is even}\}$, namely E and one for $\{\mathcal{B}_\lambda(\phi) : \phi \text{ is odd}\}$, namely O . From Theorem 3.1, we conclude that we only need to keep O for the next iteration with only $N/2$ elements at a

depth λ . In contrast, the decoder will use E in the current iteration only, and therefore the decoder can use the same space $\mathcal{B}_\lambda(0)$ for all $\{\mathcal{B}_\lambda(\phi), \phi \text{ is even}\}$ at a depth λ by overwriting it. The number of memory elements required for E is exactly the same as required for L , i.e., $(2N - 1)$.

The decoder also needs to specify the indexing of both E and O . As noted in [5], ϕ does not convey any information in indexing memory location for any $\mathcal{L}_\lambda(\phi)$, because the decoder writes all the values to the same location $\mathcal{L}_\lambda(0)$. Since E is similar to L in the sense that the SCAN decoder does not need E from one iteration to the other, the decoder can use the same indexing for both E and L . One such memory indexing function is

$$f(\lambda, \omega) = \omega + 2^{(n+1)} - 2^{(n+1-\lambda)}. \quad (3.8)$$

Since O is used only for odd values of ϕ , we can convert these odd values into the natural numbers by a simple transformation and then use it to index O . One such indexing function is

$$g(\lambda, \phi, \omega) = \omega + (\phi - 1)2^{(n-\lambda-1)} + (\lambda - 1)2^{(n-1)}. \quad (3.9)$$

Figure 3.3 presents a small example of a rate-1/2 polar code. In this example, the SCAN decoder reuses $\mathcal{B}_2(0)$ and $\mathcal{B}_3(0)$ (shown with green rectangles) by overwriting them with the values of $\mathcal{B}_2(2)$, $\mathcal{B}_3(2)$, $\mathcal{B}_3(4)$ and $\mathcal{B}_3(6)$, and does not need extra memory for them. On the other hand, the SCAN decoder keeps the values for $\{\mathcal{B}_\lambda(\phi), \forall \lambda, \phi \text{ is odd}\}$ as they are required for the next iteration.

We summarize the details of the proposed low-complexity SCAN decoder in Algorithm 3.4, 3.5 and 3.6. Algorithm 3.4 is the top-level wrapper for the SCAN decoder, similar to Algorithm 3.1. The SCAN decoder successively calls Algorithm 3.5 and 3.6 as it traverses all the uncoded bits from $i = 0$ to $N - 1$. Algorithm 3.6 updates the two portions of B using L as prior information: E for the groups with ϕ even and O for the groups with ϕ odd, whereas Algorithm 3.5 updates L using E and O as prior information. It is noteworthy that in all the algorithms we have indexed E and O using (3.8) and (3.9), respectively.

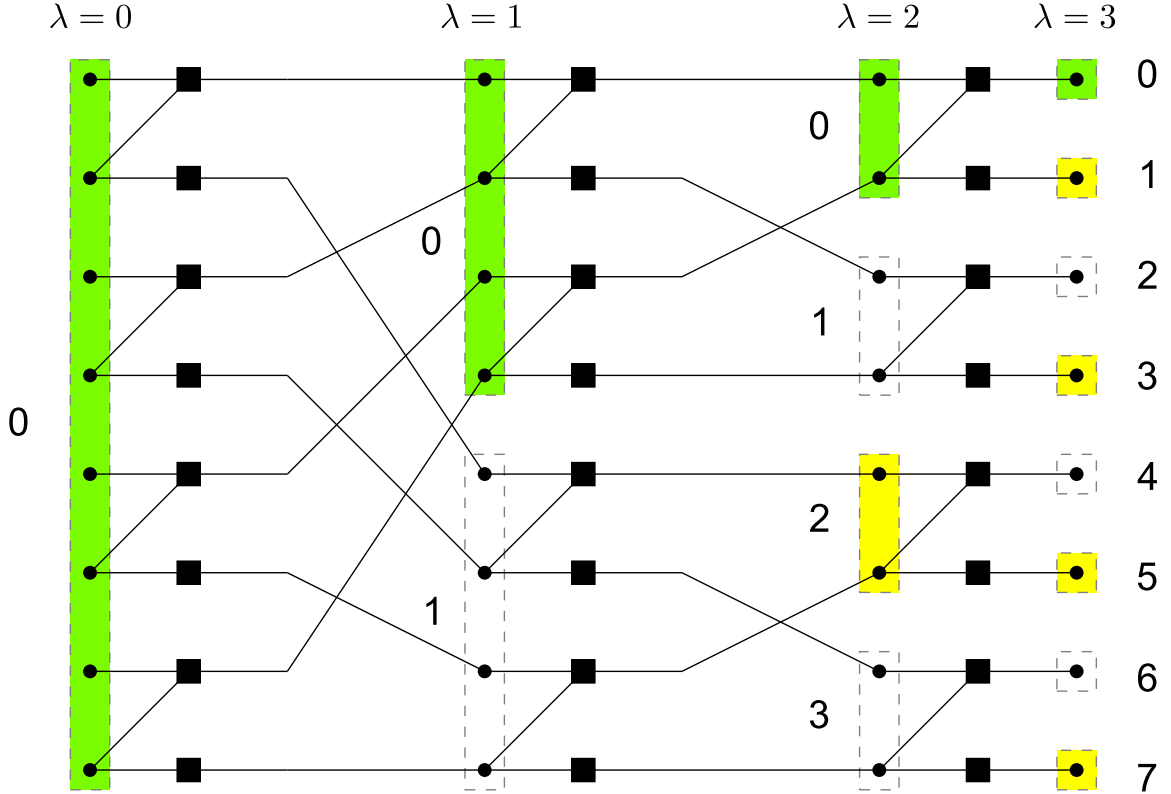


Figure 3.3: Memory elements required to store B with corresponding ϕ displayed next to a particular $\mathcal{B}_\lambda(\phi)$. In any iteration, the SCAN decoder does not need $\{\mathcal{B}_\lambda(\phi) : \phi \text{ is even}\}$ for the next iteration, and we can overwrite $\mathcal{B}_\lambda(0)$ (shown with green rectangles) at any depth λ with $\{\mathcal{B}_\lambda(\phi) : \phi \text{ is even}, \phi \neq 0\}$ (shown with yellow rectangles). On the other hand, the SCAN decoder requires $\{\mathcal{B}_\lambda(\phi) : \phi \text{ is odd}\}$ (shown with white rectangles) for processing in the next iteration, and therefore it will keep these memory locations as they are. In this small example, we save five memory elements corresponding to $\mathcal{B}_2(2)$, $\mathcal{B}_3(2)$, $\mathcal{B}_3(4)$ and $\mathcal{B}_3(6)$.

3.3 A Comparison with the Flooding Schedule

In this section, we compare the flooding schedule of the BP decoder with the SCAN schedule using Figure 3.3.

Consider first the operation of the BP decoder on the factor graph shown in Figure 3.3. Just like the SCAN decoder, the BP decoder also uses two memory locations L and B . The decoder starts by updating LLRs $L_3(0,0)$, $L_3(1,0)$, $B_2(0,0)$ and $B_2(0,1)$ using $\mathcal{L}_2(0)$, $B_3(0,0)$ and $B_3(1,0)$. In this way, the decoder updates the LLRs corresponding to the top-right protograph and then repeats the same process for all the four protographs under $\lambda = 2$. After the updates in the protographs under $\lambda = 2$, the decoder updates the

Algorithm 3.4: The SCAN decoder with reduced memory requirement

Result: Extrinsic LLRs $\{E_0(0, \omega)\}_{\omega=0}^{N-1}$
1 $\{L_0(0, i)\}_{i=0}^{(N-1)} \leftarrow$ LLRs from channel
2 $\{O_n(i, 0)\}_{i \in \mathcal{I}^c, i \text{ is odd}} \leftarrow \infty$
3 **for** $i = 1 \rightarrow I$ **do**
4 **for** $\phi = 0 \rightarrow (N - 1)$ **do**
5 updatellrmap(n, ϕ)
6 **if** ϕ is even **then**
7 **if** $\phi \in \mathcal{I}^c$ **then** $E_m(\phi, 0) \leftarrow \infty$
8 **else** $E_m(\phi, 0) \leftarrow 0$
9 **end**
10 **else** updatebitmap(n, ϕ)
11 **end**
12 **end**

Algorithm 3.5: updatellrmap(λ, ϕ)

1 **if** $\lambda = 0$ **then** return
2 $\psi \leftarrow \lfloor \frac{\phi}{2} \rfloor$
3 **if** ϕ is even **then** updatellrmap($\lambda - 1, \psi$)
4 **for** $\omega = 0 \rightarrow (2^{n-\lambda} - 1)$ **do**
5 **if** ϕ is even **then** $L_\lambda(\phi, \omega) \leftarrow L_{\lambda-1}(\psi, 2\omega) \boxplus [L_{\lambda-1}(\psi, 2\omega + 1) + E_\lambda(\phi + 1, \omega)]$
6 **else** $L_\lambda(\phi, \omega) \leftarrow L_{\lambda-1}(\psi, 2\omega + 1) + L_{\lambda-1}(\psi, 2\omega) \boxplus O_\lambda(\phi - 1, \omega)$
7 **end**

four protographs under $\lambda = 1$ and then $\lambda = 0$ completing its first iteration. The following points are noteworthy in this schedule:

1. The BP decoder updates L and B on a protograph-by-protograph basis.
2. In any iteration to update any LLR in both L and B , the BP decoder uses the values in B that are updated in the current iteration and the values in L updated in the previous iteration (or in the case of first iteration, the initialized values of L).
3. When the BP decoder is updating the LLRs under $\lambda = 0$ at the end of the first iteration, the information received from the channel in $\mathcal{L}_0(0)$ moves from the protographs under $\lambda = 0$ to the protographs under $\lambda = 1$. Therefore, in the first iteration the information from the fixed bits travels from the right-most end of the factor graph to the left-most end, but the information received from the channel moves only to the neighboring protographs, i.e., the protographs under $\lambda = 1$. Following

Algorithm 3.6: updatebitmap(λ, ϕ)

```

1  $\psi \leftarrow \lfloor \frac{\phi}{2} \rfloor$ 
2 if  $\phi$  is odd then
3   for  $\omega = 0 \rightarrow (2^{n-\lambda} - 1)$  do
4     if  $\psi$  is even then
5        $E_{\lambda-1}(\psi, 2\omega) \leftarrow E_{\lambda}(\phi - 1, \omega) \boxplus [O_{\lambda}(\phi, \omega) + L_{\lambda-1}(\psi, 2\omega + 1)]$ 
6        $E_{\lambda-1}(\psi, 2\omega + 1) \leftarrow O_{\lambda}(\phi, \omega) + E_{\lambda}(\phi - 1, \omega) \boxplus L_{\lambda-1}(\psi, 2\omega)$ 
7     end
8     else
9        $O_{\lambda-1}(\psi, 2\omega) \leftarrow E_{\lambda}(\phi - 1, \omega) \boxplus [O_{\lambda}(\phi, \omega) + L_{\lambda-1}(\psi, 2\omega + 1)]$ 
10       $O_{\lambda-1}(\psi, 2\omega + 1) \leftarrow O_{\lambda}(\phi, \omega) + E_{\lambda}(\phi - 1, \omega) \boxplus L_{\lambda-1}(\psi, 2\omega)$ 
11    end
12  end
13 if  $\psi$  is odd then updatebitmap( $\lambda - 1, \psi$ )
14 end

```

the same procedure, we can show that in every iteration, the information about the fixed bits traverses the whole factor graph, whereas the information received from the channel moves to the neighboring protographs only, and it requires n iterations to reach the right-most end of the factor graph.

The SCAN decoder updates $\mathcal{L}_1(0)$, $\mathcal{L}_2(0)$, $\mathcal{L}_3(0)$ and $\mathcal{L}_3(1)$ in this order. After the update in $\mathcal{L}_3(1)$, the SCAN decoder updates $\mathcal{B}_2(0)$ using $\mathcal{L}_2(0)$ that has just been updated. In this way, as the SCAN decoder updates $\mathcal{L}_3(i)$ from $i = 0$ to 7, it populates B using the updated values in L . At the end of the first iteration, the information received from the channel moves from left end of the factor graph to the right while the information about the fixed bits move from the right end to the left. The following points are noteworthy in this schedule:

1. The SCAN decoder does not update L and B on protograph-by-protograph basis; instead it is a node-by-node basis update schedule except in the protographs under $\lambda = 2$. For example, the SCAN decoder first updates $\mathcal{L}_1(0)$, $\mathcal{L}_2(0)$, $\mathcal{L}_3(0)$ that are

the updates corresponding to the top-right node of the protographs involved.

2. In any iteration to update any LLR in B , the SCAN decoder uses B as well as L updated in the current iteration. To update any LLR in L , the decoder uses L and $\{\mathcal{B}_\lambda(\phi) : \phi \text{ even}\}$ updated in the current iteration while $\{\mathcal{B}_\lambda(\phi) : \phi \text{ odd}\}$ updated in the previous iteration.
3. In any iteration, the information about both the fixed bits in $\{\mathcal{B}_3(i)\}_{i=0}^7$ and the information received from the channel in $\mathcal{L}_0(0)$ traverse the entire factor graph.

As described above, the BP decoder needs at least n iterations to disperse the information contained in $\{\mathcal{B}_n(i)\}_{i=0}^{(N-1)}$ and $\mathcal{L}_0(0)$ in the entire factor graph, whereas the SCAN decoder achieves this with only one iteration. In this way, the SCAN decoder achieves a faster convergence by better disseminating the information in the factor graph than the BP decoder, as pointed out by the last two points of the schedules in both the decoders.

3.4 Performance Results

In this section, we compare the error-rate performance of the SCAN decoder with the SC decoder and the BP decoder for polar codes, and the BP decoder for LDPC codes.

3.4.1 The AWGN Channel

Figure 3.4 demonstrates the improved performance of our algorithm in the AWGN channel. We have simulated the SC and the SCAN decoder for a polar code of block length $N = 32768$ and dimension $K = 16384$. The polar code is optimized for $E_b/N_0 = 2.35$ dB in the AWGN channel using the method of [1]. The design $E_b/N_0 = 2.35$ dB is obtained by sweeping design E_b/N_0 for a range of values and picking up the one that resulted in the best FER performance. We have simulated a maximum of 10^6 frames to calculate error rates on all E_b/N_0 values, terminating the simulation if 100 or more frames are found in error.

In terms of frame error rates, the SCAN decoder with one iteration performs worse than the SC decoder. The worse performance is in agreement with Proposition 3.1, as the rate of polarization for the SCAN decoder with only one iteration is lower than that of the SC decoder. By clipping the LLRs for already detected bits to extreme values of infinity, the

SC decoder converges faster than the SCAN decoder with one iteration. However, with only two iterations, the SCAN decoder outperforms the SC decoder, providing a gain of 0.1 dB in the required E_b/N_0 for a frame error rate of 10^{-4} . Further increase in the number of iterations of the SCAN decoder to four does not provide any significant gain.

In contrast to the FER performance, the SCAN decoder with only one iteration has better bit error rate (BER) performance than that of the SC decoder. The better performance of the SCAN decoder is due to the fact that in case of incorrect decoding, the SC decoder converges to an incorrect but valid codeword, because it produces hard bit decisions for message bits that combined with frozen bits has one-to-one correspondence with a codeword in the code. Therefore, whenever the SC decoder is unable to decode a message, it produces at least d_{min} errors, where d_{min} is the minimum Hamming distance of the code and is usually a large number for powerful codes. Recall that the Hamming distance between two codewords is the number of positions in which the two codewords differ, and the minimum Hamming distance d_{min} of a code is the minimum Hamming distance between any two codewords of the code. In contrast to the SC decoder, the SCAN decoder does not have the restriction of converging to a valid codeword in case of decoding failure. The SCAN decoder, by nature, is a distributed algorithm, and its codeword decisions may not correspond to message decisions at all, because they belong to different parts of the factor graph. The SCAN decoder's bit error rate performance improves even further with increasing number of iterations, and with only two iterations, provides approximately 0.2 dB gain to achieve FER= 10^{-4} . With four iterations, the SCAN decoder's performance saturates and does not improve any further with increasing number of iterations.

3.4.2 Partial Response Channels

Figure 3.5 shows the performance of the SCAN decoder on the dicode channel for a polar code of length $N = 8192$ and dimension $K = 4096$ under turbo equalization architecture [6]. We have designed the polar code using the method of [1] for the AWGN channel with $E_b/N_0 = 1.4$ dB. The design $E_b/N_0 = 1.4$ dB is obtained by calculating FER corresponding to a range of design E_b/N_0 values and picking up the one that resulted in the best FER. In

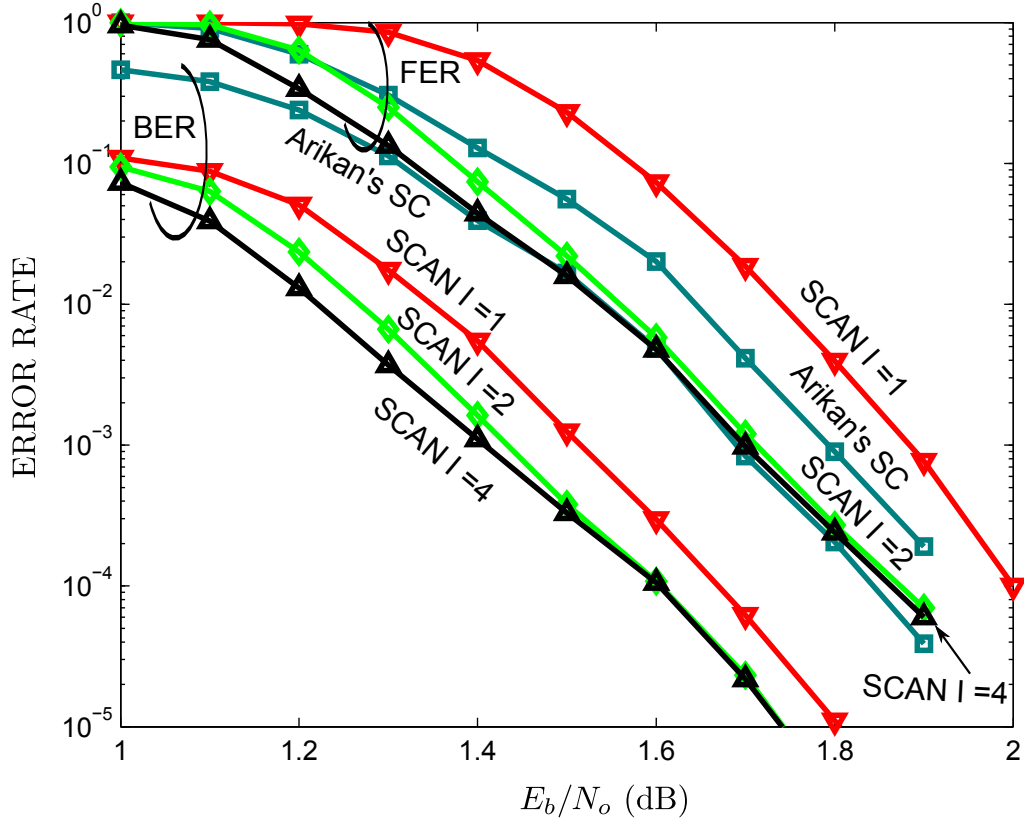


Figure 3.4: FER and BER performance of the SCAN decoder in the AWGN channel for $N = 32768$. We have optimized the polar code for $E_b/N_0 = 2.35$ dB using the method of [1].

all simulations, a maximum of 15 turbo iterations are used.

The SCAN decoder with only two iterations outperforms the BP decoder with 60 iterations on the dicode channel, where the complexity of one iteration of both the decoders is the same. With further increase in number of iterations, the performance improves, and with only eight iterations the SCAN decoder provides about 0.3 dB gain in the required E_b/N_0 over the BP decoder to achieve $\text{FER} = 10^{-3}$.

Figure 3.5 also shows the performance of the SCAN decoder on the EPR4 channel for a polar code of length $N = 8192$ and dimension $K = 4096$, designed using the method of [1] for the AWGN channel with $E_b/N_0 = 1.55$ dB. The design E_b/N_0 is obtained by the same E_b/N_0 sweeping for a range of values as used for the dicode channel. The SCAN decoder shows the same performance improvement over the BP decoder for polar codes as

shown in the dicode channel, and with only two iterations, performs comparable to the BP decoder with 60 iterations in the EPR4 channel. With eight iterations, the SCAN decoder provides about 0.2 dB gain in the required E_b/N_0 over the BP decoder for polar codes with 60 iterations to achieve FER= 10^{-3} .

We also compare the polar code's performance with the SCAN decoder to that of an irregular LDPC code of the variable node distribution $\lambda(x) = 0.2184x + 0.163x^2 + 0.6186x^3$, check node distribution $\rho(x) = 0.6821x^4 + 0.3173x^5 + 0.0006x^6$, average column weight $d_v = 3.4$ and row weight $d_c = 5.31$ decoded using the BP algorithm and constructed using [21], [22] and [23]. The performance difference between this LDPC code with the BP algorithm and the polar code with the SCAN decoder (using four iterations) is approximately 0.3 dB for FER = 10^{-3} on the dicode channel. The performance loss in the case of the EPR4 channel is larger than that in the case of the dicode channel.

Furthermore, it has been shown that polar codes outperform LDPC codes if concatenated with very simple codes [5], [24] in the AWGN channel. In this respect, the SCAN decoder can have potential applications for turbo decoding of concatenated codes because of their ability to provide soft outputs.

3.5 Complexity Analysis

Table 1 compares the complexity of the BP decoder for LDPC codes with that of the BP and the SCAN decoder for polar codes. We have used the complexity analysis for LDPC codes given in [25], where one iteration consists of variable-to-check and then check-to-variable message passing. We have further assumed that the decoder uses table lookup method to calculate both $\tanh(\cdot)$ and $\tanh^{-1}(\cdot)$.

The processing requirement of the SCAN decoder with two iterations is only 4% of that of the BP decoder with 60 iterations for polar codes while both of the decoders deliver approximately the same frame error rate performance in both the dicode and the EPR4 channel. With eight iterations, the SCAN decoder has processing requirement of only 13% of that of the BP decoder with 60 iterations but has gain in the required E_b/N_0 of approximately 0.3 dB and 0.2 dB to achieve FER = 10^{-3} in the dicode and the EPR4

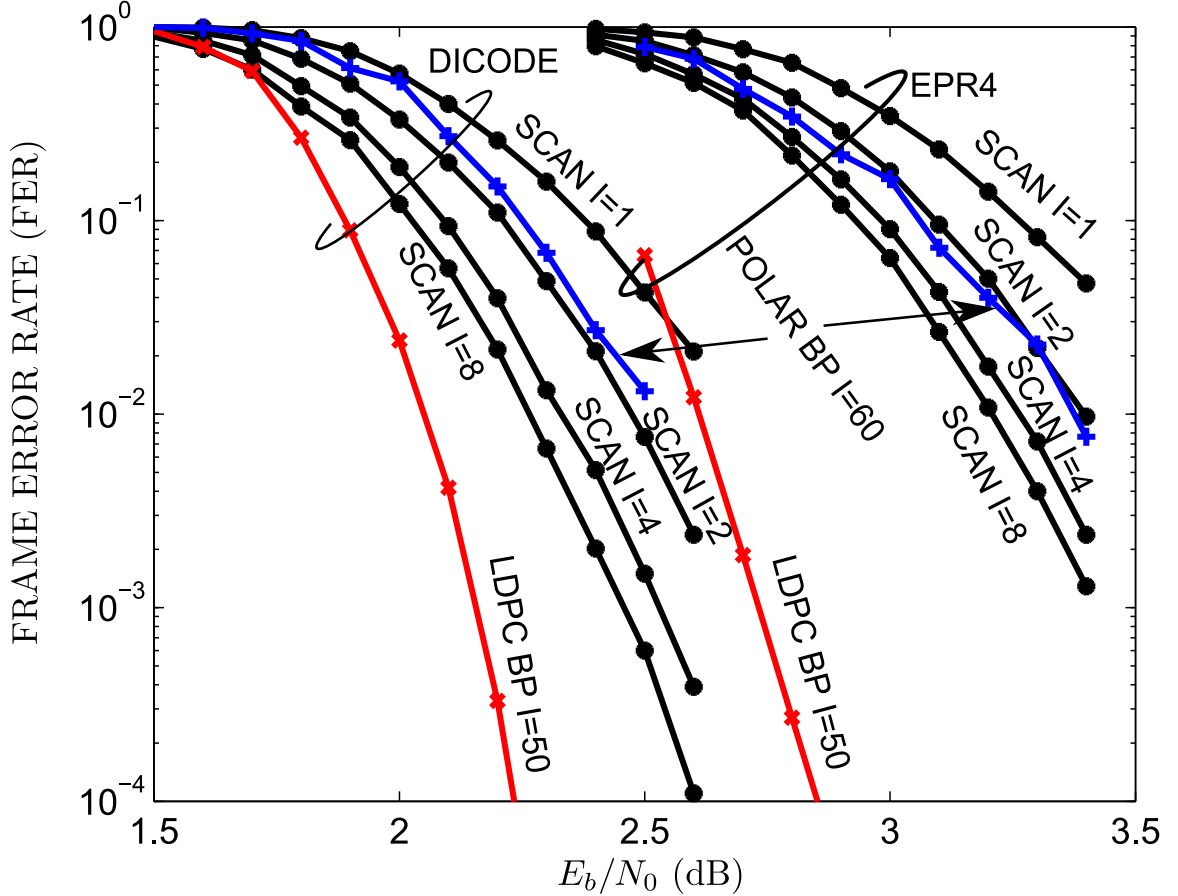


Figure 3.5: FER performance of the SCAN decoder in partial response channels for $K = 4096$ and $N = 8192$. We have optimized the polar code for $E_b/N_0 = 1.4$ dB (dicode) and $E_b/N_0 = 1.55$ dB (EPR4) using the method of [1].

channels, respectively.

The number of operations required for the SCAN decoder with four iterations is approximately equal to 60% of that required for the BP decoder for the LDPC code with 50 iterations. The complexity reduction comes at the price of higher E_b/N_0 requirement to achieve the same error-rate performance, as shown in Figure 3.5.

Figure 3.6 shows how the normalized memory requirement of the SCAN decoder with respect to the BP decoder for polar codes decreases with the increase in n . The BP decoder uses $N(n+1)$ real memory elements for each of L and B . The SCAN decoder uses $2N-1$ and $4N-2+Nn/2$ real memory elements for L and B , respectively. Figure 3.6 shows that the memory required by the SCAN decoder at two practical frame lengths of 4096 and 32768 is 43% and 39% of that required by the BP decoder, respectively. In summary,

Table 1: Complexity Comparison of Different Decoders

Operation	Complexity/Iteration	
	LDPC BP	Polar SCAN/BP
Table Lookups	$(N - K)(d_c + 1)$	$6Nn$
Multiplications	$(N - K)(d_c - 1)$	$2Nn$
Divisions	$(N - K)d_c$	0
Additions/Subtractions	$2Nd_v$	$2Nn$
Total Operations	$5Nd_v$	$10Nn$

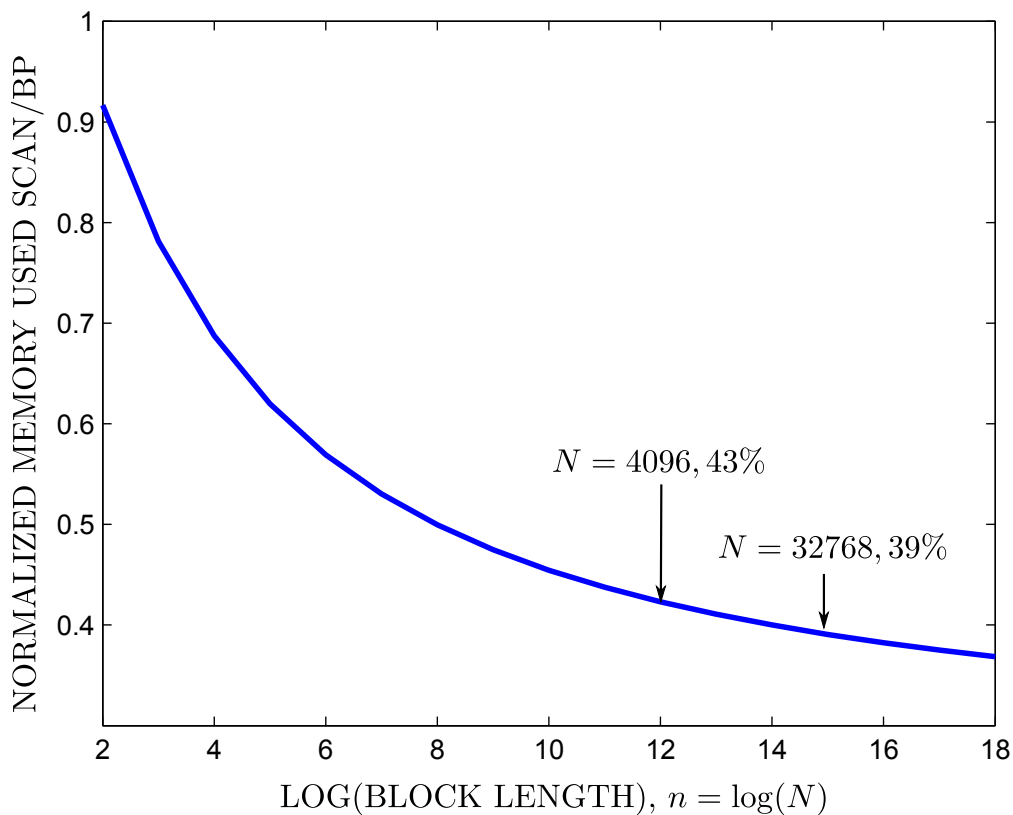


Figure 3.6: Memory efficiency improves with increasing block length.

the SCAN decoder requires approximately half the memory required by the BP decoder for polar codes for practical block lengths.

3.6 Summary

In this chapter, we have introduced *SCAN*, a soft-output decoder for polar codes that offers good performance, low computational complexity and low memory requirements. The

proposed decoder achieves its complexity reduction by adopting a serial schedule instead of a flooding schedule of the BP decoder. The SCAN decoder's computational complexity with two iterations is approximately 4% that of the BP decoder with 60 iterations on the decode channel, with comparable performance. Furthermore, the SCAN decoder requires $Nn/2$ (unlike $N(n + 1)$ for the BP decoder) memory elements to pass from one iteration to the next. Using this fact, a memory-splitting method is proposed in which the decoder keeps one portion of the memory needed for the next iterations as it is and optimizes the other one that it uses in the current iteration. With the proposed modification, the memory required by the SCAN decoder is approximately 39% of that required by the BP decoder at a block length $N = 32768$ in one example.

CHAPTER IV

AN ENHANCED SCAN DECODER WITH HIGH THROUGHPUT AND LOW COMPLEXITY

In this chapter, we propose an enhanced SCAN (eSCAN) decoder that outperforms the SCAN decoder of the previous chapter in the following ways: computational complexity, latency and memory usage.

In the previous chapter, we showed that changing the schedule of message updates in the BP decoder drastically reduces the complexity of soft-output decoding of polar codes. Although the new serial schedule reduces the complexity of the decoder, its serial nature severely hampers the decoder's throughput. The SC decoder faces the same problem, because its schedule for message update is the same as the SCAN decoder. Fortunately, for the SC decoder a number of techniques have been proposed to reduce this high latency problem, and many of them are directly applicable to the SCAN decoder. One of these techniques is the simplified successive cancellation (SSC) decoding of Alamdar-Yazdi and Kschischang [11]. However, a direct implementation of the SSC principle to the SCAN decoder requires large memory and the knowledge whether LLRs in different parts of the factor graph are fixed to ∞ , zero or take value from \mathbb{R} .

In this chapter, we prove that the location of frozen bits exhibit structural properties for a class of polar codes that provide the knowledge about LLR values in different parts of the factor graph of a polar code. The class of polar codes include the ones constructed for binary erasure channel using Arikan's method [4] and the AWGN channel using Gaussian approximation based density evolution [1]. The proposed properties define the structure of the complete factor graph of a polar code using just the location of frozen bits, and thus help in the extension of the SSC principle to the SCAN decoder, reducing the SCAN decoder's latency and computational complexity. In addition to the application of the SSC principle to the SCAN decoder, we also propose a technique based on the structural properties to

reduce the memory requirement of the SCAN decoder. The memory reduction is in addition to the reduction in the computational complexity and the latency of the SCAN decoder that come from the application of the SSC principle.

The structure of the chapter is as follows. Section 4.1 introduces the structural properties of polar codes and Section 4.2 provides an intuitive explanation for these properties. In Section 4.3, we apply these properties to propose a memory-efficient, low-complexity and low-latency enhanced SCAN (eSCAN) decoder. Section 6.2.2 analyzes the proposed high-throughput low-complexity SCAN decoder.

4.1 The Properties of Polar Codes

One can construct the generator matrix for any (N, K, R) polar code by first taking the Kronecker power of a kernel matrix of small dimension (such as 2×2 in the case of classical polar codes [4]) and then removing $N - K$ rows of the matrix by fixing corresponding message bits to zero. The construction of polar codes is explained in depth in Section 2.3.

The Kronecker power introduces a pattern in the structure of both the encoder and decoder which is a very desirable feature from hardware implementation perspective as it generally reduces area utilization and wiring congestion [7]. On the other hand, the location of frozen bits does not show any pattern whatsoever.

The construction of polar codes consists of specifying the location of frozen bits. Arikan proposed a DE-based technique to construct polar codes for the BEC only. Mori and Tanaka employed DE to construct polar codes for the AWGN channel [14], but the method is limited to moderate block lengths as the complexity of DE is very high. Trifonov and Semenov [1] approximated DE of [14] by assuming Gaussian distribution on the messages exchanged in the factor graph. Tal and Vardy approached this construction problem using channel upgradation/degradation [15] principles.

In this section, we prove that in the class of polar codes constructed using density evolution (DE) for the BEC and Gaussian assumption based DE [1] for the AWGN channel, only a few patterns of the location of fixed bits are possible. The patterns in the location of fixed bits force some node groups in the factor graph to take zero, infinity

or real log-likelihoods, thereby reducing the processing from a node-by-node basis to a group-by-group basis. We also identify these patterns in the entire factor graph, and as an application, exploit these patterns for an efficient implementation of a fast low-complexity soft-output decoder for polar codes. Specifically, if we pair two consecutive bit locations in the detection order of the SC decoder, then either both of the bits are fixed, free or the fixed bit precedes the free bit. We further prove that patterns similar to the ones in the location of fixed bits emerge in the entire factor graph of a polar code under the SCAN decoder. In general, any pair of consecutive node groups at any depth in the factor graph are restricted to a few patterns based on whether LLRs corresponding to all the nodes in individual node groups of the pair are zero, ∞ or from \mathbb{R} .

Now we will formally introduce and prove the properties of the polar codes constructed using the method of [1]. The proofs for the case of the BEC are identical and are skipped.

At this point, we urge the reader to revisit Section 2.3 to refresh the notation and the concepts related to the construction of polar codes. The following proofs and explanation will heavily rely on Section 2.3.

Let

$$\mathcal{B}_\lambda(\phi) \leftarrow \eta \text{ denotes } B_\lambda(\phi, \omega) \in \eta, \text{ for all } \omega \in \{0, 1, \dots, 2^\lambda - 1\}.$$

For $\eta \in \{\{0\}, \{\infty\}\}$, we can interpret the notation \leftarrow as ‘will stick to’, e.g., $\mathcal{B}_\lambda(\phi) \leftarrow \{0\}$ implies that all the elements in $\mathcal{B}_\lambda(\phi)$ will stick to zero for all the iterations of the decoder.

We first prove two lemmas for the construction method of [1] described in Section 2.3.2.

Lemma 4.1.

$$2x - x^2 > x^2, \text{ for } 0 < x < 1.$$

Proof.

$$x > x^2 \implies 2x > 2x^2 \implies 2x - x^2 > x^2.$$

□

Lemma 4.2.

$$2x > x > g(x), \text{ for } 0 < x < 1,$$

where $g(\cdot)$ is defined in (2.20).

Proof.

$$2x > x = h^{-1}(h(x)) = h^{-1}(2h(x) - h(x)).$$

Since $h(x)$ is monotonically decreasing and $h(x) < 1$,

$$2x > x > h^{-1}(2h(x) - h(x)^2) = h^{-1}(1 - (1 - h(x))^2) = g(x).$$

□

Consider values in B corresponding to the basic protograph in the upper-right corner of Figure 4.1 that builds the entire factor graph of a polar code. This protograph has two inputs on the right and two outputs on the left. We call the sets from which these inputs and outputs take value the *input* and the *output* set, respectively. Table 2 shows all possible input sets for this protograph, corresponding output sets and a distinct ID for the protograph based on input/output sets. We use P_i as the designator for the protograph with ID i .

Given a design set \mathcal{I} , let $p(P_i)$ denotes the probability (in the frequentist sense) of protograph P_i appearing at depth $\lambda = n$.

Theorem 4.1 (Special Prohibited Pairs Property).

$$p(P_i) = 0, \text{ for } i \in \{3, 4, 5, 6, 7, 8\}. \quad (4.1)$$

Proof. We know from Line 3 and 4 in Algorithm 3.1 that the decoder initializes B by assigning infinity and zero LLRs at depth $\lambda = n$ corresponding to fixed and free bits, respectively. From the SCAN decoder operation, we know that it does not update these LLRs in the entire decoding process. Therefore, for the entire decoding process, $\{\mathcal{B}_n(i)\}_{i=0}^{N-1}$ has elements either from $\{0\}$ or $\{\infty\}$. Mathematically,

$$\{\mathcal{B}_n(i)\}_{i=0}^{N-1} \leftarrow \{0\} \text{ or } \{\infty\}.$$

Table 2: Protograph Input/Output Set Relationship

Protograph ID	Input		Output	
0	$\{\infty\}$	$\{\infty\}$	$\{\infty\}$	$\{\infty\}$
1	$\{\infty\}$	$\{0\}$	\mathbb{R}	\mathbb{R}
2	$\{0\}$	$\{0\}$	$\{0\}$	$\{0\}$
3	$\{\infty\}$	\mathbb{R}	\mathbb{R}	\mathbb{R}
4	\mathbb{R}	$\{0\}$	\mathbb{R}	\mathbb{R}
5	\mathbb{R}	\mathbb{R}	\mathbb{R}	\mathbb{R}
6	$\{0\}$	$\{\infty\}$	$\{0\}$	$\{\infty\}$
7	$\{0\}$	\mathbb{R}	$\{0\}$	\mathbb{R}
8	\mathbb{R}	$\{\infty\}$	\mathbb{R}	$\{\infty\}$

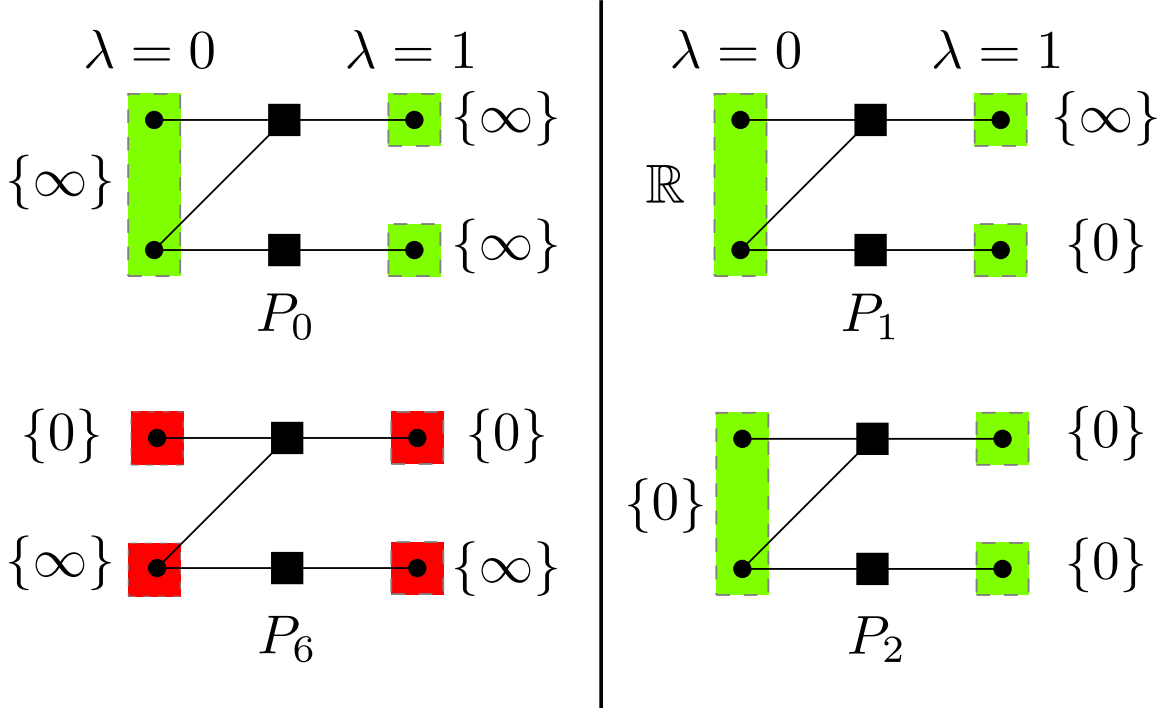


Figure 4.1: Only P_0 , P_1 and P_2 are possible at depth n in the factor graph of the polar codes. The inputs on the right of these three protographs specify whether bit is free (in case of $\{0\}$) or fixed (in case of $\{\infty\}$). In case of P_0 , P_1 and P_2 , both of the output nodes have LLRs from the same set. For example for P_0 , the values in $B_0(0)$ corresponding to both the output nodes on the left have LLRs from the set $\{\infty\}$, i.e., the LLRs in both of these nodes are stuck to ∞ . On the other hand in P_6 , LLRs corresponding to output nodes come from the set $\{0, \infty\}$, i.e., both the values are different unlike other three protographs.

Therefore, $p(P_i) = 0$ is trivially true for all $i \in \{3, 4, 5, 7, 8\}$, because all these protographs have \mathbb{R} as either of their input sets, and \mathbb{R} is not possible as an input set at depth n . Therefore, we only need to prove the theorem for $i = 6$.

Recall from Section 2.3.2 that for the construction method based on Gaussian assumption, LLRs in $\mathcal{L}_\lambda(\phi)$ have Gaussian distribution with mean $m_\lambda(\phi)$ and variance $2m_\lambda(\phi)$. Using the recursions in (2.19), we know that for any given $m_{n-1}(\phi)$ and for all $\phi \in \{0, 1, \dots, N/2 - 1\}$,

$$\begin{aligned} m_n(2\phi + 1) &= 2m_{n-1}(\phi) \\ &> g(m_n(\phi)) \\ &= m_n(2\phi). \end{aligned} \tag{4.2}$$

We can convert the relationship between two mean values $m_n(2\phi + 1)$ and $m_n(2\phi)$ in (4.2) into a relationship between the probability of error in (2ϕ) th and $(2\phi + 1)$ th bit, respectively as follows:

$$\begin{aligned} P_e(2\phi) &= Q(\sqrt{m_n(2\phi)}/2) \\ &> Q(\sqrt{m_n(2\phi + 1)}/2) && Q(\cdot) \text{ is monotonically decreasing} \\ &= P_e(2\phi + 1). \end{aligned} \tag{4.3}$$

It is shown in (2.17) of Section 2.3 that to construct a polar code, we need to construct a set of free indices \mathcal{S} such that $\sum_{i \in \mathcal{S}} P_e(i)$ is minimized. To minimize the sum, we need to include the bits with lowest error probabilities to \mathcal{S} . Therefore, we will never pick $(2\phi + 1)$ th node as fixed bit compared to (2ϕ) th bit for all $\phi \in \{0, 1, \dots, N/2 - 1\}$, because $P_e(2\phi) > P_e(2\phi + 1)$ as proved in (4.3). \square

Theorem 4.1 describes the pattern in the location of fixed bits and prohibits any free bit preceding a fixed bit in any pair of consecutive bits in the detection order of the SC decoder.

Following theorem generalizes the result of Theorem 4.1 to rest of the factor graph.

Theorem 4.2 (General Prohibited Pairs Property). *Let $\mathcal{B}_\lambda(2\phi)$ and $\mathcal{B}_\lambda(2\phi + 1)$ be two consecutive groups at any depth $\lambda \in \{1, \dots, n\}$ and for any $\phi \in \{0, 1, 2, \dots, 2^{\lambda-1} - 1\}$. The following group patterns are impossible in the polar code constructed using the method in [1]:*

1. $(\mathcal{B}_\lambda(2\phi), \mathcal{B}_\lambda(2\phi + 1)) \leftarrow (\{0\}, \{\infty\})$.
2. $(\mathcal{B}_\lambda(2\phi), \mathcal{B}_\lambda(2\phi + 1)) \leftarrow (\{0\}, \mathbb{R})$.
3. $(\mathcal{B}_\lambda(2\phi), \mathcal{B}_\lambda(2\phi + 1)) \leftarrow (\mathbb{R}, \{\infty\})$.

Proof. We prove this theorem by contradiction. From Theorem 4.1, only protographs P_0, P_1 and P_2 are possible at depth $\lambda = n$, and the proof is complete for $\lambda = n$. For $\lambda = k$, $k \in \{1, \dots, (n - 1)\}$, we investigate all the cases separately.

1. Case 1: Let us contrary assume that two consecutive $\mathcal{B}_\lambda(2\phi)$ and $\mathcal{B}_\lambda(2\phi + 1)$ exist such that $(\mathcal{B}_k(2\phi), \mathcal{B}_k(2\phi + 1)) \leftarrow (\{0\}, \{\infty\})$, for some $\phi \in \{0, 1, 2, \dots, 2^{k-1} - 1\}$. The contrary assumption is true only if all the elements of X correspond to free bits, and all the elements of Y correspond to fixed bits, where

$$X = \{2^{(n-k)}(2\phi), \dots, 2^{(n-k)}(2\phi + 1) - 1\}, \quad (4.4)$$

$$Y = \{2^{(n-k)}(2\phi + 1), \dots, 2^{(n-k)}(2\phi + 2) - 1\}. \quad (4.5)$$

Mathematically,

$$\mathcal{B}_n(i) \leftarrow \begin{cases} \{0\} & i \in X \\ \{\infty\} & i \in Y \end{cases}. \quad (4.6)$$

Figure 4.2 explains this case of the proof for $k = 1$ and $\phi = 0$. For $k = 1$ and $\phi = 0$, the contrary assumption becomes $(\mathcal{B}_1(0), \mathcal{B}_1(1)) \leftarrow (\{0\}, \{\infty\})$, which implies that all the bits in $X = \{0, \dots, 3\}$ are free while all the bits in $Y = \{4, \dots, 7\}$ are fixed.

Since all the elements in X and Y correspond to free and fixed bits, respectively, the error probabilities will follow the following relationship:

$$P_e(i) < P_e(j), \quad \text{for any } i \in X, j \in Y. \quad (4.7)$$

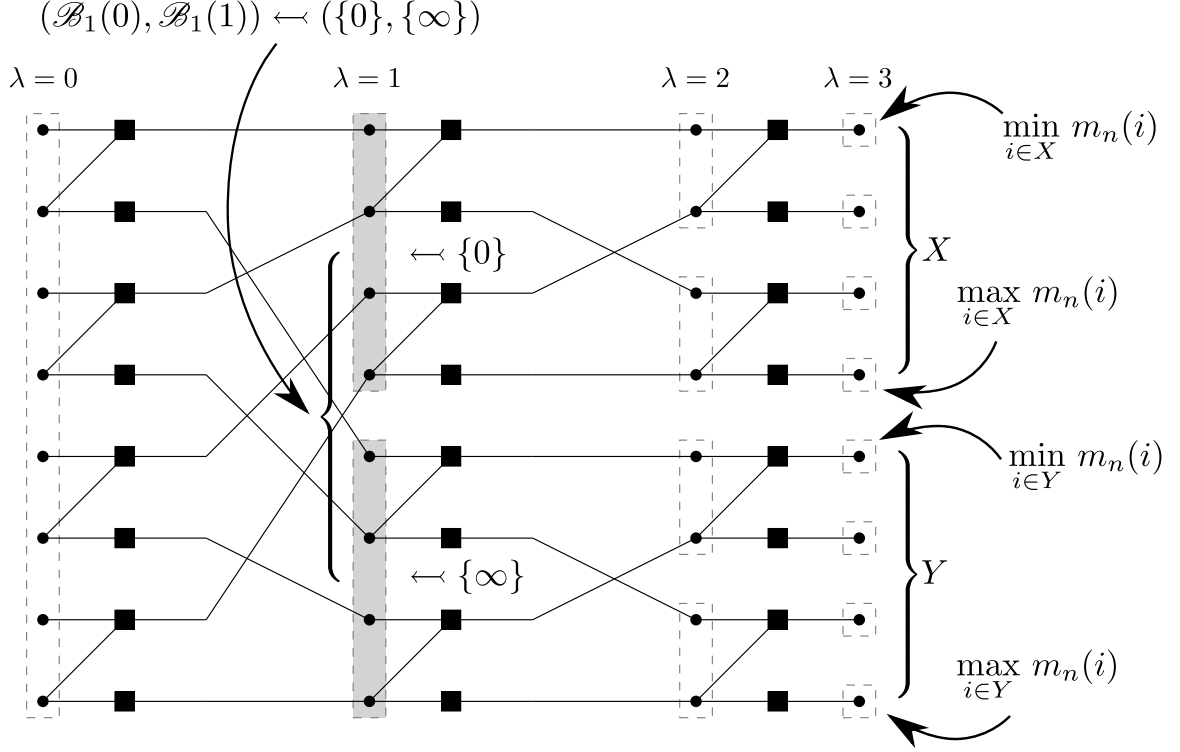


Figure 4.2: The notation used in the proof of Theorem 4.2 is explained.

We can equivalently write (4.7) as

$$m_n(i) \geq m_n(j), \quad \text{for any } i \in X, j \in Y,$$

which implies

$$\min_{i \in X} m_n(i) \geq \max_{j \in Y} m_n(j). \quad (4.8)$$

By repeated application of Lemma 4.2, we can easily show that

$$\begin{aligned} \min_{i \in X} m_n(j) &= m_n(2^{(n-k)}(2\phi)) \\ &= g^{o(n-k+1)}(m_{k-1}(\phi)), \end{aligned}$$

and

$$\begin{aligned} \max_{j \in Y} m_n(i) &= m_n(2^{(n-k)}(2\phi + 2) - 1) \\ &= 2^{(n-k+1)}m_{k-1}(\phi), \end{aligned}$$

where $g^{o(j)}$ denotes the j -times application of the function $g(x)$. So, (4.8) becomes,

$$g^{o(n-k+1)}(m_{k-1}(\phi)) \geq 2^{(n-k+1)}m_{k-1}(\phi).$$

But from repeated application of Lemma 4.2 on $m_{k-1}(\phi)$, we have

$$g^{o(n-k+1)}(m_{k-1}(\phi)) < 2^{(n-k+1)}m_{k-1}(\phi).$$

Therefore, our original assumption is wrong, and no such case exists.

2. Case 2: Let us contrary assume that two consecutive $\mathcal{B}_\lambda(2\phi)$ and $\mathcal{B}_\lambda(2\phi + 1)$ exist such that $(\mathcal{B}_k(2\phi), \mathcal{B}_k(2\phi + 1)) \leftarrow (\{0\}, \{\mathbb{R}\})$, for some $\phi \in \{0, 1, 2, \dots, 2^{k-1} - 1\}$. This implies that all the bits in X and at least one bit in Y are free bits, where X and Y are as defined in (4.4) and (4.5). Equivalently,

$$m_n(i) \geq m_n(j), \text{ for any } i \in X, \text{ at least one } j \in Y,$$

which implies

$$\min_{i \in X} m_n(i) \geq \min_{j \in Y} m_n(j). \quad (4.9)$$

By repeated application of Lemma 4.2, we can easily show that

$$\begin{aligned} \min_{i \in X} m_n(i) &= m_n(2^{(n-k)}(2\phi)) \\ &= g^{o(n-k)}(m_k(2\phi)), \end{aligned}$$

and

$$\begin{aligned} \min_{j \in Y} m_n(i) &= m_n(2^{(n-k)}(2\phi + 1)) \\ &= g^{o(n-k)}(m_k(2\phi + 1)), \end{aligned}$$

where $g^{o(j)}$ denotes the j -times application of the function $g(x)$. So, (4.9) becomes,

$$g^{o(n-k)}(m_k(2\phi)) \geq g^{o(n-k)}(m_k(2\phi + 1)).$$

Since $g(\cdot)$ is a monotonically increasing function and $m_k(2\phi + 1) > m_k(2\phi)$, we have

$$g^{o(n-k)}(m_k(2\phi)) < g^{o(n-k)}(m_k(2\phi + 1)),$$

that is a contradiction. Hence, no such case exists.

3. Case 3: Let us contrary assume that two consecutive $\mathcal{B}_\lambda(2\phi)$ and $\mathcal{B}_\lambda(2\phi + 1)$ exist such that $(\mathcal{B}_k(2\phi), \mathcal{B}_k(2\phi + 1)) \leftarrow (\{\mathbb{R}\}, \{\{\infty\}\})$, for some $\phi \in \{0, 1, 2, \dots, 2^{k-1} - 1\}$. This implies that at least one bit in X is a free bit, and all the bits in Y are fixed bits, where X and Y are as defined in (4.4) and (4.5). Equivalently,

$$\max_{i \in X} m_n(i) \geq \max_{j \in Y} m_n(j). \quad (4.10)$$

By repeated application of Lemma 4.2, we can easily show that

$$\begin{aligned} \max_{i \in X} m_n(i) &= m_n(2^{(n-k)}(2\phi + 1) - 1) \\ &= 2^{n-k}(m_k(2\phi)), \end{aligned}$$

and

$$\begin{aligned} \max_{j \in Y} m_n(i) &= m_n(2^{(n-k)}(2\phi + 2) - 1) \\ &= 2^{n-k}(m_k(2\phi + 1)). \end{aligned}$$

So, (4.10) becomes,

$$2^{n-k}(m_k(2\phi)) \geq 2^{n-k}(m_k(2\phi + 1)).$$

Since $m_k(2\phi + 1) > m_k(2\phi)$, we have

$$2^{n-k}(m_k(2\phi)) < 2^{n-k}(m_k(2\phi + 1)),$$

that is a contradiction. Hence, no such case exists. □

Example 4.1. Consider a polar code with $\mathcal{I}^c = \{0, 1, 2, 4\}$ and $N = 8$, constructed using the method of [1] for the AWGN channel with design $E_b/N_0 = 2$ dB. Figure 4.3 shows the structure of the factor graph for this construction. The code has the following group patterns:

1. $(\mathcal{B}_1(0), \mathcal{B}_1(1)) \leftarrow (\mathbb{R}, \mathbb{R})$.
2. $(\mathcal{B}_2(0), \mathcal{B}_2(1)) \leftarrow (\{\infty\}, \mathbb{R})$,
 $(\mathcal{B}_2(2), \mathcal{B}_2(3)) \leftarrow (\mathbb{R}, \{0\})$.

3. $(\mathcal{B}_3(0), \mathcal{B}_3(1)) \leftarrow (\{\infty\}, \{\infty\}),$
 $(\mathcal{B}_3(2), \mathcal{B}_3(3)) \leftarrow (\{\infty\}, \{0\}),$
 $(\mathcal{B}_3(4), \mathcal{B}_3(5)) \leftarrow (\{\infty\}, \{0\}),$
 $(\mathcal{B}_3(6), \mathcal{B}_3(7)) \leftarrow (\{0\}, \{0\}).$

It is clear that none of the group patterns described in Theorem 4.2 is present in the list above.

Corollary 4.1. For any $\lambda \in \{0, \dots, n\}$, $\phi \in \{0, \dots, 2^\lambda - 1\}$,

$$\mathcal{B}_\lambda(\phi) \leftarrow \eta, \quad \eta \in \{\{\infty\}, \{0\}, \mathbb{R}\}.$$

Proof. We prove this corollary by induction. The corollary is trivially true for the base case of $\lambda = n$ as the size of the groups is one. Suppose the corollary is true for $\lambda = k$, and we need to show that the corollary holds for $\lambda = k - 1$. We observe from the factor graph in Figure 4.1 that two consecutive $\mathcal{B}_\lambda(2\phi)$ and $\mathcal{B}_\lambda(2\phi + 1)$ combine to produce output in $\mathcal{B}_\lambda(\lfloor \phi/2 \rfloor)$. Therefore, the cases in which $\mathcal{B}_\lambda(\lfloor \phi/2 \rfloor)$ will have mixed values are:

1. $(\mathcal{B}_k(2\phi), \mathcal{B}_k(2\phi + 1)) \leftarrow (\{0\}, \{\infty\}).$
2. $(\mathcal{B}_k(2\phi), \mathcal{B}_k(2\phi + 1)) \leftarrow (\{0\}, \mathbb{R}).$
3. $(\mathcal{B}_k(2\phi), \mathcal{B}_k(2\phi + 1)) \leftarrow (\{\mathbb{R}\}, \{\infty\}).$

Since from Theorem 4.2, these cases are not possible, all the $\mathcal{B}_\lambda(\phi)$ will either have real values or will stick to ∞ or zero. □

Equivalently, Corollary 4.1 says that all $\mathcal{B}_\lambda(\phi)$ will either have real values or will stick to zero or ∞ for the entire decoding process. It specifically removes the possibility of any $\mathcal{B}_\lambda(\phi)$ having mixed values such as from the set $\{0, \infty\}$.

Corollary 4.2. For any $\lambda \in \{0, \dots, n\}$ and $\phi \in \{0, \dots, 2^\lambda - 1\}$, given $\mathcal{B}_\lambda(\phi) \leftarrow \eta$, where $\eta \in \{\{0\}, \{\infty\}\}$ then

$$\mathcal{B}_\lambda(\phi) \leftarrow \begin{cases} \{\infty\} & \text{if } \phi \text{ is even and } \mathcal{B}_\lambda(\phi + 1) \not\leftarrow \{\infty\}, \\ \{0\} & \text{if } \phi \text{ is odd and } \mathcal{B}_\lambda(\phi - 1) \not\leftarrow \{0\}. \end{cases}$$

Proof. Assume on the contrary that for some even ϕ , $\mathcal{B}_\lambda(\phi) \leftarrow \{0\}$. From Theorem 4.2, Case 1 and Case 2 are not possible when ϕ is even. Thus, $\mathcal{B}_\lambda(\phi) \leftarrow \{\infty\}$. The proof for ϕ odd is similar and is omitted. \square

Corollary 4.3. Consider $\mathcal{B}_\lambda(\phi)$ for any $\lambda \in \{1, \dots, n\}$ with $\mathcal{B}_\lambda(\phi) \leftarrow \eta$, where $\eta \in \{\{0\}, \{\infty\}\}$. For even values of ϕ , if $\mathcal{B}_\lambda(\phi + 1) \not\leftarrow \eta$ then

$$\mathcal{B}_\lambda(\phi + 1) \leftarrow \begin{cases} \mathbb{R} & \text{if } 2^{n-\lambda}(\phi + 1) \in \mathcal{I}^c, \\ \{0\} & \text{otherwise,} \end{cases}$$

whereas for odd values of ϕ , if $\mathcal{B}_\lambda(\phi - 1) \not\leftarrow \eta$ then

$$\mathcal{B}_\lambda(\phi - 1) \leftarrow \begin{cases} \{\infty\} & \text{if } 2^{n-\lambda}\phi - 1 \in \mathcal{I}^c, \\ \{\mathbb{R}\} & \text{otherwise.} \end{cases}$$

Proof. Consider any $\mathcal{B}_\lambda(\phi) \leftarrow \eta$, where $\eta \in \{\{0\}, \{\infty\}\}$. For even values of ϕ , from Corollary 4.2, we know that $\mathcal{B}_\lambda(\phi) \leftarrow \{\infty\}$ or $\mathcal{B}_\lambda(\phi) \leftarrow \mathbb{R}$. Suppose if $\mathcal{B}_\lambda(\phi) \leftarrow \{\infty\}$ then

$$\mathcal{B}_\lambda(\phi + 1) \leftarrow \{0\} \iff Y \subset \mathcal{I} \implies 2^{n-\lambda}(\phi + 1) \in \mathcal{I},$$

where $Y = \{2^{n-\lambda}(\phi + 1), \dots, 2^{n-\lambda}(\phi + 2) - 1\}$.

Now suppose if $\mathcal{B}_\lambda(\phi) \leftarrow \mathbb{R}$, then at least one element of Y should belong to \mathcal{I} , where Y is as defined above. Equivalently, by repeated application of Lemma 4.2,

$$\arg \min_{i \in Y} m_n(i) = 2^{n-\lambda}(\phi + 1) \in \mathcal{I}^c.$$

Similarly, for odd values of ϕ the proof is similar and is omitted. \square

Example 4.2. Consider the construction of polar code in Figure 4.3. Since $\mathcal{B}_2(0) \leftarrow \{\infty\}$ and $\mathcal{B}_2(1) \not\leftarrow \{\infty\}$ with $\phi = 0$ being even, the conditions in Corollary 4.3 are satisfied. To know whether $\mathcal{B}_2(1) \leftarrow \{0\}$ or $\mathcal{B}_2(1) \leftarrow \mathbb{R}$, we only need to check if $2^{n-\lambda}(\phi + 1) = 2^{3-2}(0+1) = 2 \in \mathcal{I}^c$. In this example, u_2 is a fixed bit and therefore according to Corollary 4.3, $\mathcal{B}_2(1) \leftarrow \mathbb{R}$.

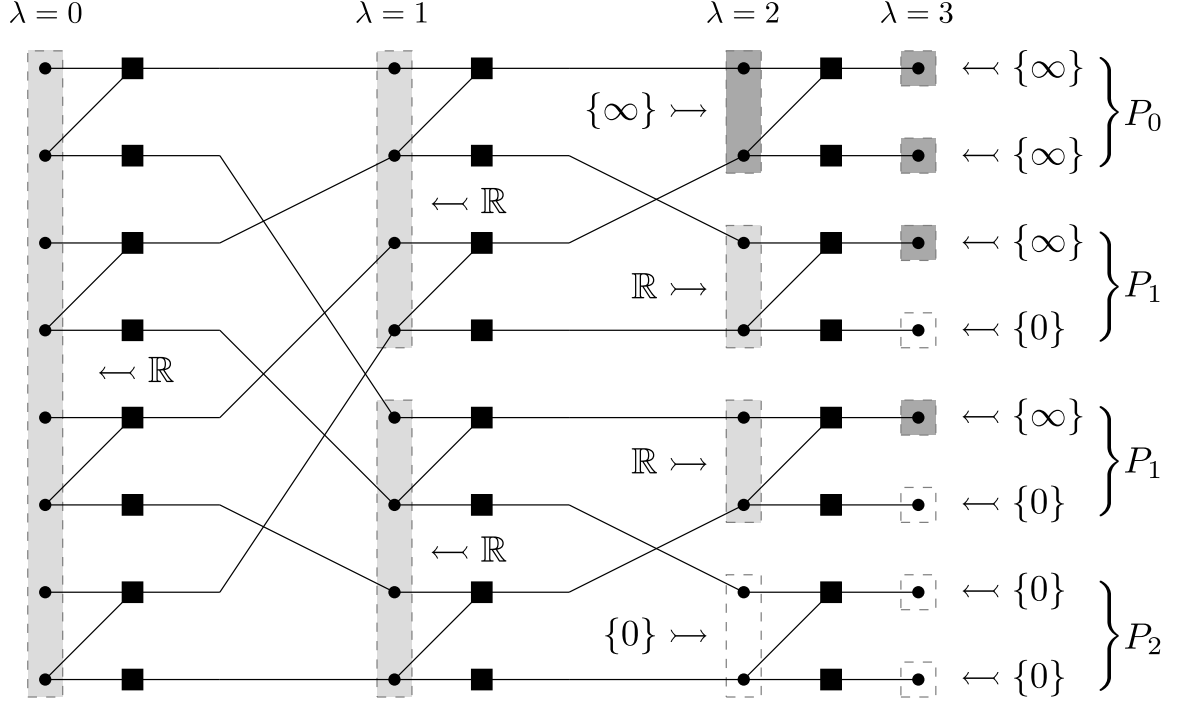


Figure 4.3: An example design of a rate one-half polar code validates the properties. Only protographs P_0, P_1 and P_2 appear at depth $\lambda = n$ (Special Prohibited Pairs Property). In the entire factor graph, P_6, P_7 and P_8 do not occur (General Prohibited Pairs Property). All the node-groups have LLRs from either of the sets $\{\{0\}, \{\infty\}, \mathbb{R}\}$ (Corollary 4.1).

4.2 Discussion on the Properties of Polar Codes

In this section, we discuss the rationale behind the properties derived in Section 4.1. Figure 4.4 shows all the protographs in Table 2 except P_0 and P_1 , along with their reduced forms, which are similar to the ones presented by Forney [26] in the context of Reed Muller codes. The reduced forms of protographs in Table 2 emerge from the values of LLRs in B corresponding to the nodes on the right-hand side of these protographs.

For example, consider P_1 in Figure 4.4. By using $B_\lambda(\phi - 1, \omega) = \infty$ and $B_\lambda(\phi, \omega) = 0$ in (3.5), we get

$$B_\lambda(\psi, 2\omega) = L_\lambda(\psi, 2\omega + 1),$$

$$B_\lambda(\psi, 2\omega + 1) = L_\lambda(\psi, 2\omega).$$

The aforementioned equations correspond to the reduced form of P_1 shown below the

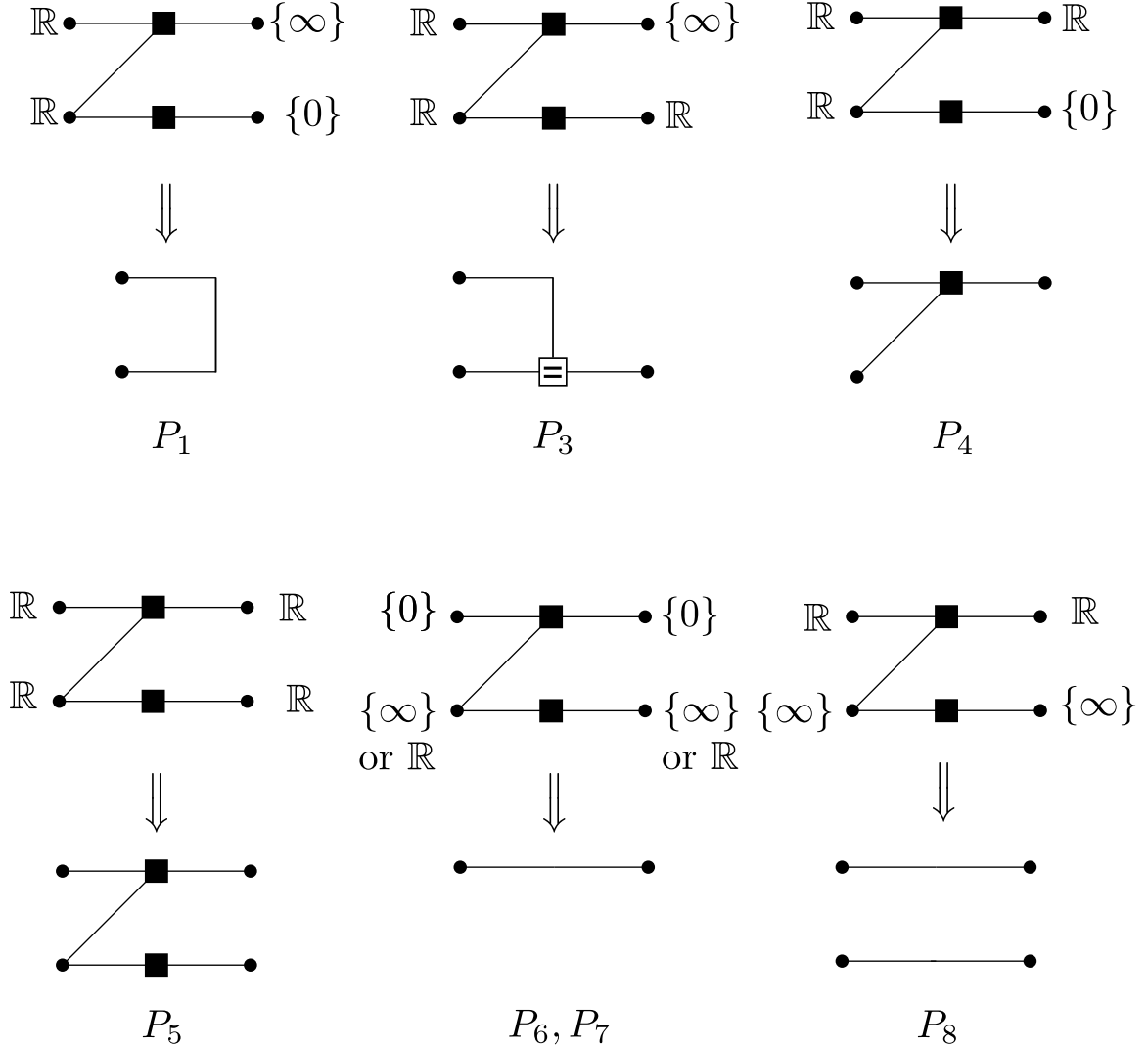


Figure 4.4: Every type of protograph has an equivalent reduced form.

protograph in Figure 4.4. In words, the equations show that in this protograph, two values corresponding to $L_\lambda(\phi - 1, 2\omega)$ and $L_\lambda(\phi - 1, 2\omega + 1)$ go as they are in B but in swapped locations. It is noteworthy here that LLRs in L always come from \mathbb{R} and there is no guarantee that these LLRs will stick to either ∞ or zero for the entire decoding process. Since B in this protograph gets values from L , the output of the protograph shows \mathbb{R} on both the left nodes.

The reduced forms for P_3 and P_4 are an equality check code and a parity check code, respectively. P_5 is equivalent to two parity checks (note that the bottom parity check is equivalent to an equality check). Each of P_1, P_3, P_4 and P_5 takes part in error correction

or checking, whereas P_0 and P_2 yield P_1, P_3, P_4 and P_5 under the general prohibited pair property. Therefore, $P_i, i \in \{0, 1, \dots, 5\}$ give rise to the error-correction capability of polar codes.

In contrast to P_i for $i \in \{0, 1, \dots, 5\}$, P_6 and P_7 result in the loss of a dimension. The reduced forms of both of P_6 and P_7 are equivalent to two *short-circuited* upper nodes. In the reduced form of P_8 , both upper and lower pair of nodes are *short circuited* with no error-correction capability. In this context, we can easily conclude that the construction of [4] and [1] discourage the ineffective protograph formations of P_6, P_7 and P_8 .

4.3 A High-Throughput, Low-Complexity Soft-Output Decoder for Polar Codes

In applications requiring large block lengths, design constraints other than error-rate performance become stringent. The design constraints include latency, computational complexity and storage requirement of the decoder. The latency of the decoder dictates its throughput, whereas the higher computational complexity and storage requirement of the decoder in general, result in higher power and area utilization in the hardware implementation [7]. In this section, we apply the structural properties of polar codes discussed in the previous section by proposing a memory-efficient extension of the SSC principle to the SCAN decoder, called the enhanced SCAN (eSCAN) decoder.

We first demonstrate that like the SSC decoder, we can skip rate-one and rate-zero subcodes in the SCAN decoder as well, and that the properties of polar codes can be used to locate these subcodes using only \mathcal{I} . This straightforward extension results in a computation complexity and latency reduction as discussed in [11]. We then demonstrate that by using the properties of polar codes discussed in Section 4.1, we can reduce the memory utilization of the decoder in addition to the reduction in computational complexity and latency by the application of the SSC principle. Memory utilization in the SC or the SSC decoder is not an issue, because memory for already detected bits (in the detection order of the SC decoder) in the factor graph is binary valued, and any further reduction or optimization will not reduce the overall memory budget of the SC decoder. On the other hand, in the SCAN decoder memory for both L and B is real valued, and memory reduction

in general, will reduce area utilization and power consumption of the decoder.

Consider the basic decision element on the top-right corner in Figure 4.1. The SC (or SSC) decoder processes these decision elements locally, throughout the factor graph using (2.12), (2.13), (2.14), (2.15) and (2.16). If both the values $B_\lambda(\phi, \omega)$ and $B_\lambda(\phi - 1, \omega)$ are zero for some ϕ and ω (signifying that these are free bits with no prior information about their values), $B_{\lambda-1}(\psi, 2\omega)$ and $B_{\lambda-1}(\psi, 2\omega + 1)$ will remain zero for all the iterations of the decoder. Similarly, if both the values $B_\lambda(\phi, \omega)$ and $B_\lambda(\phi - 1, \omega)$ represent fixed bits with LLRs ∞ , $B_{\lambda-1}(\psi, 2\omega)$ and $B_{\lambda-1}(\psi, 2\omega + 1)$ will stick to ∞ for all the iterations of the decoder. We can greatly reduce the complexity and latency of the decoder if we skip processing on these rate-one and rate-zero subcodes as discussed in [11]. We first show how we can apply the SSC principle to the SCAN decoder described in Algorithm 3.4, 3.5 and 3.6 with the help of the properties discussed in the previous section, and then propose a memory reduction strategy.

Algorithms 4.1 describes the wrapper for all the low-level functions of the eSCAN decoder with LLR skipping. In case of a rate-one or rate-zero subcode, the algorithm calculates the subcode's length ℓ and calls Algorithm 4.4 to fix $\mathcal{B}_\lambda(\phi)$ with $\lambda = n - \log_2(\ell)$ to either zero or ∞ . Corollary 4.2 helps the decoder by fixing $\mathcal{B}_\lambda(\phi)$ to ∞ and 0 for ϕ even and odd, respectively. Algorithms 4.1 calls Algorithm 4.2 and 4.3 for rate one-half subcodes, where we need $\mathcal{O}_\lambda(\phi + 1)$ and $\mathcal{E}_\lambda(\phi - 1)$ to update $\mathcal{L}_\lambda(\phi)$ for ϕ even and odd, respectively. To update $\mathcal{L}_\lambda(\phi)$ for ϕ even, the decoder needs to figure out if $\mathcal{O}_\lambda(\phi + 1) \leftarrow \mathbb{R}$ or $\mathcal{O}_\lambda(\phi + 1) \leftarrow \{0\}$. Apparently, it seems that the decoder needs tracking of the fixed blocks for all depths $\lambda \in \{1, \dots, n\}$. According to Corollary 4.3, the decoder only needs to check if $2^{n-\lambda}(\phi + 1)$ th node belongs to the fixed bits. Similarly, for ϕ odd, the decoder can distinguish between the cases of $E_\lambda(\phi - 1, \omega) \leftarrow \{\infty\}$ or \mathbb{R} by checking if $(2^{n-\lambda}\phi - 1)$ th node belongs to the fixed or the free bits, respectively.

To understand the need for memory reduction in the SCAN decoder, consider the operation of the SSC decoder on the factor graph in Figure 4.3. The SSC decoder has only one iteration (similar to the SC decoder) and does not need to retain any information from previous iterations. The authors in [5] showed that the memory required at any depth

Algorithm 4.1: Low-complexity low-latency eSCAN decoder

Data: LLRs from channel
Result: $\mathcal{B}_0(0)$

```

1   $j \leftarrow 0$ 
2  for  $k = 1 \rightarrow J$  do
3    for  $i = 0 \rightarrow (N - 1)$  do
4      if  $i$  belongs to rate-one or rate-zero subcode then
5         $j \leftarrow j + 1$ 
6        if  $i$  is the last node of the subcode then
7           $\zeta \leftarrow (n - \log(j))$ 
8           $\psi \leftarrow i/j$ 
9           $j \leftarrow 0$ 
10         fixblock( $\zeta, \psi$ )
11        end
12      end
13      else
14        if  $i$  is odd then
15          updatellrmap( $n - 1, \lfloor i/2 \rfloor$ )
16           $B_{n-1}(\lfloor i/2 \rfloor, 1) \leftarrow L_{n-1}(\lfloor i/2 \rfloor, 0)$ 
17           $B_{n-1}(\lfloor i/2 \rfloor, 0) \leftarrow L_{n-1}(\lfloor i/2 \rfloor, 1)$ 
18          updatebitmap( $n - 1, \lfloor i/2 \rfloor$ )
19        end
20      end
21    end
22 end

```

λ for B in the SC (or the SSC) is $2^{(n-\lambda+1)}$, i.e., the memory required for two $\mathcal{B}_\lambda(\phi)$. For example, the SSC decoder only needs $\mathcal{B}_2(0)$ and $\mathcal{B}_2(1)$ for the operation at depth $\lambda = 2$. Therefore, there is no memory requirement issue in the SSC decoder, because it already uses a small number of memory elements at a depth λ . Additionally, since the memory for B is of boolean type, any further optimization (if possible) will not have a significant impact on the overall memory budget.

In case of the SCAN decoder, we have to pass on information in some of the memory elements from one iteration to the other. The information passed on from one iteration to the next is of real type, and can significantly impact the decoder's memory budget. In the memory-efficient SCAN decoder discussed in Section 3.2, we divided the memory for B in $E = \{\mathcal{B}_\lambda(\phi) : \phi \text{ is even}\}$ and $O = \{\mathcal{B}_\lambda(\phi) : \phi \text{ is odd}\}$. We further showed that only O is required from one iteration to the other of the SCAN decoder, and E can be optimized

Algorithm 4.2: updatellrmap(λ, ϕ)

```
1 if  $\lambda = 0$  then return
2  $\psi \leftarrow \lfloor \frac{\phi}{2} \rfloor$ 
3  $j \leftarrow 2^{n-\lambda}(\phi + 1)$ 
4  $k \leftarrow 2^{n-\lambda}(\phi) - 1$ 
5 if  $\phi$  is even then updatellrmap( $\lambda - 1, \psi$ )
6 for  $\omega = 0 \rightarrow (2^{n-\lambda} - 1)$  do
7   if  $\phi$  is even then
8      $\alpha \leftarrow L_{\lambda-1}(\psi, 2\omega + 1)$ 
9     if  $j \in \mathcal{J}^c$  then  $\alpha \leftarrow \alpha + O_{\lambda}(\phi + 1, \omega)$ 
10     $L_{\lambda}(\phi, \omega) \leftarrow L_{\lambda-1}(\psi, 2\omega) \boxplus \alpha$ 
11  end
12  else
13     $\alpha \leftarrow L_{\lambda-1}(\psi, 2\omega)$ 
14    if  $k \in \mathcal{J}$  then  $\alpha \leftarrow \alpha \boxplus E_{\lambda}(\phi - 1, \omega)$ 
15     $L_{\lambda}(\phi, \omega) \leftarrow L_{\lambda-1}(\psi, 2\omega + 1) + \alpha$ 
16  end
17 end
```

Algorithm 4.3: updatebitmap(λ, ϕ)

```
1  $\psi \leftarrow \lfloor \frac{\phi}{2} \rfloor$ 
2  $k \leftarrow 2^{n-\lambda}(\phi) - 1$ 
3 if  $\phi$  is odd then
4   for  $\omega = 0 \rightarrow (2^{n-\lambda} - 1)$  do
5      $\alpha \leftarrow O_{\lambda}(\phi, \omega) + L_{\lambda-1}(\psi, 2\omega + 1)$ 
6      $\beta \leftarrow L_{\lambda-1}(\psi, 2\omega)$ 
7     if  $k \in \mathcal{J}$  then
8        $\alpha \leftarrow \alpha \boxplus E_{\lambda}(\phi - 1, \omega)$ 
9        $\beta \leftarrow \beta \boxplus E_{\lambda}(\phi - 1, \omega)$ 
10    end
11     $\beta \leftarrow \beta + O_{\lambda}(\phi, \omega)$ 
12    if  $\psi$  is even then
13       $E_{\lambda-1}(\psi, 2\omega) \leftarrow \alpha$ 
14       $E_{\lambda-1}(\psi, 2\omega + 1) \leftarrow \beta$ 
15    end
16    else
17       $O_{\lambda-1}(\psi, 2\omega) \leftarrow \alpha$ 
18       $O_{\lambda-1}(\psi, 2\omega + 1) \leftarrow \beta$ 
19    end
20  end
21 if  $\psi$  is odd then updatebitmap( $\lambda - 1, \psi$ )
22 end
```

Algorithm 4.4: fixblock(λ, ϕ)

```

1  $\psi \leftarrow \lfloor \frac{\phi}{2} \rfloor$ 
2 if  $\phi$  is even then
3    $\mathcal{E}_\lambda(\phi) \leftarrow \infty$ 
4   updatellrmap( $\lambda - 1, \psi$ );
5 end
6 else
7   for  $\omega = 0 \rightarrow (2^{n-\lambda} - 1)$  do
8      $\alpha \leftarrow E_\lambda(\phi - 1, \omega) \boxplus L_{\lambda-1}(\psi, 2\omega + 1)$ 
9      $\beta \leftarrow E_\lambda(\phi - 1, \omega) \boxplus L_{\lambda-1}(\psi, 2\omega)$ 
10    if  $\psi$  is even then
11       $E_{\lambda-1}(\psi, 2\omega) \leftarrow \alpha$ 
12       $E_{\lambda-1}(\psi, 2\omega + 1) \leftarrow \beta$ 
13    end
14    else
15       $O_{\lambda-1}(\psi, 2\omega) \leftarrow \alpha$ 
16       $O_{\lambda-1}(\psi, 2\omega + 1) \leftarrow \beta$ 
17      if  $\lambda \geq 2$  then updatebitmap( $\lambda - 1, \psi$ )
18    end
19  end
20 end

```

by overwriting. Now we explain how we can optimize $O = \{\mathcal{B}_\lambda(\phi) : \phi \text{ is odd}\}$ as well by observing that there are only a few memory elements at any depth λ in B of type real, and rest of the memory is of boolean type. For example, the seven greyed ϕ -groups correspond to O in the factor graph shown in Figure 4.5 as their ϕ indices are all odd. Out of the seven ϕ -groups, only $\mathcal{B}_1(1)$ and $\mathcal{B}_2(1)$ carry real values in decoding process. We can save memory by not storing LLRs of the ϕ -groups corresponding to rate-zero and rate-one codes, but by not storing some LLRs on different depths of the factor graph, we require different memory sizes for O on different depths. Therefore, the decoder cannot use the memory addressing (3.9) proposed for O in Chapter 3, which assumes $N/2$ memory elements on all the depths $\lambda \in \{1, \dots, n\}$, and therefore, requires a memory of total size $nN/2$.

To skip $\mathcal{O}_\lambda(\phi)$ belonging to rate-zero and rate-one codes, we propose the following variable-offset memory addressing technique. Let F_λ be the number of nodes at depth λ for which $\mathcal{B}_\lambda(\phi) \leftarrow \mathbb{R}$. In this notation, the SCAN decoder needs a memory of size $F = \sum_{\lambda=1}^n F_\lambda$ to store real LLRs in O . To distinguish among the memory locations corresponding

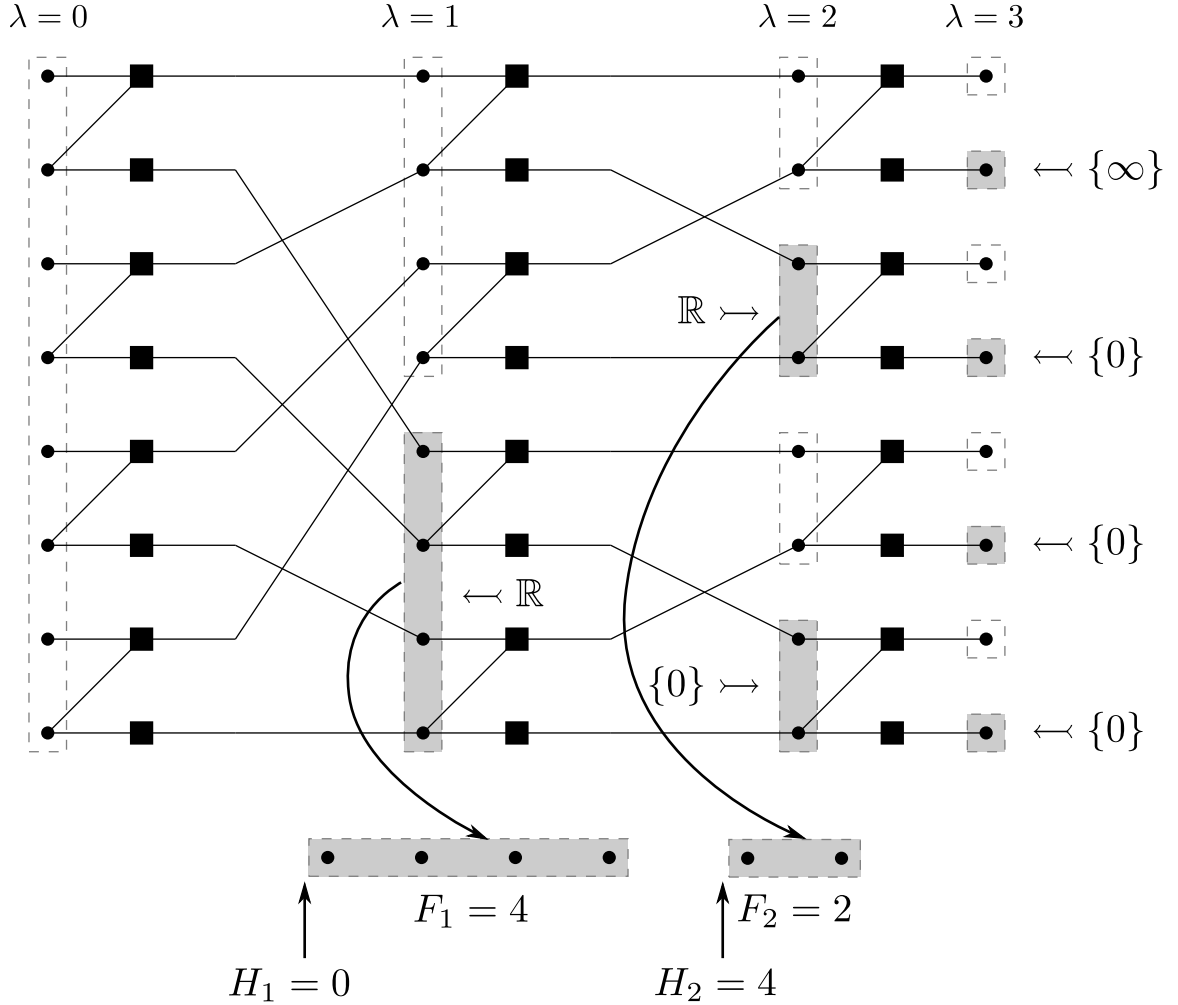


Figure 4.5: The memory required for O is reduced by not storing the LLRs corresponding to rate-one and rate-zero subcodes.

to different depths of the factor graph, we define n memory offset values $H_\lambda = \sum_{i=1}^{\lambda-1} F_i$, for $\lambda \in \{1, \dots, n\}$, corresponding to each portion in the memory of size F_λ . The values of H_λ depend on the construction of polar code and are fixed for a given set of free bits \mathcal{S} .

Figure 4.5 shows an example of the memory reduction in the case of a polar code of length eight. The decoder only need to store $\mathcal{B}_1(1)$ and $\mathcal{B}_2(1)$ of lengths four and two, respectively. Therefore, the size of the memory required by O is only six instead of 12 required for O without the optimization, highlighting a 50% decrease in the required memory in this example.

We have addressed the start of memory location for an individual depth in the factor graph using H_λ . The last step in the addressing technique is to specify how we will address

each memory node on a particular offset H_λ in the memory for O . From Lemma 1 in [27], we know that at any depth λ , the SCAN decoder reads from and writes to B traversing the nodes in increasing order. Therefore, we can use two counters at every depth λ to address $\{\mathcal{B}_\lambda(\phi) : \phi \text{ is odd}\}$: one counter for the write and one for the read operations. The counters are incremented each time the decoder writes to or reads from the memory for a particular node. This completes the implementation of the eSCAN decoder with SSC principle and reduced memory requirement.

4.4 Latency and Complexity Analysis

Figure 4.6 shows the normalized values of the number of computations, memory and latency of the eSCAN decoder with respect to the SCAN decoder of Chapter 3 for a block length $N = 32768$. We have constructed polar codes using the method in [1] for design $E_b/N_0 = 2^{2R} - 1$. For analysis, we have assumed that *eSCAN* has $N/2$ processing elements with each capable of implementing both (3.3), (3.4) and (3.5), (3.6) in τ clock cycles. Additionally, we have assumed that fixing of a block $\mathcal{B}_\lambda(\phi)$ with ϕ even occurs instantly.

Under these assumptions, the update in any $\mathcal{L}_\lambda(\phi)$ or $\mathcal{B}_\lambda(\phi)$ takes τ clock cycles implying that the latency of one iteration of the eSCAN decoder equals τ times the number of $\mathcal{L}_\lambda(\phi)$ and $\mathcal{B}_\lambda(\phi)$ the decoder updates. In any iteration, the decoder updates $2N - 2$ times in L and $N - 1$ times in B with total clock cycles of $(3N - 3)\tau$, significantly higher than $(2N - 2)\tau$ for the SC decoder. Fortunately, the eSCAN decoder can compute $\mathcal{L}_n(i)$, $\mathcal{L}_n(i + 1)$, $\mathcal{B}_{n-1}(\lfloor i/2 \rfloor)$ for i even in parallel, unlike the SC decoder that computes them in 2τ clock cycles. The parallel computation of LLRs in parallel reduces the number of updates in $\mathcal{L}_\lambda(\phi)$ to $N - 2$, and as a result the total number of clock cycles to $(2N - 3)\tau$: slightly less than $(2N - 2)\tau$ required for the SC decoder.

We computed the latency of the eSCAN decoder by subtracting the number of $\mathcal{L}_\lambda(\phi)$ and $\mathcal{B}_\lambda(\phi)$ corresponding to rate-one and rate-zero subcodes from $2N - 3$. We observe in Figure 4.6 that for a polar code of length 32768, the normalized latency stays below 0.2 for all rates: a significant 80% reduction in the latency. Specifically, for the rate-0.7 code the normalized latency decreases to approximately 0.14 which is 86% reduction in latency with

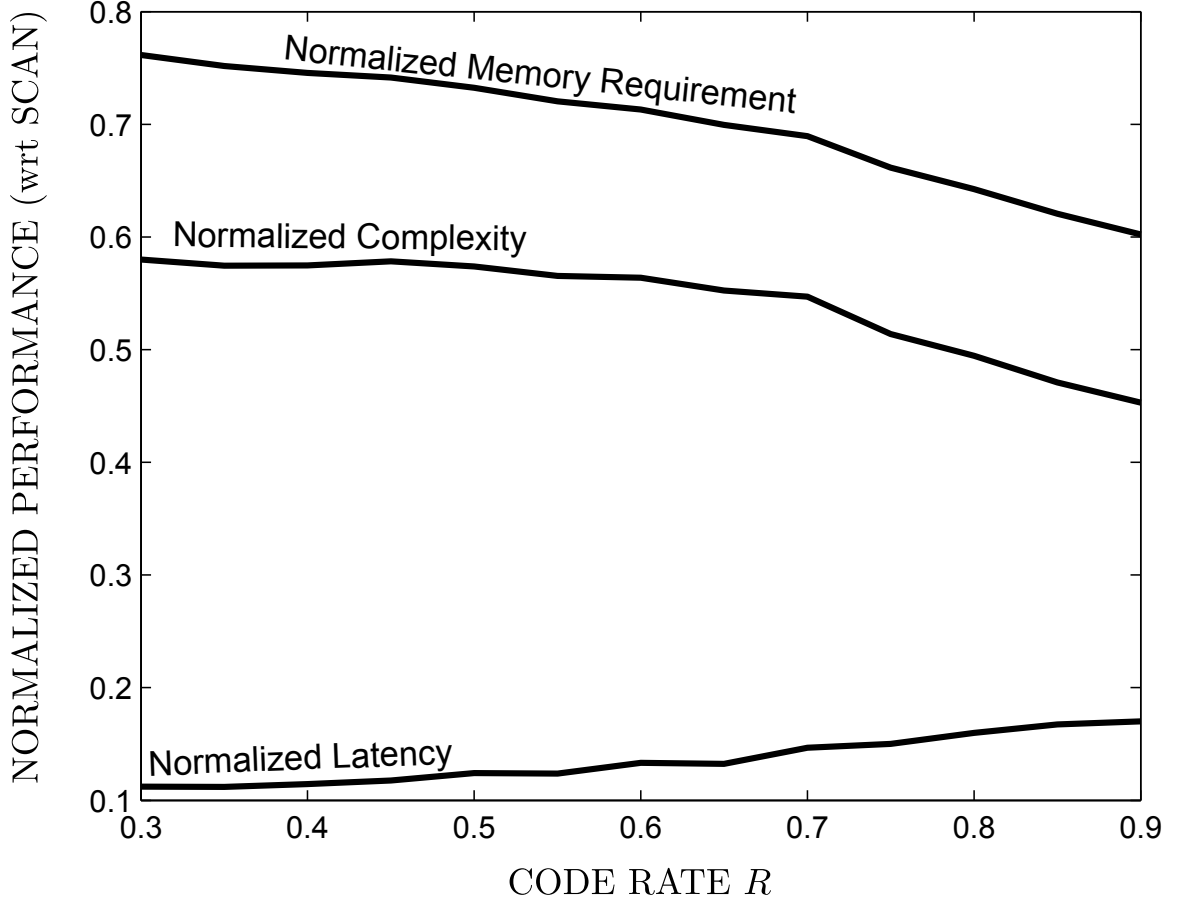


Figure 4.6: The normalized number of computations, memory requirement and latency of the eSCAN decoder with LLR-skipping stays less than those of the SCAN decoder without LLR-skipping for a range of code rates.

respect to the latency of the SCAN decoder in Chapter 3.

The normalized complexity of the eSCAN decoder can be calculated by counting number of operations required for the nodes with $\mathcal{B}_\lambda(\phi) \leftrightarrow \mathbb{R}$. Figure 4.6 shows the decrease in the normalized complexity of the eSCAN decoder in comparison with the SCAN decoder as described in Chapter 3. For rates greater than 0.7, it stays below 0.59 and approaches 0.45 for rates near 0.9 that is less than half the complexity of the SCAN decoder.

The normalized memory requirement of the eSCAN decoder with proposed memory reduction for O with respect to the SCAN decoder of Section 3.2 decreases with increasing rate of the code and goes as low as 0.6, highlighting almost 40% reduction in memory requirement.

Figure 4.7 shows the complexity versus power trade-off for different decoders of polar

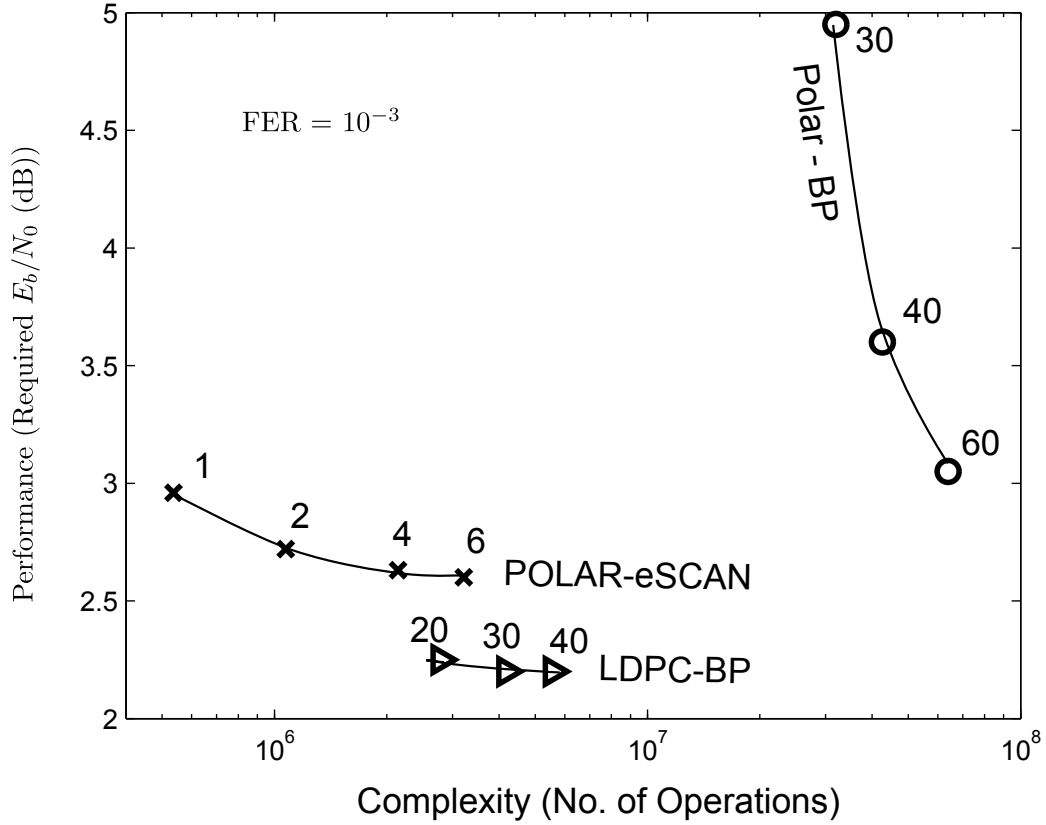


Figure 4.7: The polar code with eSCAN decoding has approximately the same complexity/power trade-off trend as the LDPC code with BP decoding. However, polar codes require approximately 0.4 dB higher E_b/N_0 to achieve the same frame error rate on the dicode channel.

and LDPC codes on the dicode channel. All the simulation conditions are the same as for Figure 2.10. The slope of the eSCAN decoder curve is approximately the same as that of the BP decoder for LDPC codes showing that unlike BP decoder for polar codes, the eSCAN decoder's performance does not vary much with increasing number of iterations and quickly saturates with only four iterations. The same slope of the curves for the eSCAN decoder and the BP decoder for LDPC codes shows that both of the decoders have the same performance versus complexity trade-off. Moreover, the eSCAN decoder with six iterations and BP decoder for LDPC codes with 30 iterations have approximately the same complexity with 0.4 dB difference in required E_b/N_0 to achieve a frame error rate of 10^{-3} .

As a final note, we mention here that the error-rate performance of the eSCAN decoder

does not change with the LLR-skipping and the proposed memory reduction, and is exactly the same, as shown in Figure 3.4.

4.5 Summary

We have proved that the polar codes constructed using density evolution for the BEC and Gaussian approximation based density evolution for the AWGN channel exhibit the *special prohibited patterns property* that prohibits certain patterns of the location of free/frozen bits. Specifically, we have shown that a free bit will never precede a fixed bit in any pair of uncoded bits. We have also proved that under the SCAN decoder, the *special prohibited patterns property* gives rise to the *general prohibited patterns property* in the entire factor graph of the polar code that allows only a few patterns of node groups to appear. As an example application, we have applied the properties in the implementation of a low-latency low-complexity SCAN decoder, called the enhanced SCAN (eSCAN) decoder for polar codes using the SSC decoder principle. The properties of the construction of polar codes buy us an extra saving in memory required using a variable-offset memory access method. Our analysis reveals that for the practical block lengths, the latency of the eSCAN decoder stays within 10% to 20% of the SCAN decoder for a range of code rates, whereas the computational complexity and the memory requirement stays within 45% to 67% and 60% to 76%, respectively. With this multifaceted (complexity, performance, latency and memory) improvement, the eSCAN decoder stands out as a promising soft-output decoder for polar codes.

CHAPTER V

OPTIMIZED POLAR CODE DESIGN FOR INTERSYMBOL INTERFERENCE CHANNELS

An effective strategy for error-control decoding over an intersymbol interference (ISI) channel is turbo equalization [6], in which the cascade of the encoder and ISI channel is viewed as a serial concatenation, and the receiver iteratively exchanges soft information between the ISI detector and decoder. In Chapter 3 and 4, we designed the soft-output decoder for polar codes that enabled polar codes in this turbo-based framework. In addition to the soft-output decoder, a turbo-based system requires codes designed for the ISI channel. While codes designed for the AWGN channel can perform adequately in this setting, better performance can be achieved when the code is specifically tailored to match the characteristics of the given ISI channel.

Code design for ISI channels has been limited to LDPC codes, and in this setting, three different strategies for code design have emerged: density evolution is used in [28] and [29], the extrinsic information transfer (EXIT) charts of ten Brink [30] are used in [31], and multistage decoding of multilevel codes is used in [32]. Although there has been much work regarding polar code design for the AWGN channel as well as soft-output decoders for polar codes based on belief propagation [33] and SCAN [34], the problem of designing good polar codes for ISI channels, to the best of our knowledge, remains unexplored in literature until now.

This chapter proposes a solution to the problem of designing polar codes for ISI channels with iterative decoding. We describe a design methodology to construct polar codes tailored for an ISI channel and with performance close to LDPC codes. Specifically, we employ the multilevel description of polar codes [1], analyze the shape of the EXIT curve under multilevel decoding, and following [30] and [31] formulate the problem of code design as one of matching the EXIT curve of the polar code with that of the ISI channel. We then

propose a graphical strategy to design the rates of different component polar codes in the multilevel description to achieve the required curve matching. We present numerical results demonstrating that the polar codes designed using our method outperform the codes designed for the AWGN channel when used over an ISI channel. For example, for the EPR4 and E2PR4 channels we observe a gain of 0.6 dB and 0.9 dB, respectively, using our designs when compared to polar codes designed for the AWGN channel.

The structure of the chapter is as follows. We introduce polar codes as generalized concatenated codes as done by Trifonov and Semenov [1] and then give a primer on EXIT charts. Then, we describe our EXIT curve analysis of polar codes in Section 5.3. Section 5.4 describes the design methodology based on the EXIT chart analysis, and in Section 5.5, we present our conclusions.

5.1 Polar Codes as Generalized Concatenated Codes

Trifonov and Semenov [1] demonstrated that polar codes are a class of generalized concatenated codes, and that successive cancellation decoding is an instance of multistage decoding.

As a special case, we can view a parent polar code of length N as the concatenation of two outer polar codes of length $N/2$ with an inner polar code of length N , as shown in Figure 5.1. Similarly, we can decode this polar code of length N using a multistage decoder in which we individually decode one of the polar codes of length $N/2$, use its output as prior input to the inner decoder, and then decode the other polar code of length $N/2$.

Figure 5.1 shows an example concatenation of two length-four outer polar codes to a rate-one inner code of length eight, constructing a parent polar code of length eight. To decode this code, we can first use any decoder (the SC or any of its variants such as the successive cancellation list decoder [5]) to decode the outer code \mathcal{C}_0 . The inner decoder uses extrinsic LLRs in $\{B_1(0, i)\}_{i=0}^{N/2}$ to compute $\{L_1(1, i)\}_{i=0}^{N/2}$, which is input to the decoder of \mathcal{C}_1 . After successful decoding of \mathcal{C}_1 , the multistage decoder uses (3.5) and (3.6) at $\lambda = 1$ to calculate $\{B_0(0, i)\}_{i=0}^N$ and completes the decoding of the parent code.

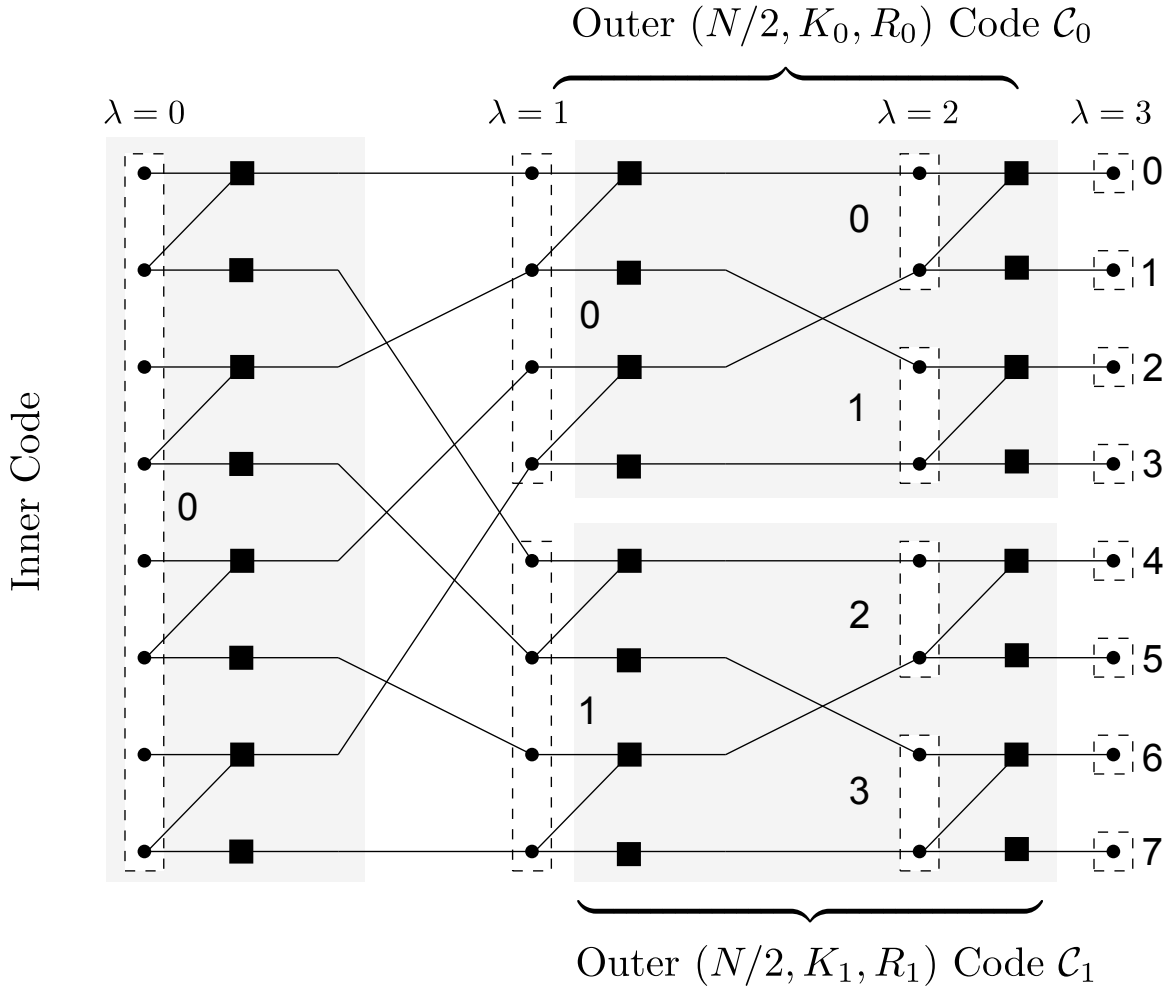


Figure 5.1: The factor graph of a parent polar code of length $N = 8$ is a concatenation of two outer codes of length four with an inner code of length eight.

5.2 An Introduction to EXIT Charts

EXIT charts provide an efficient method to design [35] and analyze [30] iterative coding schemes. In iterative decoding, the component decoders exchange extrinsic LLRs, where the extrinsic LLR is the difference between the *a posteriori* LLR and *a priori* LLR. EXIT charts track average mutual information between the extrinsic LLRs and corresponding bits throughout the decoding process. As a result, these charts provide a trajectory for the mutual information exchanged between the two decoders along with the following useful properties:

1. The decoding is successful if an *open convergence tunnel* exists between the EXIT

curves of the two decoders [30].

2. One can design efficient codes by matching the two curves of the component decoders using curve-fitting techniques [35]. The better the matching is, the higher the code rate is and the more iterations are required.

We follow the notation of [35] to describe the following different methods of computing the EXIT curves:

1. Using Monte Carlo Simulations: This method applies to any decoder, specially for which analytical methods do not exist such as the BCJR decoder. In this method, to compute the EXIT curve of the BCJR decoder/equalizer for a channel of certain SNR, we compute histogram of extrinsic LLRs corresponding to a large number of frames, assuming that a Gaussian source generates *a priori* LLRs of mutual information I_A . This histogram gives us the extrinsic mutual information I_E . Figure 5.2 explains this method and the step-by-step procedure to calculate I_E corresponding to a given I_A is as follows:

- (a) *A Priori LLRs L_A Generation:* Generate Gaussian-distributed LLRs by adding $\sigma_A^2 x_i/2$ to a Gaussian source $\mathcal{N}(0, \sigma_A^2)$, where $\sigma_A = J^{-1}(I_A)$, $x_i \in \{-1, 1\}$ are source symbols, and functions $J(\cdot)$ and $J^{-1}(\cdot)$ are defined in [35, Appendix].
- (b) *Channel LLRs L_C Generation:* Pass source symbols \mathbf{x} through the ISI channel and the AWGN channel of zero mean and variance σ_N^2 . The output of the AWGN channel multiplied by $2/\sigma_N^2$ gives us channel LLRs L_C .
- (c) *Extrinsic LLRs L_E Generation:* Given the channel observations in L_C and a priori information from L_A , compute extrinsic LLRs L_E using the BCJR equalizer/decoder.
- (d) *Calculation of Extrinsic Information:* Given L_E , calculate histogram $p(L_E/x_i =$

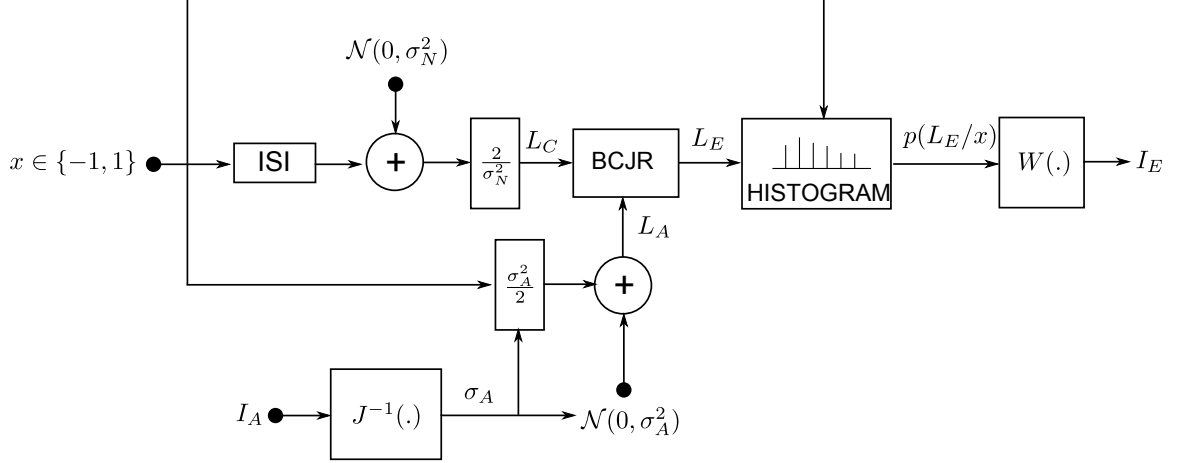


Figure 5.2: The computation of EXIT chart of the BCJR decoder/equalizer boils down to computing three LLRs: a priori LLRs L_A , channel LLRs L_C and extrinsic LLRs L_E .

0) and $p(L_E/x_i = 1)$, and compute

$$I_E = W[p(L_E/X = x)] = \frac{1}{2} \sum_{x \in \{-1, 1\}} \int_{-\infty}^{\infty} p(L_E/X = x) \times \log_2 \left(\frac{2 \cdot p(L_E/X = x)}{p(L_E/X = -1) + p(L_E/X = +1)} \right) dL_E.$$

A numerical evaluation of the above integration will be useful for software implementation.

The procedure above gives us one point on the EXIT curve, and we can repeat the same procedure for various values of I_A to generate a complete EXIT curve.

2. Using Analysis of Check and Variable Nodes: Let I_A denote the average mutual information between *a priori* LLRs and corresponding bits of a check or variable node then the EXIT curve $I_{E,VND}(I_A, d_v)$ for a degree d_v variable node (assuming no incoming message from the channel) is [35]

$$I_{E,VND}(I_A, d_v) = J(\sqrt{d_v - 1} J^{-1}(I_A)), \quad (5.1)$$

and the EXIT curve $I_{E,CND}(I_A, d_c)$ for a degree d_c check node is

$$I_{E,CND}(I_A, d_c) \approx 1 - I_{E,VND}(1 - I_A, d_c). \quad (5.2)$$

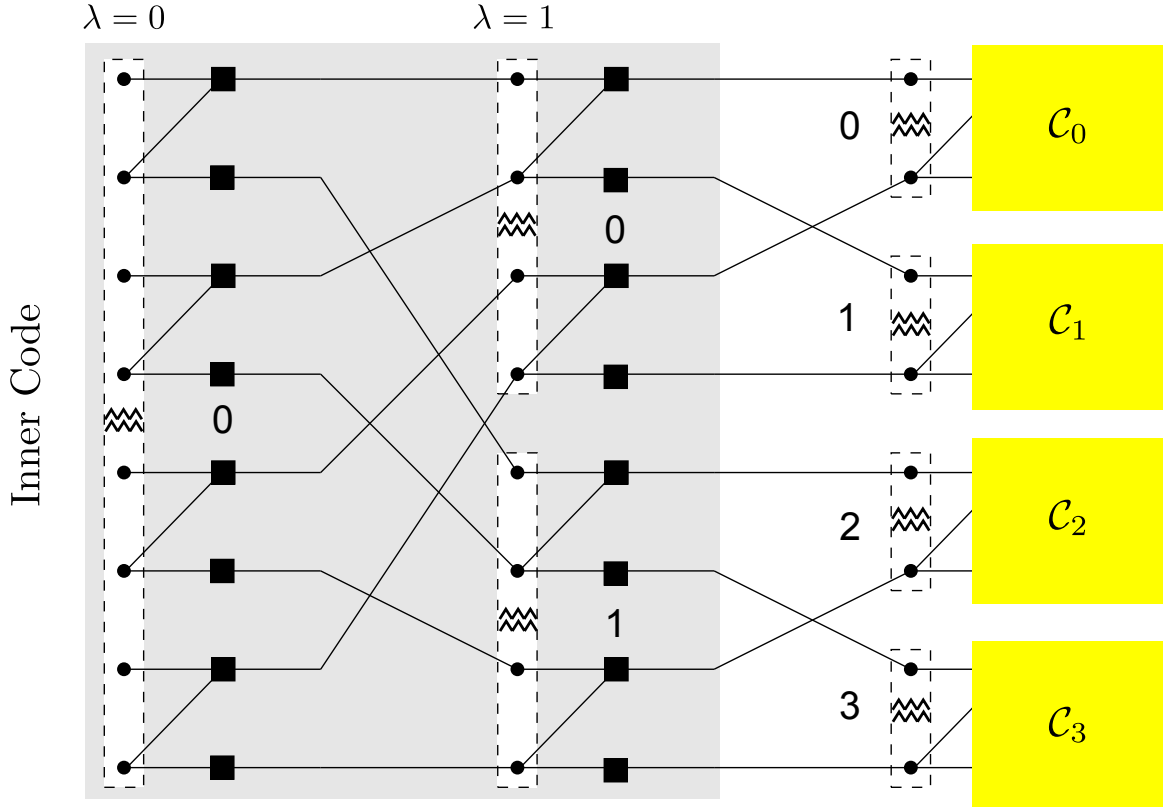


Figure 5.3: The polar code of length N can be viewed as the concatenation of four outer codes $\mathcal{C}_0, \mathcal{C}_1, \mathcal{C}_2$ and \mathcal{C}_3 using an inner code.

5.3 EXIT Chart Analysis of Polar Codes with Multistage Decoding

The EXIT chart analysis of polar codes with multistage decoding depends on how many levels or stages have been considered. For example, the special case of Figure 5.1 has two stages of decoding, whereas Figure 5.3 shows an example of four stages of decoding. In this section, we present the EXIT chart analysis of polar codes under multistage decoding with two and four stages.

5.3.1 Multistage Decoding with Two Stages

Consider the multistage decoder for polar codes with two stages and its operation as explained in Section 5.1 under the assumption that the outer codes are capacity-achieving codes.

We draw the EXIT curve for this decoder by sweeping I_A from zero to one and calculating

I_E , where

$$I_A = I(\{L_0(0, i)\}_{i=0}^{N-1}, \mathbf{v}) \text{ and } I_E = I(\{B_0(0, i)\}_{i=0}^{N-1}, \mathbf{v}).$$

Let I_{A, \mathcal{C}_i} and I_{E, \mathcal{C}_i} denote the input and output mutual information of the decoder for outer code \mathcal{C}_i . Let R_i denote the rate of the code \mathcal{C}_i .

The following description of multilevel decoding applies directly if the component decoders are SC or the SCL decoders. In the case of the SCAN decoder, the following description applies to the last iteration of the decoder.

As we increase the values of I_A , we observe the following different stages of this EXIT curve in the inverted graph (I_A versus I_E):

1. Lower Face: This is the first part of the EXIT curve, as we increase I_A from zero. As described in Section 5.1, the multistage decoder first decodes \mathcal{C}_0 , assuming no information from the decoder of \mathcal{C}_1 and converts the inner code into a mixture of check nodes of degree three, as shown in Figure 5.5. Since the EXIT curve of a code mixture is average of the EXIT curves of the component codes [35], the mutual information corresponding to *a priori* input to the decoder of \mathcal{C}_0 is $I_{A, \mathcal{C}_0} = I_{E, \text{CND}}(I_A, 3)$. As we have assumed that the outer code \mathcal{C}_0 is capacity-achieving, the decoder will remain unsuccessful for as long as $R_0 \geq I_{A, \mathcal{C}_0}$. Alternatively,

$$I_E = 0 \text{ for } 0 \leq I_A \leq I_{E, \text{CND}}^{-1}(R_0, 3).$$

We call the region of $I_E = 0$ the *lower face*.

2. Lower Plateau: As soon as $I_A > I_{E, \text{CND}}^{-1}(R_0, 3)$, the decoder for outer code \mathcal{C}_0 successfully decodes the message $\{u_0, u_1, \dots, u_{N/2-1}\}$, and therefore, the average extrinsic mutual information at the output of the decoder for \mathcal{C}_0 is maximum, i.e., $I_{E, \mathcal{C}_0} = 1$. Thus, the perfect recovery of bits corresponding to $\{B_1(0, i)\}_{i=0}^{N/2-1}$ converts the inner code into a repetition code by removing the top right edge of all the protographs in the inner code, as shown in Figure 5.5.

When the inner code is behaving as a repetition code, and the decoder for \mathcal{C}_1 is unsuccessful, $I_E = I_{E, \text{CND}}(I_A, 2) = I_A$. The equality $I_E = I_A$ can also be explained

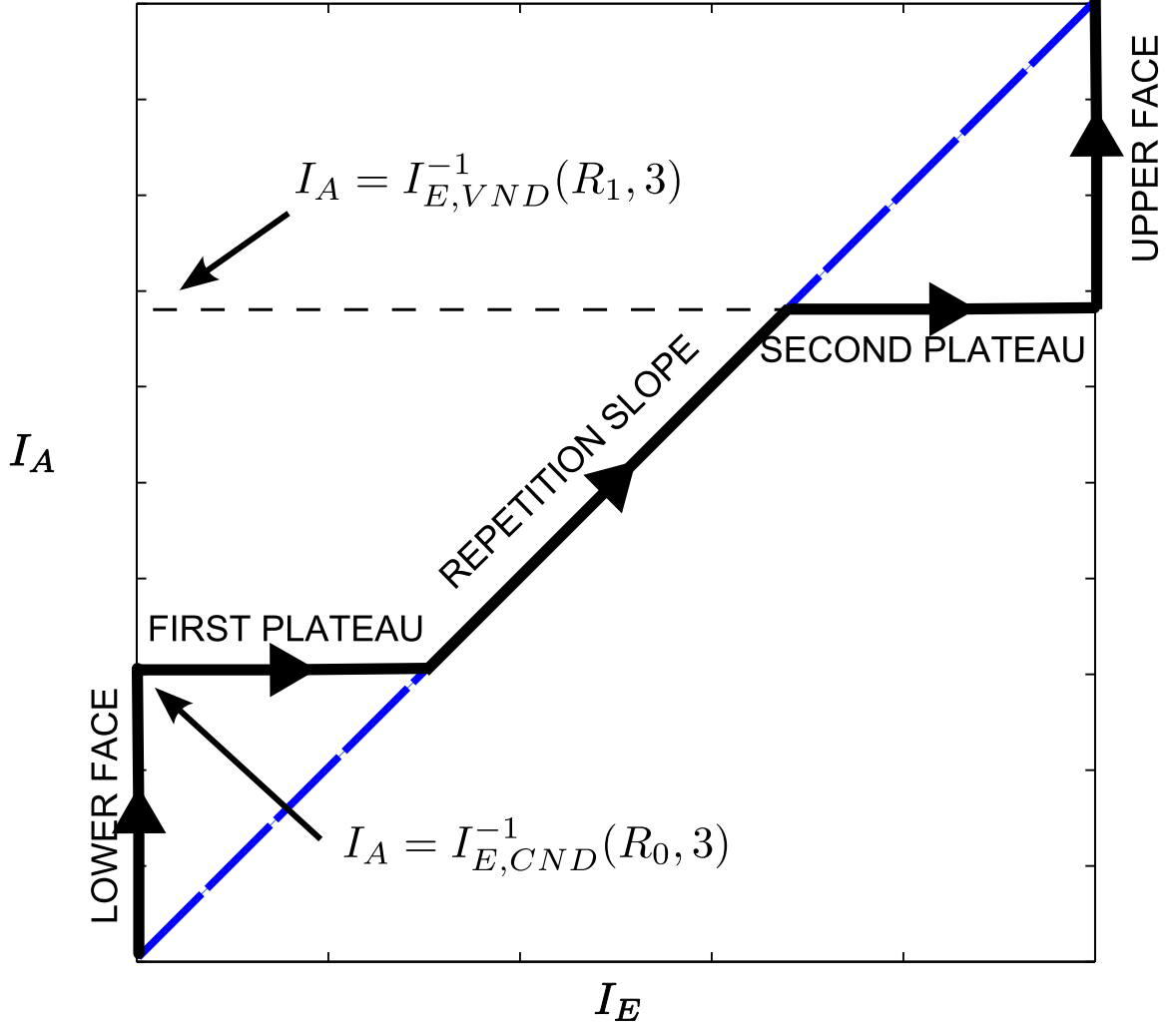


Figure 5.4: The EXIT curve of polar codes follows a hill-like trajectory with two faces, two plateaus and one slope.

with the help of LLRs. In case the decoder for \mathcal{C}_0 is successful, whereas the decoder for \mathcal{C}_1 is not, we can write

$$B_0(0, 2i) = L_0(0, 2i + 1) \text{ and } B_0(0, 2i + 1) = L_0(0, 2i),$$

where $i \in \{0, 1, 2, \dots, N/2 - 1\}$. Since the extrinsic LLRs in $\{B_0(0, i)\}_{i=0}^{N-1}$ are the same LLRs in $\{L_0(0, i)\}_{i=0}^{N-1}$ but in different positions, the corresponding mutual information is equal, implying $I_E = I_A$. Therefore, as soon as $I_A > I_{E,CND}^{-1}(R_0, 3)$, the EXIT curve jumps from $I_E = 0$ to a line of slope one, or the line $I_E = I_A$. The sudden jump in the output I_E produces a plateau, which we call the *lower plateau*.

3. Repetition Slope: As soon as $I_A > I_{E,CND}^{-1}(R_0, 3)$, the EXIT curve jumps as explained in the previous step and reaches the repetition slope as shown in Figure 5.4. The EXIT curve follows this unity slope line until the decoder for \mathcal{C}_1 is successful. Assuming \mathcal{C}_1 is also capacity-achieving, the decoder will successfully decode $\{u_{N/2}, u_{N/2+1}, \dots, u_{N-1}\}$ when

$$I_{A,C_1} = I_{E,VND}(I_A, 3) > R_1.$$

Equivalently, $I_E = I_A$ in the region

$$I_{E,CND}^{-1}(R_0, 3) \leq I_A \leq I_{E,VND}^{-1}(R_1, 3).$$

We call this unity slope line the *repetition slope*.

4. Upper Plateau and Face: When $I_A = I_{E,VND}^{-1}(R_1, 3)$, the decoder for \mathcal{C}_1 successfully decodes $\{u_{N/2}, u_{N/2+1}, \dots, u_{N-1}\}$, and $I_{E,C_0} = I_{E,C_1} = I_E = 1$. The successful decoding of $\{u_{N/2}, u_{N/2+1}, \dots, u_{N-1}\}$ produces a jump to $I_E = 1$, completing the decoding operation. We call the region of sudden jump from $I_{E,VND}^{-1}(R_1, 3)$ to $I_E = 1$ the *upper plateau* and the line where $I_E = 1$, the *upper face*.

In short, for this case of two outer and one inner codes, the EXIT curve traverses portions of the three curves ($I_E = 0$, $I_E = I_A$ and $I_E = 1$), where the rates of outer codes determine the jump points from one curve to the other (from $I_E = 0$ to $I_E = I_A$ and $I_E = I_A$ to $I_E = 1$).

5.3.2 Multistage Decoding with Four Stages

In the case of more than two outer codes such as four or eight, the number of curves that the EXIT curve traverses increases. Figure 5.8 shows the EXIT curve in the case of four outer codes.

Consider four outer codes $\mathcal{C}_0, \mathcal{C}_1, \mathcal{C}_2$ and \mathcal{C}_3 connected to each other using the inner code, as shown in Figure 5.3. Now suppose we gradually increase I_A from zero to one. Since the decoders for all four outer codes are unsuccessful, the inner code acts like a mixture of check nodes of degree five for outer code \mathcal{C}_0 , as shown on the right in Figure 5.6.

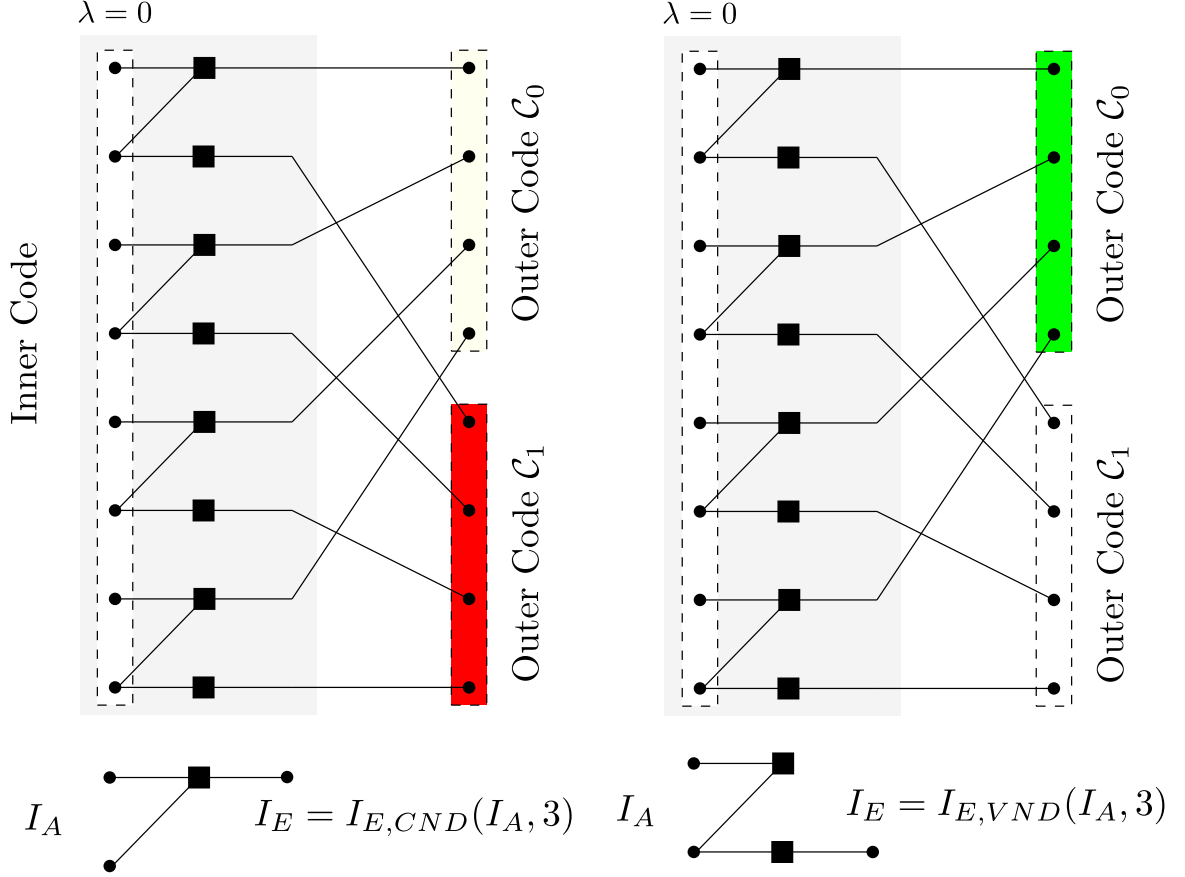


Figure 5.5: The inner code serves as the parity check and repetition code of degree three when the decoder for \mathcal{C}_1 is unsuccessful and the decoder for \mathcal{C}_0 is successful, respectively.

Consider the mixture of degree-five check nodes on the right in Figure 5.6. The extrinsic mutual information of this code mixture, which is also the input mutual information for the decoder of \mathcal{C}_0 , is $I_{A,\mathcal{C}_0} = I_{E,CND}(I_A, 5)$. Since \mathcal{C}_0 is unsuccessful, the extrinsic mutual information I_{E,\mathcal{C}_0} from the decoder for \mathcal{C}_0 is zero. As a result of unsuccessful decoding by all the outer decoders, the extrinsic mutual information I_E of the multistage decoder is also zero.

As we have assumed that the outer code \mathcal{C}_0 is capacity-achieving, the decoder for \mathcal{C}_0 will remain unsuccessful for as long as $R_0 \geq I_{A,\mathcal{C}_0}$. Alternatively,

$$I_E = 0 \text{ for } 0 \leq I_A \leq I_{E,CND}^{-1}(R_0, 5).$$

As soon as $I_A > I_{E,CND}^{-1}(R_0, 5)$, the decoder for \mathcal{C}_0 is successful. When the decoder for \mathcal{C}_0 is successful, the inner code becomes the concatenation of degree-three check and

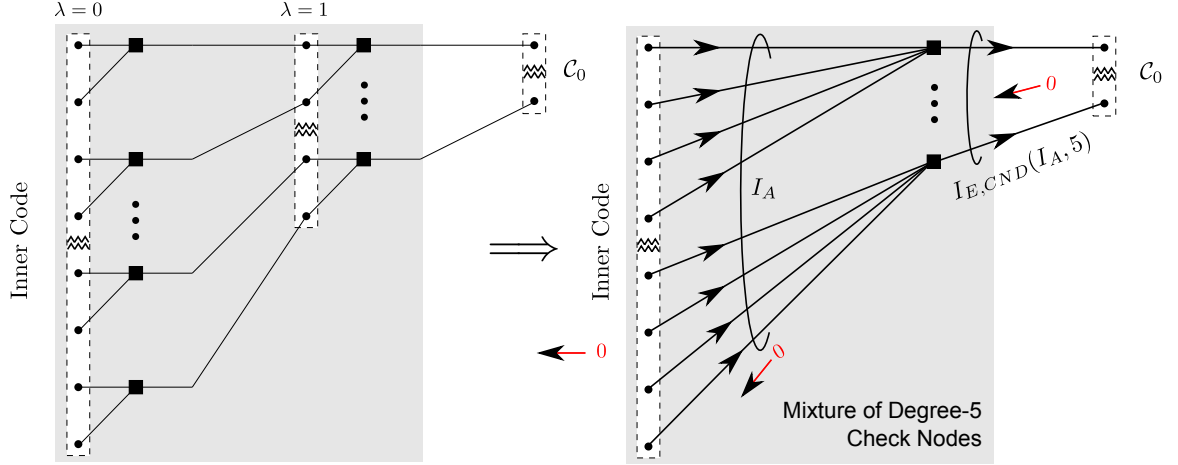


Figure 5.6: When decoders for outer codes C_0 , C_1 , C_2 and C_3 are unsuccessful, the inner code acts like a mixture of degree-five parity-check codes. The extrinsic mutual information at the output of the multistage decoder is zero, because all the decoders for C_0 , C_1 , C_2 and C_3 are unable to decode the message.

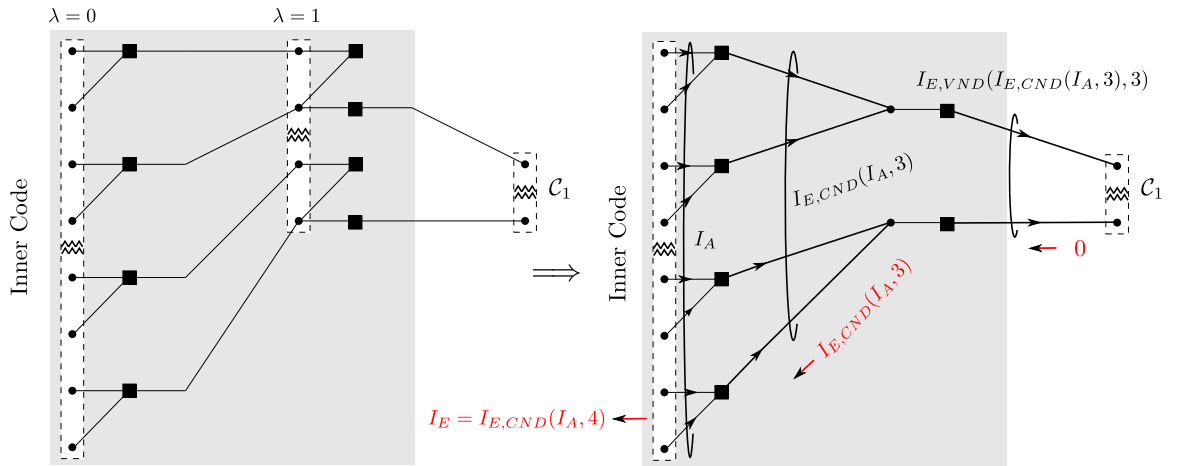


Figure 5.7: When the decoders for outer code C_0 and C_1 are successful and unsuccessful, respectively, the inner code becomes a code mixture of serially concatenated degree-three parity-check and degree-three variable nodes.

and degree-three variable nodes, as shown on the right of Figure 5.7. The extrinsic mutual information of this concatenated code, which is also the input mutual information for the decoder of code C_1 , is $I_{E,VND}(I_{E,CND}(I_A,3),3)$. Since the decoder for C_1 is unsuccessful, $I_{E,C_1} = 0$, which essentially removes the edges connecting C_1 and inner code. As a result, the extrinsic mutual information I_E of the multistage decoder is the extrinsic mutual information of a mixture of degree-four parity-check codes $I_{E,CND}(I_A,4)$.

The EXIT curve stays on the curve $I_E = I_{E,CND}(I_A,4)$ until the decoder for C_1

succeeds when the input mutual information $I_{A,C_1} = I_{E,VND}(I_{E,CND}(I_A, 3), 3) > R_1$. At this point, the EXIT curve jumps to $I_E = I_A$ in a similar way to the *lower plateau* in Section 5.3.1. The EXIT curve traverses $I_E = I_A$ until the decoder for C_2 succeeds at $I_{A,C_2} = I_{E,CND}(I_{E,VND}(I_A, 3), 3)$. Equivalently, the EXIT curve stays on $I_E = I_A$ line for as long as

$$I_{E,CND}^{-1}(I_{E,VND}^{-1}(R_1, 3), 3) \leq I_A \leq I_{E,VND}^{-1}(I_{E,CND}^{-1}(R_2, 3), 3).$$

When $I_A > I_{E,VND}^{-1}(I_{E,CND}^{-1}(R_2, 3), 3)$, the decoder for C_3 succeeds, and the EXIT curve jumps to $I_E = I_{E,VND}(I_A, 4)$.

The EXIT curve follows $I_E = I_{E,VND}(I_A, 4)$ until the decoder for C_3 succeeds when $I_{A,C_3} = I_{E,VND}(I_A, 5) > R_3$ with a jump to $I_E = 1$ curve. At this point, the decoding of the message \mathbf{u} is complete.

5.4 EXIT Chart Based Design of Polar Codes

Figure 5.9 shows the EXIT curve for the BCJR equalizer in the dicode, the EPR4 and the E2PR4 channels, defined by the impulse response

$$\begin{aligned} \mathbf{h} &= \begin{bmatrix} 1 & -1 \end{bmatrix} / \sqrt{2}, \\ \mathbf{h} &= \begin{bmatrix} 1 & 1 & -1 & -1 \end{bmatrix} / 2, \\ \mathbf{h} &= \begin{bmatrix} 1 & 2 & 0 & -2 & -1 \end{bmatrix} / \sqrt{10}, \end{aligned}$$

respectively. It is evident that with the increasing intersymbol interference, the EXIT curves of the channels become steeper, and for better performance under iterative decoding, the EXIT curve of the code needs to match to these steep curves as closely as possible.

As explained in Section 5.3, by changing the rates of the component codes in the multistage description of polar codes, we can produce the jump points giving the EXIT curve a sloped shape. The sloped EXIT curve provides better matching to the EXIT curve of the ISI channel, which facilitates an *open convergence tunnel* between the two curves. This open tunnel allows the iterative decoder to follow a trajectory that ends at $I_E = 1$ or equivalently successful decoding. Based on this observation, we propose the following design method for polar codes of rate R for ISI channels.

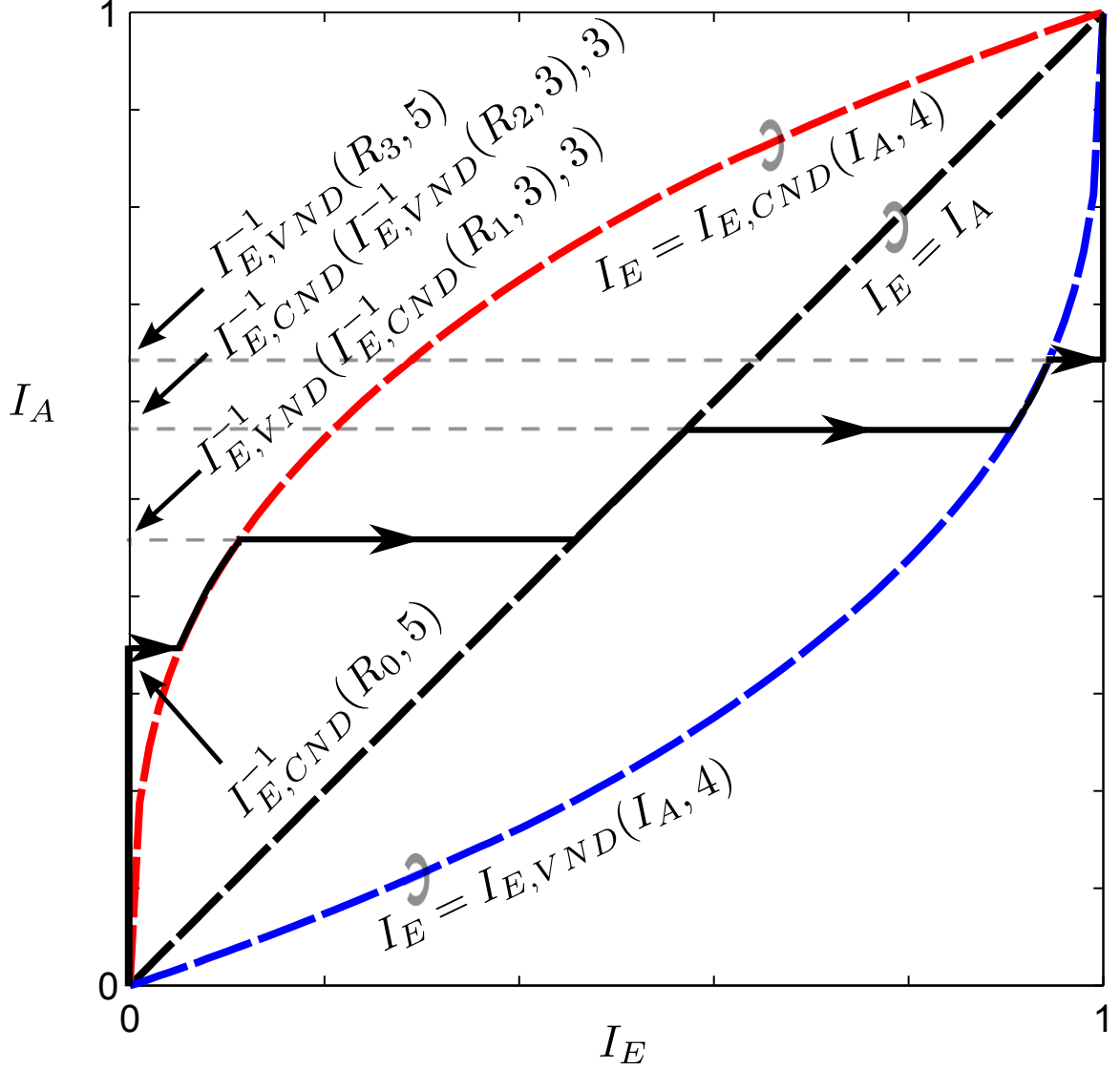


Figure 5.8: The EXIT curve of polar codes follows a hill-like trajectory for four-level codes.

5.4.1 For Decoding with Two Stages

1. Fix the search space size as M codes. Draw the EXIT curve of the ISI channel for $(E_b/N_0)_R \times (1 + \Delta)$, where $\Delta > 0$ is arbitrarily small, and $(E_b/N_0)_R$ denotes the E_b/N_0 required by a capacity-achieving modulation scheme to transmit on an ISI channel with rate R and an independent, uniformly distributed (IUD) binary source. One simulation-based technique to compute $(E_b/N_0)_R$ is discussed in [36]. Let $(0, a)$ be the intersection point of this curve with y -axis ($I_E = 0$).
2. Draw a unity slope line connecting the points $(0,0)$ and $(1,1)$. Let (b, b) be the

intersection point of the unity slope line with the line of step 1.

3. If

$$R + M/N > (I_{E,CND}(a, 3) + I_{E,VND}(b, 3))/2,$$

go to step 1 and repeat with increased Δ , else proceed to step 4.

4. Perform a search in the following region for the code with best frame error rate (FER):

$$R_0 < I_{E,CND}(a, 3),$$

$$R_1 < I_{E,VND}(b, 3),$$

$$R = \left(\frac{R_0 + R_1}{2} \right).$$

5.4.2 For Decoding with Four Stages

1. Fix the search space size as M codes. Draw the EXIT curve of the ISI channel for $(E_b/N_0)_R \times (1 + \Delta)$, where $\Delta > 0$ is arbitrarily small, and $(E_b/N_0)_R$ denotes the E_b/N_0 required by a capacity-achieving modulation scheme to transmit on an ISI channel with rate R and an independent, uniformly distributed (IUD) binary source. One simulation-based technique to compute $(E_b/N_0)_R$ is discussed in [36]. Let the curve be $I_E = I_{E,CH}(I_A)$

2. Let $(0, y_0), (\cdot, y_1), (\cdot, y_2)$ and (\cdot, y_3) be the intersection points of this curve with the lines $I_E = 0$, $I_A = I_{E,CND}^{-1}(I_E, 4)$, $I_A = I_E$ and $I_A = I_{E,VND}^{-1}(I_E, 4)$, respectively and

$$\rho_0 = I_{E,CND}(y_0, 5) \tag{5.3}$$

$$\rho_1 = I_{E,CND}(I_{E,VND}(y_1, 3), 3) \tag{5.4}$$

$$\rho_2 = I_{E,VND}(I_{E,CND}(y_2, 3), 3) \tag{5.5}$$

$$\rho_3 = I_{E,VND}(y_3, 5) \tag{5.6}$$

3. If

$$R + M/N > \sum_{i=0}^3 \rho_i,$$

repeat from step 1 with an increased Δ , else proceed to step 4.

4. Perform a search in the following region for the code with best frame error rate (FER):

$$1 - (\rho_0 + \rho_1) < R_1 < \rho_2 + \rho_3.$$

5.4.3 Computation of Design SNR

The second design parameter is the SNR to which the component polar codes will be optimized. One empirically good design strategy we found is to design component polar codes optimized to the design SNR γ_0 and γ_1 given by

$$\gamma_0 = \frac{h^{-1}\left(1 - [1 - h(2\gamma)]^2\right)}{2} \text{ and } \gamma_1 = 2\gamma, \quad (5.7)$$

where

$$h(x) = \begin{cases} e^{-0.4527x^{0.86} + 0.0218} & x > 10, \\ \sqrt{\frac{\pi}{x}} e^{-\frac{x}{4}} \left[1 - \frac{10}{7x}\right] & \text{otherwise.} \end{cases} \quad (5.8)$$

γ_0 and γ_1 represent the SNRs corresponding to the LLRs in $\{L_1(0, i)\}_{i=0}^{N/2}$ and $\{L_1(1, i)\}_{i=0}^{N/2}$, respectively calculated using the density evolution (DE) based on Gaussian assumption [1]. The DE procedure assumes that the SNR γ corresponding to the LLRs in $\{L_0(0, i)\}_{i=0}^N$ is given by

$$\gamma = (E_b/N_0)_R \times \Delta E_b(N) \times 2R, \quad (5.9)$$

where $\Delta E_b(N)$ is excess energy per bit over the energy per bit required to achieve capacity for a block length N . γ is a crude guess about the SNR required to achieve rate- R communication over the ISI channel at a finite block length N . We refer the interested reader to [37] for the computation of $\Delta E_b(N)$ and will just state the quantity wherever needed.

Example 5.1 (EPR4 Channel). *Suppose we want to design a polar code of length 8192 with $R = 1/2$ for the EPR4 channel. For this example, we apply the design method for the two-level description of polar codes. We first fix the search space size to $M = 50$ codes. Using the method in Section 5.2, we draw EXIT curve for the EPR4 channel using the BCJR equalizer for $(E_b/N_0)_{1/2} = 1.16$ dB which is the minimum E_b/N_0 required for rate-0.5 (to*

be precise 0.5012) transmission [36]. A linear approximation to this EXIT curve generates

$$I_E = 0.16I_A + 0.44. \quad (5.10)$$

Solving (5.10) and $I_E = I_A$ results in $b = 0.5238$. Since

$$\left(\frac{I_{E,CND}(a, 3) + I_{E,VND}(b, 3)}{2} \right) = 0.4929 < 0.5 + 0.0061,$$

we cannot achieve rate-0.5 transmission with the rate pair (R_0, R_1) , where $R_0 = I_{E,CND}(a, 3)$ and $R_1 = I_{E,VND}(b, 3)$. We go back to step 1 and repeat with increased Δ . After a few iterations, we reach the EXIT curve for the EPR_4 channel with $E_b/N_0 = 1.8$ dB. This curve has the following linear approximation:

$$I_E = 0.17I_A + 0.46, \quad (5.11)$$

with $a = 0.46$. Solving (5.11) and $I_E = I_A$ results in $b = 0.5542$. Since

$$\left(\frac{I_{E,CND}(a, 3) + I_{E,VND}(b, 3)}{2} \right) = 0.5067 > 0.5 + 0.0061,$$

according to step 3, the design is possible. The code search region is as follows:

$$R_0 < 0.2267, \quad R_1 < 0.7867, \quad \left(\frac{R_0 + R_1}{2} \right) = 0.5,$$

that simplifies to

$$1 - R_0 < R_1 < 0.7867 \implies 0.7733 < R_1 < 0.7867$$

in terms of rates and

$$3167 < K_1 < 3222,$$

in terms of dimensions of component codes of length 4096, respectively. For the design SNR of different component codes, we know the following parameters for the EPR_4 channel:

$$(E_b/N_0)_{1/2} = 1.16 \text{ dB}, \quad \Delta E_b(8192) \approx 0.4 \text{ dB},$$

where ΔE_b is calculated to achieve an error rate of 10^{-5} . Using these parameters in (5.9), we calculate SNR $\gamma = 1.6$ dB (after rounding off). This γ along with (5.7) gives $\gamma_0 = -1.45$ dB and $\gamma_1 = 4.6$ dB.

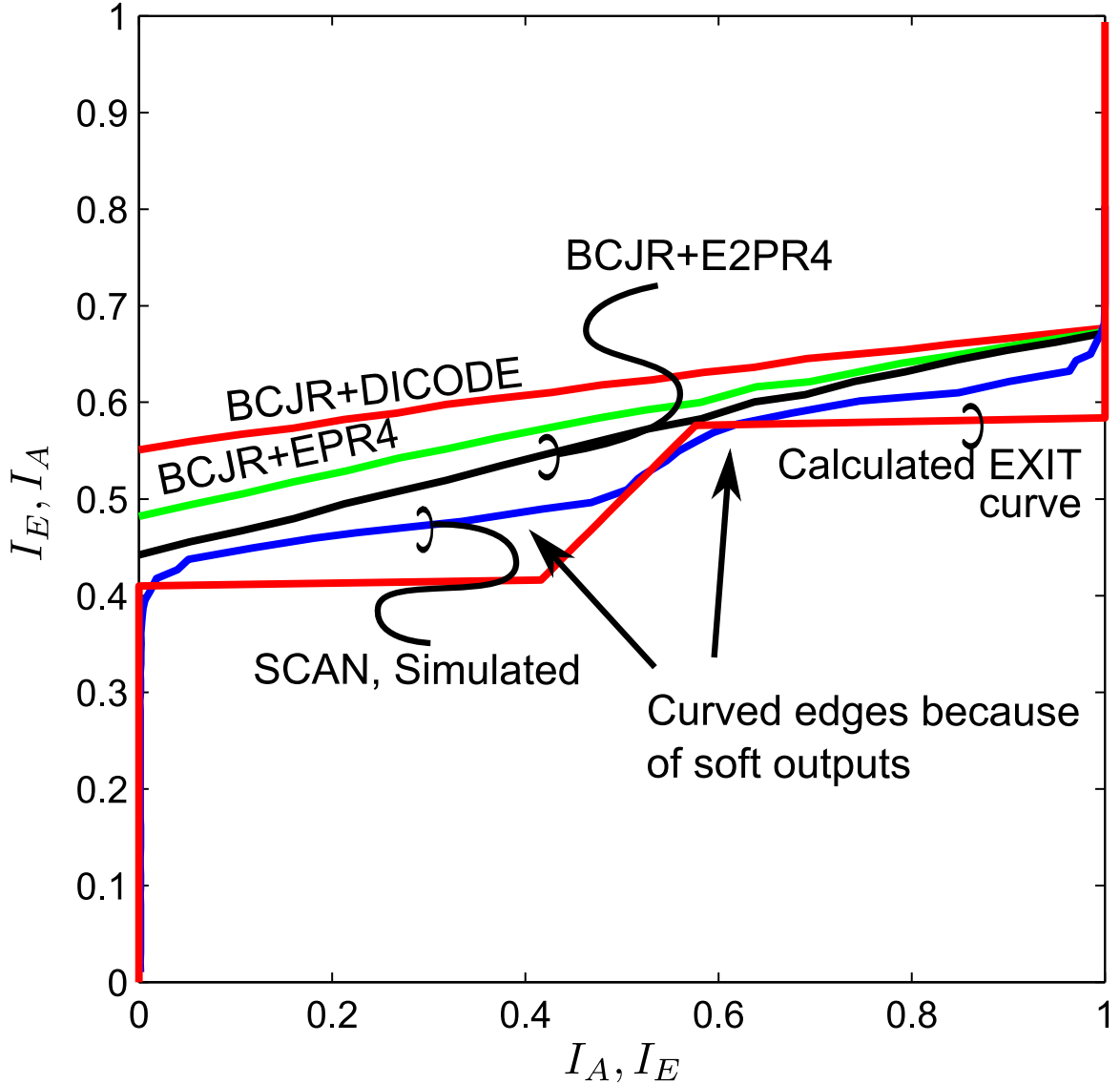


Figure 5.9: The EXIT curve of polar codes calculated from Section 5.3 approximates that obtained through Monte Carlo simulations.

Example 5.2 (E2PR4 Channel). *Suppose we want to design a polar code of length 8192 with $R = 1/2$ for the E2PR4 channel. For this example, we employ the design method for the four-level description of polar codes. We fix the search space size to $M = 50$ codes. We start with the EXIT curve for the E2PR4 channel for $(E_b/N_0)_{1/2} = 1.48$ dB, and after a few iterations of step 1 to step 3, we finally find the EXIT curve satisfying the condition in step 3. The second order approximation to this EXIT curve generates*

$$I_E = 0.420712 + 0.253236I_A - 0.027686I_A^2. \quad (5.12)$$

Using (5.12) in step 3 results in

$$y_0 = 0.420712, y_1 = 0.447026, y_2 = 0.552080, y_3 = 0.999751,$$

$$\rho_0 = 0.041606, \rho_1 = 0.375103, \rho_2 = 0.623617, \rho_3 = 1.000000.$$

Since

$$\frac{1}{4} \sum_{i=0}^3 \rho_i = 0.510082 > 0.500000 + 0.006104,$$

according to step 3, the design is possible. The code search region is as follows:

$$R_0 < (\rho_0 + \rho_1)/2, \quad R_1 < (\rho_2 + \rho_3)/2,$$

$$\left(\frac{R_0 + R_1}{2} \right) = 0.5,$$

that simplifies to

$$1 - R_0 < R_1 < 0.811809 \implies 0.791645 < R_1 < 0.811809$$

in terms of rates and

$$3243 < K_1 < 3326,$$

in terms of dimensions of component polar codes of length 4096, respectively. For design SNR, following the similar approach to the previous example, we get the following:

$$(E_b/N_0)_{1/2} = 1.48 \text{ dB}, \quad \Delta E_b(8192) \approx 0.4 \text{ dB},$$

$$\gamma = 1.9 \text{ dB}, \quad \gamma_0 = -1.0189 \text{ dB}, \quad \gamma_1 = 4.9 \text{ dB}.$$

5.5 Simulation Results

In this section, we show that the EXIT curve of polar codes with the SCAN decoder follows the approximation presented in Section 5.3. We further compare the error-rate performance of the polar codes designed using our proposed method with the polar codes designed for the AWGN channel when decoded using the SCAN decoder in turbo equalization framework.

Table 3: Design Parameters

Channel	Code	N	K	Design SNR
	\mathcal{C}_0	4096	894	-1.45 dB
EPR4	\mathcal{C}_1	4096	3202	4.6 dB
	Classical	8192	4096	1.4 dB
	\mathcal{C}_0	4096	770	-1.01 dB
E2PR4	\mathcal{C}_1	4096	3326	4.9 dB
	Classical	8192	4096	1.6 dB

5.5.1 Accuracy of EXIT Curve Approximation

We have calculated the EXIT curve of the SCAN decoder for the polar code in Example 5.2 using Monte Carlo simulations, as explained in Section 5.3. The jump points in the simulated curve closely follow the predicted jump points in the EXIT curve calculated using the analysis in Section 5.3.

We also observe smooth edges in the EXIT curve for the SCAN decoder on the two jump points (at the start of both the plateaus) rather than the sudden transitions in the calculated EXIT curve. This smoothness is because we assumed in Section 5.3 that the outer decoders are capacity-achieving and hard-output, i.e., either they deliver complete information with $I_E = 1$ or no information $I_E = 0$, but not in between. On the other hand, the SCAN decoder is a soft-output decoder that provides a smooth transition instead of a sudden jump. This smooth transition reduces the area between the EXIT curve of the SCAN decoder and that of the ISI channel relative to the calculated EXIT curve and directly corresponds to the reduction in the rate loss ($C - R$) [38], where C is the capacity of the channel for IUD binary source.

5.5.2 Code Performance

We have simulated polar codes designed in Example 5.1 and 5.2 and compared them with classical polar codes. We have designed the classical as well as both the component polar codes in the two examples using the method of [1]. For classical polar codes, we swept the design SNR from 1 dB to 3 dB with a step of 0.1 dB and picked the one that resulted in

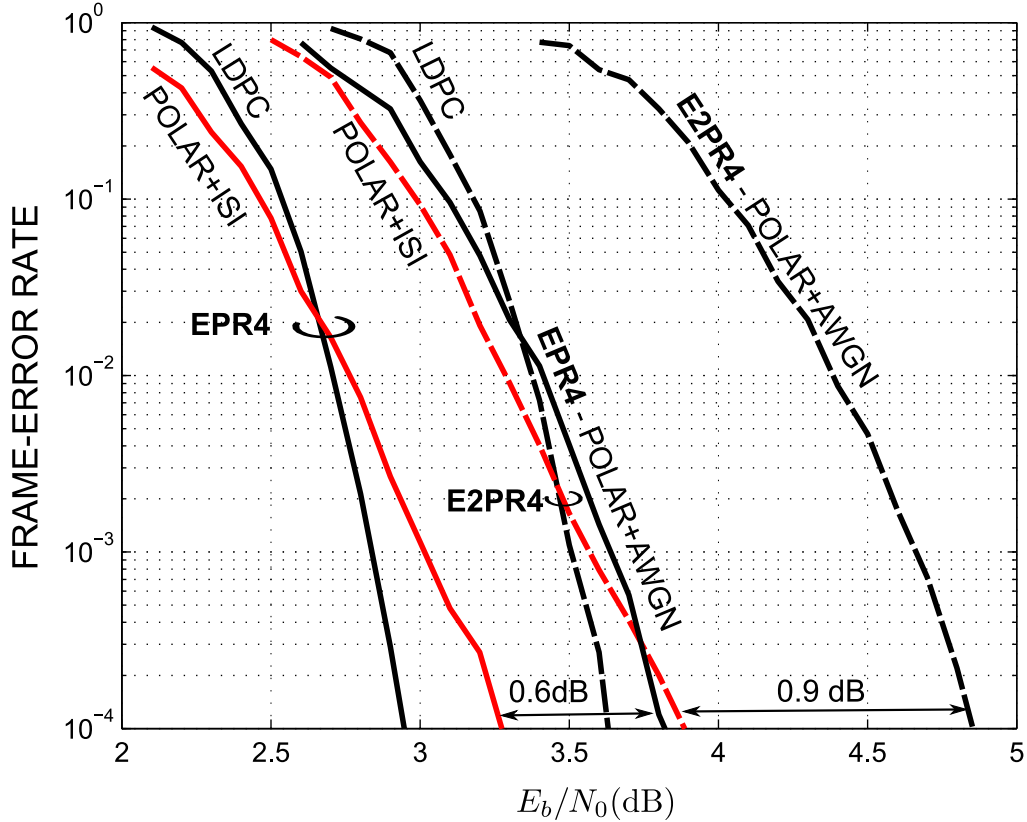


Figure 5.10: Polar codes constructed through the proposed method provide approximately 0.6 dB and 0.9 dB gain in FER performance on EPR4 and E2PR4 channels, respectively, relative to the ones optimized for AWGN.

the best FER performance at a certain E_b/N_0 . For all polar code simulations, a maximum of six turbo iterations and eight SCAN iterations are used.

In the code search space in both of the examples, we observed that the majority of the codes perform well with negligible difference in error rate from each other. Therefore, the search for $M = 50$ codes in both of the examples suffices to reach a code that performs either equal or closer to the best code in the entire code search space. Table 3 summarizes different polar codes used in Figure 5.10. We observed a gain of 0.6 dB and 0.9 dB in the proposed design of polar codes as compared to the classical designs for $\text{FER} = 10^{-4}$.

We also compared the proposed polar codes to an irregular LDPC code of the variable node distribution $\lambda(x) = 0.2184x + 0.163x^2 + 0.6186x^3$ and check node distribution $\rho(x) = 0.6821x^4 + 0.3173x^5 + 0.0006x^6$ designed using progressive edge growth (PEG) method

[23], [21], [22]. For LDPC simulations, we have used a maximum of six turbo and 40 BP iterations. We observed that polar codes for both EPR4 and E2PR4 channels perform approximately 0.25 dB and 0.2 dB away from respective LDPC codes.

In fairness, we mention here that the simulated LDPC code is optimized for the AWGN channel with lower values of maximum variable and check node degrees and LDPC codes optimized for ISI channels exist such as reported in [28]. But, the caveat, however, is that such optimal LDPC codes usually have very higher maximum variable node and check node degrees that make these codes difficult to realize in hardware.

5.6 Summary

In this chapter, we presented a method to design polar codes for intersymbol interference channels. The proposed method utilizes the multilevel description of polar codes and optimizes the rates of component codes for ISI channels under iterative decoding. We showed that by changing the rates of the component polar codes, we can match the EXIT curve of a polar code to that of a ISI channel. We also provided numerical results demonstrating significant gains relative to codes designed for the AWGN channel. Specifically, we observed a gain of 0.6 dB and 0.9 dB in the proposed designs for EPR4 and E2PR4 channels, respectively, relative to the classical design of polar codes for the AWGN channel.

CHAPTER VI

CONTRIBUTIONS AND FUTURE RESEARCH

This thesis presents polar codes as a strong candidate for magnetic recording application. In current state, polar codes have neither the optimized designs nor near-optimal, low-complexity, soft-output decoders for magnetic recording channels. This thesis provides an error-correcting system based on optimized polar codes for magnetic recording channels and a low-complexity, high-throughput soft-output decoder for polar codes. In this chapter, we summarize all the contributions of this thesis and then discuss a few directions in which this work can be extended.

6.1 Contributions

Following are the main contributions of this thesis:

1. In Chapter 3, we proposed a low-complexity soft-output decoder called the soft-cancellation (SCAN) decoder. We demonstrated that the serial schedule of message updates in the SCAN decoder converges much faster than the flooding schedule of previous BP decoder, resulting in drastically reduced computational complexity. The low complexity of *SCAN* combined with other properties of polar codes such as universal rate adaptability, puts polar codes in a strong position with other competing code families in magnetic recording application. The complexity reduction does not compromise error-rate performance at all, and the SCAN decoder outperforms the SC and the BP decoders in both the AWGN and the ISI channels.
2. In Chapter 4, we demonstrated that polar codes exhibit *special prohibited pair property* according to which only a few of all the possible patterns in the location of *frozen bits* are possible. Specifically, if we pair two consecutive bits in the successive-cancellation detection order, a free bit will never precede a fixed bit. We also showed that this property generalizes to the *general prohibited pair property* under *SCAN* in the

sense that a few of all the possible patterns of node groups are possible. Both of the properties describe the type of LLRs in the entire factor graphs based on the location of fixed bits. We apply these properties to the SCAN decoder and propose a high-throughput and memory-efficient implementation of the SCAN decoder called the enhanced SCAN (eSCAN) decoder.

3. In Chapter 5, we proposed a method to design polar codes for ISI channels when the SCAN decoder is used. The method is based on the well-known result that under turbo equalization, EXIT curves of optimal codes match those of ISI channels. This result reduces the problem of finding better codes into a curve-fitting problem in which we try to fit the EXIT curve of the code to that of the ISI channel. The better this matching is, the better the codes perform in terms of error rates. We demonstrated that polar codes can have a sloped EXIT curve matched to that of an ISI channel, outperforming the codes designed for the AWGN channel under turbo equalization. We also provide a method to achieve this matching for a given channel. The polar codes designed using the proposed method buy us a gain of 0.6 dB and 0.9 dB for EPR4 and E2PR4 channels, respectively compared to the the codes designed for the AWGN channel.

6.2 *Future Directions*

In the previous section, we outlined the main contributions of this thesis. This section discusses a few directions in which our work can be extended.

6.2.1 **Error Floor Analysis of Polar Codes with the SCAN Decoder**

Error-rate curves for the iterative decoding usually exhibit two main regions as we increase the SNR from a lower value to a higher one; namely, the *waterfall* region and the *error-floor* region [39]. As we increase the SNR from a lower value, the error rate stays at some lower value as well until it reaches a certain value of SNR. After this SNR, the error rate decreases rapidly. This region of rapid error-rate drop is called the *waterfall* region. As we increase the SNR even further, it is observed that the error rate stops to decrease as rapidly as it

does in the *waterfall* region. This region of slow error-rate drop is called the *error-floor* region.

All the performance curves in this thesis concern only the *waterfall* region as they are easy to simulate using computer software. The *waterfall* region broadly defines the performance of a coded system in most cases, however, some applications such as magnetic recording and optical communication channels have stringent error-floor requirements. To assess the performance of polar codes with the SCAN decoder in the *error-floor* region, we need high-speed hardware platforms that can reach such low error rates. This necessitates the research for hardware implementations of the SCAN decoder.

6.2.2 Analysis of the SCAN Decoder

All codes of rate R require a minimum block length N to achieve a certain frame-error probability P_e . Although a single relationship between these three parameters is of immense practical significance, it is usually very hard to find. Therefore, a relatively easier approach is to reduce the size of the problem by fixing one of these three parameters and look at the relationship between the remaining two variables. This reduction results in the following two important cases:

1. *Error Exponent:* If we fix rate R and study the relationship between the error-probability P_e and block length N , we end up with the concept of an *error exponent*. Precisely, if the error probability of a code decays as $P_e = e^{-N\alpha}$, then α is called the error exponent.

For instance, Arikan and Telatar [40] showed that under the SC decoder polar codes attain an exponent of $1/2$. In other words, for any $\beta < 1/2$ and $R < C$, where R is the rate of the code and C is the capacity of the channel, the block-error probability is upper bounded by 2^{-N^β} . This rapid exponential decay of error probability guarantees an error-rate curve with no error floor for moderate to large block lengths. For the SCAN decoder, no such guarantees exist; although, it outperforms the SC decoder in error-rate performance in the AWGN channel. Therefore, one possible extension of our work is to study the error exponent of polar codes under the SCAN decoding to

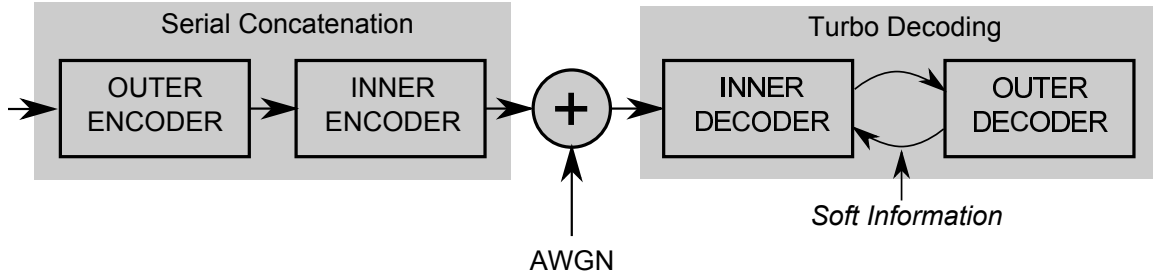


Figure 6.1: In turbo decoding, the decoder decodes the combination of two codes by exchanging soft information between two decoders.

compare them with other decoders for polar codes.

2. *Scaling Laws*: If we fix maximum error probability P_e then the relationships between rate R and block length N of a code produce scaling laws. The scaling laws are more relevant in practical applications [41], because usually a certain error probability P_e is required by an application, and we are interested in maximizing rate R on a certain block length N .

Since the seminal work in [4], the SC [42], [41]; and the SCL [43] decoder have been studied for their scaling laws. A focused study for the scaling laws of the SCAN decoder can be another possible extension of this work.

6.2.3 Performance of the SCAN Decoder in Turbo Decoding

This thesis described the performance of polar codes in turbo equalization framework. One future direction can be to assess the performance of *SCAN* in turbo decoding framework. One such system with serial concatenation of two codes is shown in Figure 6.1. In this system, we concatenate two codes of same or different families in a serial fashion and on the receiver exchange the soft information about the coded bits between the two decoders. The code that lies deeper inside the system is called the *inner code*, whereas the one that lies close to the edge of the system is called the *outer code*. It is worth mentioning that turbo decoding principle also works when two codes are combined in a parallel fashion [44] instead of a serial one.

Tal and Vardy showed that polar codes perform extremely well when concatenated with the CRC codes using the SCL decoder. Trifonov and Miloslavskaya [45] demonstrated

similar improvement in the performance of polar codes when concatenated with a short-length parity-check code and decoded with a SCL decoder. Both of these codes are examples of serially concatenated codes and can be decoded using the turbo decoding framework. Our initial investigations show that the first CRC-concatenated code is hard to decode this way, because no low-complexity soft-output decoder is available for them at moderate to long block lengths. For short-length parity-check codes, the BP decoder for LDPC codes do not work because of the relatively high-density of the code. In this context, the following two important questions demand further exploration:

1. Is there a way to decode these concatenated codes using the SCAN decoder?
2. Which of these codes perform better under *SCAN* in turbo decoding framework?

APPENDIX A

PROOF OF THE PROPERTIES OF THE SCAN DECODER

Proof of Lemma 3.1.

$$\begin{aligned}
 W^-(y_0, y_1, z_1|u_0) &= \sum_{u_1} W_2(y_0, y_1, z_1, u_1|u_0) \\
 &= \frac{1}{2} \sum_{u_1} W(y_0|u_0 \oplus u_1)W(y_1|u_1)P(z_1|u_1). \tag{A.1}
 \end{aligned}$$

$$\begin{aligned}
 W^+(y_0, y_1, z_0|u_1) &= \sum_{u_0} W_2(y_0, y_1, z_0, u_0|u_1) \\
 &= \frac{1}{2} W(y_1|u_1) \sum_{u_0} W(y_0|u_0 \oplus u_1)P(z_0|u_0), \tag{A.2}
 \end{aligned}$$

where we have used the fact that both the bits u_0, u_1 are equally likely to be 0 or 1. Using (A.1) and (A.2) with the definition of an LLR, we get (3.1) and (3.2). \square

Proof of Proposition 3.1. Consider the problem setup for (A.1) and (A.2). Recall for an SC decoder, we have from [18]

$$\begin{aligned}
 Z(W_{SC}^+) &= Z(W)^2, \\
 Z(W)\sqrt{2 - Z(W)^2} &\leq Z(W_{SC}^-) \leq 2Z(W) - Z(W)^2,
 \end{aligned}$$

where $Z(W)$ is Bhattacharyya parameter of the DMC W defined as

$$Z(W) \triangleq \sum_y \sqrt{W(y|0)W(y|1)}. \tag{A.3}$$

Since for the SCAN decoder with $I = 1$, the computation for the check-node doesn't change, the relationships for $Z(W^-)$ as described above hold. Therefore, we only need to prove

$$Z(W^+) \geq Z(W)^2.$$

$$\begin{aligned} Z(W^+) &= \sum_{y_0, y_1, z_0} \sqrt{W^+(y_0, y_1, z_0|0)W^+(y_0, y_1, z_0|1)} \\ &= \frac{1}{2}Z(W) \times A(W, P), \end{aligned} \tag{A.4}$$

where

$$A(W, P) = \sum_{y_0, z_0} \left(\sum_{u_0} W(y_0|u_0)P(z_0|u_0) \right) \times \left(\sum_{u'_0} W(y_0|u'_0 \oplus 1)P(z_0|u'_0) \right).$$

From Lemma 3.15 in [18], we have

$$A(W, P) \geq 2\sqrt{Z(W)^2 + Z(P)^2 - Z(W)^2Z(P)^2}. \tag{A.5}$$

Using (A.5) in (A.4), we get

$$\begin{aligned} Z(W^+) &= Z(W)^2 \sqrt{1 + Z(P)^2 \left(\frac{1}{Z(W)^2} - 1 \right)}, \\ &\geq Z(W)^2 \end{aligned}$$

as by definition $0 \leq Z(P), Z(W) \leq 1$. □

REFERENCES

- [1] P. Trifonov and P. Semenov, "Generalized concatenated codes based on polar codes," in *Proc. 8th Int. Symp. Wireless Commun. Syst.*, Nov. 2011, pp. 442–446.
- [2] R. Galbraith and T. Oenning. (2008) Iterative detection read channel technology in hard disk drives. [Online]. Available: [http://www.hgst.com/tech/techlib.nsf/techdocs/FB376A33027F5A5F86257509001463AE/\\$file/IDRC'WP'final.pdf](http://www.hgst.com/tech/techlib.nsf/techdocs/FB376A33027F5A5F86257509001463AE/$file/IDRC'WP'final.pdf)
- [3] A. Jimenez Felstrom and K. Zigangirov, "Time-varying periodic convolutional codes with low-density parity-check matrix," *IEEE Trans. Inf. Theory*, vol. 45, no. 6, pp. 2181–2191, Sep. 1999.
- [4] E. Arıkan, "Channel polarization: A method for constructing capacity-achieving codes for symmetric binary-input memoryless channels," *IEEE Trans. Inf. Theory*, vol. 55, no. 7, pp. 3051–3073, Jul. 2009.
- [5] I. Tal and A. Vardy, "List decoding of polar codes," in *Proc. IEEE Int. Symp. Inform. Theory*, Aug. 2011, pp. 1–5.
- [6] C. Douillard, M. Jzquel, C. Berrou, D. Electronique, A. Picart, P. Didier, and A. Glavieux, "Iterative correction of intersymbol interference: Turbo-equalization," *European Trans. on Telecommun.*, vol. 6, no. 5, pp. 507–511, 1995.
- [7] M. Mansour and N. Shanbhag, "High-throughput LDPC decoders," *IEEE Trans. VLSI Syst.*, vol. 11, no. 6, pp. 976–996, Dec. 2003.
- [8] C. Leroux, I. Tal, A. Vardy, and W. Gross, "Hardware architectures for successive cancellation decoding of polar codes," in *Proc. IEEE Int. Conf. Acoust., Speech and Signal Process.*, 2011, pp. 1665–1668.
- [9] M. Mansour and N. Shanbhag, "A 640-mb/s 2048-bit programmable ldpc decoder chip," *IEEE J. Solid-State Circuits*, vol. 41, no. 3, pp. 684–698, Mar. 2006.
- [10] T. Richardson, M. Shokrollahi, and R. Urbanke, "Design of capacity-approaching irregular low-density parity-check codes," *IEEE Trans. Inf. Theory*, vol. 47, no. 2, pp. 619–637, Feb. 2001.
- [11] A. Alamdar-Yazdi and F. Kschischang, "A simplified successive-cancellation decoder for polar codes," *IEEE Commun. Lett.*, vol. 15, no. 12, pp. 1378–1380, Dec. 2011.
- [12] E. Arıkan, "A survey of reed-muller codes from polar coding perspective," in *Information Theory Workshop (ITW), 2010 IEEE*, Jan 2010, pp. 1–5.
- [13] F. Kschischang, B. Frey, and H.-A. Loeliger, "Factor graphs and the sum-product algorithm," *IEEE Trans. Inf. Theory*, vol. 47, no. 2, pp. 498–519, 2001.

- [14] R. Mori and T. Tanaka, "Performance of polar codes with the construction using density evolution," *IEEE Commun. Lett.*, vol. 13, no. 7, pp. 519–521, Jul. 2009.
- [15] I. Tal and A. Vardy, "How to construct polar codes," *IEEE Trans. Inf. Theory*, vol. 59, no. 10, pp. 6562–6582, Oct. 2013.
- [16] L. Bahl, J. Cocke, F. Jelinek, and J. Raviv, "Optimal decoding of linear codes for minimizing symbol error rate," *IEEE Trans. Inf. Theory*, vol. 20, no. 2, pp. 284–287, Mar. 1974.
- [17] E. Arıkan, "A performance comparison of polar codes and Reed-Muller codes," *IEEE Commun. Lett.*, vol. 12, no. 6, pp. 447–449, Jun. 2008.
- [18] S. B. Korada, "Polar codes for channel and source coding," Ph.D. dissertation, EPFL, Lausanne, 2009. [Online]. Available: <http://library.epfl.ch/theses/?nr=4461>
- [19] H. Sankar and K. Narayanan, "Memory-efficient sum-product decoding of ldpc codes," *IEEE Trans. Commun.*, vol. 52, no. 8, pp. 1225–1230, Aug 2004.
- [20] E. Zimmermann and G. Fettweis, "Reduced complexity LDPC decoding using forced convergence," in *Proc. 7th Int. Symp. Wireless Personal Multimedia Communications*, 2004, p. 15.
- [21] X.-Y. Hu. Source code for Progressive Edge Growth parity-check matrix construction. [Online]. Available: <http://www.cs.toronto.edu/~mackay/PEG-ECC.html>
- [22] X.-Y. Hu, E. Eleftheriou, and D.-M. Arnold, "Progressive edge-growth tanner graphs," in *Proc. IEEE Global Commun. Conf.*, vol. 2, 2001, pp. 995–1001.
- [23] LOPT - online optimisation of LDPC and RA degree distributions. [Online]. Available: <http://sonic.newcastle.edu.au/ldpc/lopt/>
- [24] B. Li, H. Shen, and D. Tse, "An adaptive successive cancellation list decoder for polar codes with cyclic redundancy check," *IEEE Commun. Lett.*, vol. 16, no. 12, pp. 2044–2047, Dec. 2012.
- [25] S. Jeon and B. Kumar, "Performance and complexity of 32 k-bit binary LDPC codes for magnetic recording channels," *IEEE Trans. Magn.*, vol. 46, no. 6, pp. 2244–2247, 2010.
- [26] J. Forney, G.D., "Codes on graphs: normal realizations," *IEEE Trans. Inf. Theory*, vol. 47, no. 2, pp. 520–548, 2001.
- [27] U. U. Fayyaz and J. Barry, "A Low-Complexity Soft-Output decoder for polar codes," in *Proc. IEEE Global Commun. Conf.*, Atlanta, USA, Dec. 2013.
- [28] N. Varnica and A. Kavcic, "Optimized low-density parity-check codes for partial response channels," *IEEE Commun. Lett.*, vol. 7, no. 4, pp. 168–170, April 2003.
- [29] A. Kavcic, X. Ma, and M. Mitzenmacher, "Binary intersymbol interference channels: Gallager codes, density evolution, and code performance bounds," *IEEE Trans. Inf. Theory*, vol. 49, no. 7, pp. 1636–1652, July 2003.

- [30] S. Ten Brink, “Convergence behavior of iteratively decoded parallel concatenated codes,” *IEEE Trans. Commun.*, vol. 49, no. 10, pp. 1727–1737, Oct 2001.
- [31] M. Franceschini, G. Ferrari, and R. Raheli, “Exit chart-based design of LDPC codes for inter-symbol interference channels,” in *Proc. IST Mobile and Wireless Communications Summit*, 2005.
- [32] J. B. Soriaga, H. Pfister, and P. Siegel, “Determining and approaching achievable rates of binary intersymbol interference channels using multistage decoding,” *IEEE Trans. Inf. Theory*, vol. 53, no. 4, pp. 1416–1429, April 2007.
- [33] N. Hussami, S. Korada, and R. Urbanke, “Performance of polar codes for channel and source coding,” in *Proc. IEEE Int. Symp. Inform. Theory*, 2009, pp. 1488–1492.
- [34] U. U. Fayyaz and J. R. Barry, “Low-complexity soft-output decoding of polar codes,” *IEEE J. Sel. Areas Commun.*, vol. 32, no. 5, pp. 958–966, May 2014.
- [35] S. ten Brink, G. Kramer, and A. Ashikhmin, “Design of low-density parity-check codes for modulation and detection,” *IEEE Trans. Commun.*, vol. 52, no. 4, pp. 670–678, Apr. 2004.
- [36] D. Arnold and H.-A. Loeliger, “On the information rate of binary-input channels with memory,” in *Proc. IEEE Int. Conf. Commun.*, vol. 9, June 2001, pp. 2692–2695.
- [37] Y. Polyanskiy, H. Poor, and S. Verdú, “Channel coding rate in the finite blocklength regime,” *IEEE Trans. Inf. Theory*, vol. 56, no. 5, pp. 2307–2359, May 2010.
- [38] A. Ashikhmin, G. Kramer, and S. ten Brink, “Extrinsic information transfer functions: model and erasure channel properties,” *IEEE Trans. Inf. Theory*, vol. 50, no. 11, pp. 2657–2673, Nov. 2004.
- [39] T. Richardson, “Error floors of LDPC codes,” in *Proc. the 41st Annual Conf. on Commun., Control and Comput.*, 2003, pp. 1426–1435.
- [40] E. Arikan and I. Telatar, “On the rate of channel polarization,” in *Proc. IEEE Int. Symp. Inform. Theory*, Jun. 2009, pp. 1493–1495.
- [41] S. H. Hassani, K. Alishahi, and R. Urbanke, “Finite-length scaling of polar codes,” *arXiv preprint arXiv:1304.4778*, 2013.
- [42] S. Korada, A. Montanari, I. Telatar, and R. Urbanke, “An empirical scaling law for polar codes,” in *Proc. IEEE Int. Symp. Inform. Theory*, Jun. 2010, pp. 884–888.
- [43] M. Mondelli, S. H. Hassani, and R. L. Urbanke, “Scaling exponent of list decoders with applications to polar codes,” *CoRR*, vol. abs/1304.5220, 2013.
- [44] S. Benedetto and G. Montorsi, “Design of parallel concatenated convolutional codes,” *IEEE Trans. Commun.*, vol. 44, no. 5, pp. 591–600, May 1996.
- [45] P. Trifonov and V. Miloslavskaya, “Polar codes with dynamic frozen symbols and their decoding by directed search,” in *Proc. IEEE Information Theory Workshop (ITW)*, Sep. 2013, pp. 1–5.

VITA

Ubaid U. Fayyaz received the B.S. degree in electrical engineering from the University of Engineering and Technology, Lahore, Pakistan in 2005, and the M.S. degree in electrical engineering from the Georgia Institute of Technology, Georgia USA, in 2013. He is currently pursuing his Ph.D. degree in electrical engineering at the Georgia Institute of Technology Atlanta, Georgia USA. From 2006 to 2009, he worked at the Center for Advance Research in Engineering Islamabad, Pakistan, where he was responsible for the algorithm design and FPGA-based implementations of communication systems. His research interests include coding theory, information theory and signal processing. He is recipient of the William J. Fulbright, the Water and Power Development Authority Pakistan, and the National Talent scholarships.